2011

Crystal Growth of Complex Intermetallics in Search for Heavy Electron Systems

Brenton L. Drake
Louisiana State University and Agricultural and Mechanical College

CRYSTAL GROWTH OF COMPLEX INTERMETALLICS IN SEARCH FOR HEAVY ELECTRON SYSTEMS

A Dissertation

Submitted to the Graduate Faculty of the
Louisiana State University and
Agricultural and Mechanical College
In partial fulfillment of the
Requirements for the degree of
Doctor of Philosophy

In

Department of Chemistry

By
Brenton L. Drake
B.A. and B.S., Glenville State College, 2007
December 2011

DEDICATION

To the baby blues that captivate, a smile that illuminates, and love that inspires,

My Wife

To the sculptors, designers, and carpenters of personality,

My Family

To the leaning posts and crutches needed along the way,

My Friends

To those who believed in what one didn't see,

My Advisors

May our next steps together be as seamless and fruitful

ACKNOWLEDGEMENTS

Science is the quest to understand. A plethora of questions, many beginning with what, how, or why, encumber us from the day we are born. We seek advice from our parents, instructors, and elders regarding the burning questions we often quickly blurt from our mouth. In many cases the question can be quickly and satisfactorily answered. Yet there are those of us who always follow with why to expand our breadth of knowledge in order to satiate our curiosity. The incessant need to probe, question, and comprehend allows the learner to grow, moving to higher levels of cognitive understanding and mental realization. Traversing the hierarchy of questioning, one finds beauty in the simple questions that require not only an invested answer but critical analysis of the information at hand. To progress through Bloom's taxonomy we must initially allow assimilation of vast reservoirs of information. Instructors at an early age push us with how, what, and why questions slowly developing our cognitive ability such that we have the ability to answer questions that require us to make new connections and draw conclusions. Post secondary education is a pursuit to grow and further learning to a level that requires assessment of situations, evaluating outcomes, and creatively finding an answer. The ability to think critically requires training and an ardent appreciation of the question. The irony of science is that we never leave the how, what, and why questions; we only learn to better form a question such that a more specific and critical answer is required.

Recognition that questioning and development is metered in nature, it should not come as a surprise that doctoral studies lead to the actualization of a beauty in the way one approaches problem solving. Nature's beauty arises from the ability to masquerade complexity as though with one fleeting glance all can and has been perceived. Few things evoke beauty like shape, structure, and the symmetry elicited in many crystalline materials expediently left for our

discovery in nature or the laboratory. The faceted faces transmitting, absorbing, and reflecting light afford a perfect guise for the underlying intricacy in atomic structure, arrangement, and the resulting physical properties. Yet, in the quest to understand the inner workings one must question and design ways to probe, analyze, and resolve the queries at hand. Along this journey what was true beauty is modified to incorporate the concealed underpinnings of complexity and external simplicity. As much as beauty is to the eye, understanding the complexities of nature has a genuine beauty few will ever see to fruition. This realization arises when one learns to value the question, more over the pondering of the question, as much as the answer.

Memoirs are simply a retrospective collection of memories as they pertain to the intricate relations you have developed over time. My memoirs are far from complete as many influences have yet to add their stroke to the picture that is my life. Over the past 26 years many of the brush strokes are in place and an individual, the product of many contributions, can be realized in the portrait. Here in, I would like to acknowledge and thank those artists.

I would like to start by acknowledging those who painted the background and set forth the structural foundation from which I developed. I would like to thank my mother, Debra K. Drake, for the compassion and understanding only a mother can give. I would like to thank my father, Rickey L. Drake, for instilling virtues and a work ethic that are centric to my self-perception today. I would like to thank Christina Workman for always having and open ear (and tolerating my father). I would like to thank my sisters, Beverly Drake, Brittany Drake, and Brandy Drake, for tireless and unrelenting aggravation, joy, and a perspective on life that only 3 sisters can give. I would like to thank my cousin, Jason G. Moore, he was the brother I never had growing up. I would like to thank Andrea Hacker, Melissa Workman, and Robby Workman for helping me grow as a person. I would like to give thanks to my extended family, a support

system that has shaped me profoundly. Specifically, thank you Phyllis Moore, Robert (Bob or Whitey) Moore, and Karen Drake, surrogate parents during those long summer breaks when Jason and I found nothing but trouble/fun in the creeks (catching minnows and craw crabs), the yard (playing and/or catching lightning bugs), the woods (hunting and building "tree stands"), and on dirt bikes and ATV's. I would like acknowledge my parents for similar experience when Jason would venture to our house. I would like to thank my Grandparents, they are not walking with me now, but their essence remains in my heart. To my family, you're the artist whose brush strokes have outlined the man I am today. You are the basis, the stock, from which everything I have and will accomplish roots. Thank you and I love you.

I would like to thank my wife, Leslie A. Drake. You have impacted my life in so many positive ways. I am humbled by your generosity and compassion. It takes a special person to just tolerate me, and somehow I have managed to convince you to marry me. You are my best friend and I love you. I truly look forward to a fruitful future together with many new and defining brush strokes.

I would like to thank those who I am lucky enough to have as my friends. You mean more to me than you know. Thank you for the laughs, the open ears, and the experiences! We may move apart but you will always be reflected in my personality and remembered in my heart.

I would like to thank and acknowledge the professors who have made a profound mark on my life that I will not soon forget. Your focus on students and the way you handle yourself in and out of the classroom have directly impacted my vision and philosophy as a future educator. Your brush strokes will forever be visible, academically; they have made me who I am. Thank you Professors Kevin L. Evans and Joe Evans. You both knew when to push me beyond my limits, and you believed in me when I wasn't sure of myself. I consider you both dear friends

and mentors. I would like to thank Professors Julia Y. Chan and George Stanley for providing me with the tools to critically asses a situation and present solutions that may lie outside the box. You both have help me take my abilities to a new level.

I would like to thank my committee members, Professors George Stanley, David Young and Philip Adams for their advice and mentoring. Special thanks to my collaborators: Prof. David Young, Prof. Philip Adams, Prof. John DiTusa, Prof. Emilia Morosan, Prof. Cigdem Capan, Michael Kangas, W. Adam Phelan, Gregory McCandless, Neel Haldolaarachchige, Yimin Xiong, and Amar Karki for stimulating conversations and significant contributions to my dissertation work. I would like to thank Dr. Frank Fronczek, a man of many hats, crystallographer, teacher, and friend. Without his mentoring, my understanding of the theory and practical application of crystallography would be minimal at its best.

I would like to acknowledge and thank the Chan group in its many forms. A warm thank you goes to Jung Young Cho, W. Adam Phelan, Melissa Menard, Michael Kangas, Devin Schmitt (with two T's), Brad Fulfer, and Greg Morrison. Your support and camaraderie will be deeply missed.

In closing, I would like to acknowledge and thank the funding agencies who have graciously supported myself and my research: Louisiana State University – Economic Development Assistantship, National Science Foundation – Division of Materials Research (DMR – 0756281 and DMR - 1063735), and the Alfred P. Sloan Fellowship.

TABLE OF CONTENTS

LIST OF TABLES

LIST OF FIGURES

ABSTRACT

The structural solution and physical property characterization of several *Ln*-T-Al/Ga and *Ln*-T-Al-Si contain phases, which include *Ln*$(Cu,Al)_{12}$ (*Ln* = Y, Ce, Pr, Sm, and Yb), *Ln*$(Ag,Al,Si)_2$ (*Ln* = Ce and Gd), *Ln*$Cu_2(Al,Si)_5$ (*Ln* = La and Ce), *Ln*$(Cu,Al,Ga)_{13-x}$ (*Ln* = La, Ce, Pr, and Eu), α and β *Ln*$NiGa_4$ (α *Ln* = Y and Gd – Yb; β *Ln* = (Tb – Er)), and Ln_4FeGa_{12} (*Ln* = Tb – Er) will be presented in this work with an emphasis on crystal growth. The systems cover a large breadth of phase space and serve to illustrate the new and rich chemistry and physics that remain, to this day, to be discovered in these phase spaces. Additionally, these phases range in complexity, to the eloquently simple open network found in *Ln*$(Ag,Al,Si)_2$ to the more complex 3 dimensional polyhedral environments of *Ln*$(Cu,Al)_{12}$ (*Ln* = Y, Ce, Pr, Sm, and Yb) or *Ln*$(Cu,Al,Ga)_{13-x}$.

In all cases these phases were discovered from systematic progressions throughout the periodic table and can all trace their roots to one phase, $CePdGa_6$. Chapter 1 of this document describes the logic and motivation behind the exploration of the *Ln*-Cu-Al phase space and alludes to some serendipitous discoveries. Additionally, it treats the issues of a failing materials science effort in America as recently outline in a recent National Academies of Science document: *Frontiers in Crystalline Matter: From Discovery to Technology*. Time is taken to discuss what is needed to once again assume a predominate role in these ventures and how our group aligns itself with the proposed directives Chapters 2 – 5 provide in-depth discussion of selected phases as it relates to their respective crystalline growth, structure, magnetic, and transport properties.

CHAPTER 1. INTRODUCTION

1.1 Motivation

As time has shown, a development on the forefront of scientific endeavor allows a society to enjoy the benefits of a synergistic effort between the pure sciences and engineering for the betterment of technology and therefore society. At the cutting edge of this synergism are the areas of condensed matter physics, solid state chemistry, materials science, and crystal growth with interest in the electrical, magnetic, structural, or optical nature of a material. Basic research in both chemistry and physics acts as fodder for the development of new technologies, and at the heart of this is the ability to grow and characterize a material such that the intrinsic properties are observed. Though respected for advances in fundamental theory and science, the area maintains a lasting vitality that few other areas have demonstrated over the past century. From the first observation of superconductivity in mercury in 1911 by Onnes to the more recent report of pnictide-based high temperature superconductors, vitality and vigor exists with extensive collaborative efforts that few other disciplines can muster.

The search for materials with desired properties concomitantly relies on the discovery of new materials and ultimately the subsequent growth of large single crystals. In many cases a new material is identified as bolstering potential for application, to unequivocally determine the material innate properties, large single crystals, as can be seen in Figure 1.1, must be grown such that detailed studies can be completed.

It has been our focus to join these two with the maxim of a properties-driven approach by first growing and subsequently studying large single crystals of lanthanide based ternary intermetallics. By spring boarding off the synergism of single crystal growth/structural characterization and property measurement, direct growth of single crystals circumnavigates the

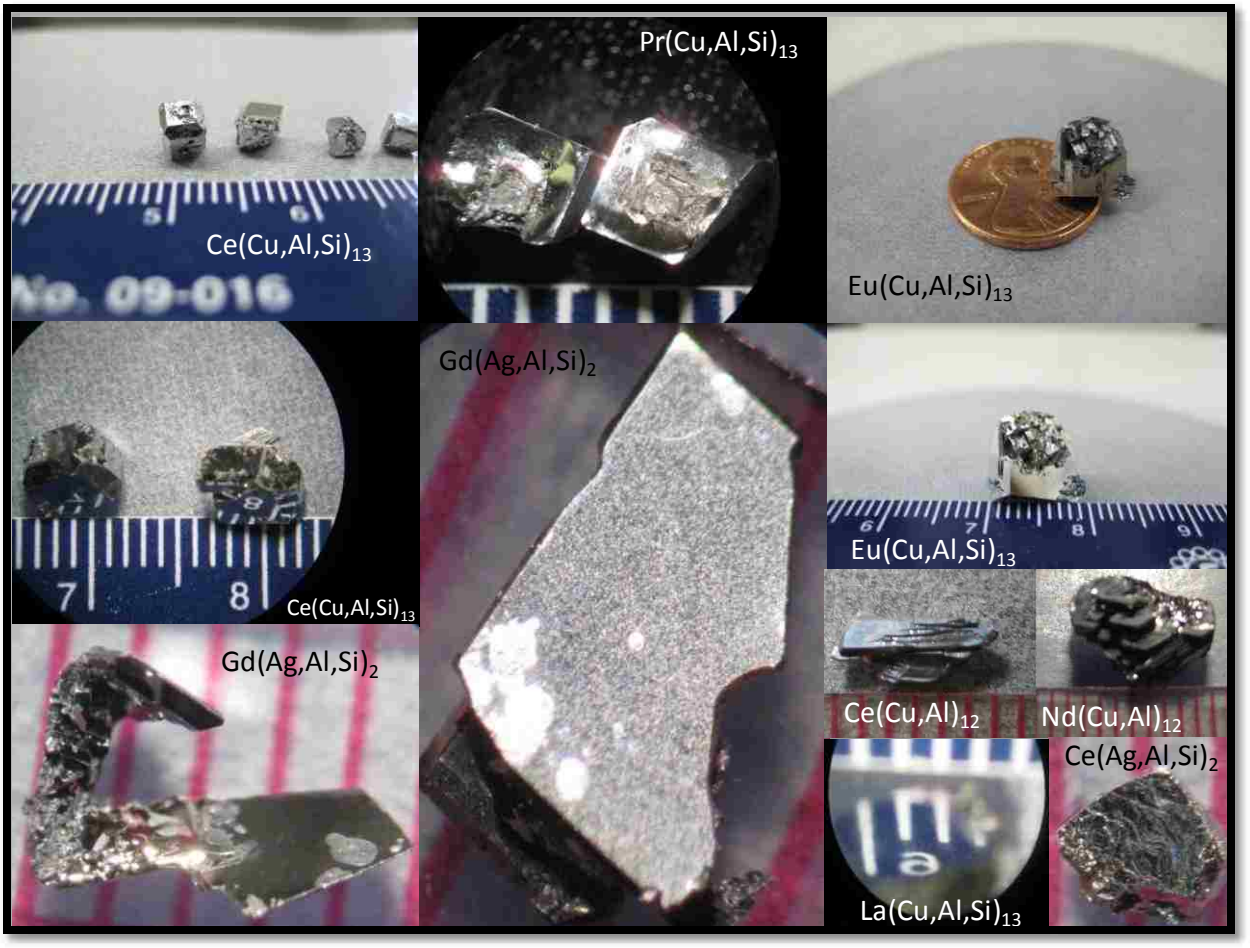

Figure 1.1 A collage of single crystals grown during my tenure as a graduate student. The crystals depicted are as follows: 1) $Ce(Cu,Al)_{12}$, and $Nd(Cu,Al)_{12}$ (Chapter 2) 2) $Ce(Ag,Al,Si)_2$ and $Gd(Ag,Al,Si)_2$ (Chapter 3) 3) $Ce(Cu,Al,Ga)_{13}$, $Pr(Cu,Al,Ga)_{13}$, $Eu(Cu,Al,Ga)_{13}$, and $La(Cu,Al,Ga)_{13}$ (Chapter 5 section 2.1).

need for subsequent growth via the adduct of the molten metal flux growth technique. Growth of large single crystals is a demanding endeavor that is rewarded by not only the beauty of a faceted single crystal, but by knowledge that the properties measured are true and intrinsic to the phase, its crystalline quality, and its orientation.

Upon reflection, the choice to join a group in which crystal growth was fervent and central to the science worked on each day in the laboratory was one initially of fascination and curiosity. To see molten metal yield beautiful, faceted crystals whose outer beauty disguise

completely the hidden complexity of the inner-workings was an opportunity that could not be surpassed.

1.2 Synthesis, X-ray diffraction, and Physical Properties

For the sake of proper and thorough discussion, the background associated with synthesis, diffraction, magnetism, and transport properties must be presented. The interdisciplinary nature of materials research requires our group to be proficient in a broad spectrum of topics, even outside our specific research scope. Our true interests lie in ascertaining the relationship of a compound's structural subunits (chemistry) and if these subunits can be associated with specific properties (physics).

1.2.1 Synthesis

The self flux growth technique is advantageous to crystal growers as the required equipment is comparably inexpensive and large single crystals of multiple phase can readily be accessed from a molten flux.[1] Here in, the foci of this dissertation are the phases grown from molten Al (Chapters 2 – 4) and Ga fluxes (sections of Chapter 5). Typical synthesis begin by charging an alumina crucible, in the following order, with chunks of 99.9% purity lanthanide, a minimum of 99.9% purity transition metal, and a large excess of > 99.9% purity main group element as a flux. Charging the crucible in this fashion ensures the flux covers the other components and assists in melting both the transition metal and lanthanide. The starting constituents are loaded in molar ratio such that the total weight of the growth is around 1 – 1.5 g for Al growths and 1.5 – 2 g for other fluxes. The charged crucible is then loaded into a fused silica tube with a filtering medium (silica wool) placed on top with the exception of Al. The use of silica wool in Al synthesis is singled out as Al will react readily with the silica wool resulting in the possible inclusion of Si into the reaction melt. Silicon inclusion, though not normally

desirable, can lead to serendipitous discoveries ($LnCu_2(Al,Si)_2$ Chapter 4). Often an inverted alumina crucible is place over the crucible containing the reactants. The fused silica tube is subsequently evacuated, sealed, and placed in a high-temperature oven. A general sythesis temperature profile and image of a typical reaction setup for aluminum flux growth is shown in Figure 1.2. After the prescribed profile is complete the sample is removed from the furnace and the bulk of the flux removed by centrifugation. Remaining flux on single crystals is remove chemically via a prescribed adduct such as an HCl, HNO_3, $C_2H_4O_2$, or NaOH.

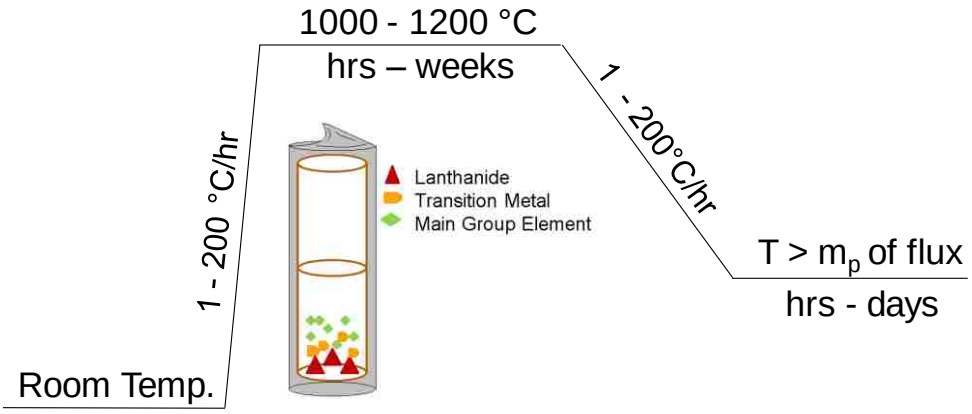

Figure 1.2 Generic temperature profile that encompasses much of the synthesis reported in later chapters. The image under the temperature profile depicts a typical Al flux growth synthesis.

Reaction ratios are determined by careful analysis of binary and if available ternary phase diagrams. Binary phase diagrams, though not fully accurate due to the incorporation of a third constituent in the melt, serves as a guide revealing stable binary phases that may contaminate the growth. In addition to determining the relative ratios used in the reaction, phase diagrams assist in the mapping of temperature profiles. The temperature profile is chosen to ensure a congruent melt, avoid secondary phase formation, and upon cooling provide spontaneous nucleation points at a sufficiently low rate to ensure optimal conditions for large crystal growth. In some cases slow cooling permits stabilization of a secondary phase and must be avoided by cooling rapidly to some temperature below that phase's formation range. After cooling to a point below the

formation range, often the cooling rate is decreased significantly to once again resume controlling the nucleation and crystal growth rates. Another powerful factor governing the chosen experimental conditions is experience and the familiarity of a given system that one acquires over time by working with related systems.

1.2.2 X-ray Diffraction

Specifics of the experimental conditions for X-ray powder and single crystal diffraction are given in each chapter. In all cases powder X-ray diffraction (XRD) were collected to ensure phase homogeneity/purity using a Bruker D8 Advance X-ray diffractometer equipped with Cu K_α radiation (λ = 1.54056 Å) source with accelerating voltages of 40 KV at 40 mA and a Ge single crystal monochromator. Powder XRD allows for confirmation of single crystal XRD models. Single crystal XRD data are collected using a Nonius Kappa CCD (charge coupled device) equipped with a Mo K_α source (λ = 0.71073 Å) and a graphite monochromator. Often a powder XRD pattern is collected and the phases cannot be identified immediately as the pattern may contain multiple phases, both of known and unknown materials, making complete identification difficult. As a group that cares about crystal growth, one of the first methods for separating phases are to identify the specific morphologies in a growth. As morphology often is insufficient to identify a phase, single crystal XRD experiments are completed on all unique morphologies. With all the morphologies of the respective structures solved, we return to the original powder XRD pattern and ensure that all observed peaks are indexed to the phases found during single crystal XRD experiments.

A thorough discussion of diffraction theory, both powder and single crystal XRD, are well beyond the scope of this dissertation. The theory of diffraction is central and pertinent to our group's niche in the scientific community. At this time, for the reader of this dissertation

who may need/desire a fundamental grasp of X-ray diffraction theory, I would like to recommend the following texts *Elements of X-ray Diffraction* (B. D. Cullity)[2] or *X-ray Structure Determination: A Practical Guide* (Stout and Jensen)[3,4].

A complementary technique, often employed when disorder is prevalent or a structure is difficult to solve, is that of scanning electron microscopy (SEM) when equipped with an energy dispersive X-ray spectroscopy probe (EDS). This technique is useful in understanding/determining the stoichiometry of the material. Fundementally, SEM/EDS can be understood from Bohr's model of the atom. A sample is irradiated with a high energy electron beam, inducing electron promotion to higher energy shells. Subsequent transitions to lower shells release photons on the energy scale of X-rays, of which the photon energies are characteristic of specific metals.

1.2.3 Physical Properties

Specific details related to the experimental conditions are contained within each chapter where physical property data such as molar magnetic susceptibility (χ_m), magnetization (M), resistivity (*p*), magnetoresistance (MR), and heat capacity are presented. Though satisfactory for individuals working in the area, it may be warranted to digress in a similar fashion as I have done on the topics of synthesis and X-ray diffraction. The statement in its own right, physical properties can be rather misleading and can be defined differently based on the area of the readers expertise. Specifically when asked about the physical properties of a compound or material, many may be requesting information related to colligative properties such as the melting point or boiling point, intrinsic properties like density, or olfactory/visual/tactile properties. In all cases, the answer delineates the physical nature of the substance, but here when

discussing the physical properties of a material, the properties to be discussed will focus on magnetism, electrical transport, magnetoresistance (MR), and heat capacity.

1.2.3.1 Magnetism

Many inorganic compounds and materials which contain transition and/or lanthanide metals display magnetism which arises from un-paired electrons associated with the *d* or *f* orbitals respectively. These spins can interact in varying degrees of strength and over a range, while, if present, interacting with an applied field resulting a plethora of magnetic ground states. The two basic magnetic states are *dia*- and *para*- magnetism. In the case of diamagnetism all electrons are spin paired and repel an applied external magnetic field. This is due to, in a classical view, circulation in a fashion to generate an opposing magnetic field. A material is paramagnetic if it contains unpaired electrons which interact with the applied magnetic field in such a fashion that they are attracted to the external source yet there is no net dipole moment. If a material is paramagnetic and undergoes cooling, a transition may occur at a critical temperature (T_C or T_N) where spins align parallel (ferromagnetism, FM), anti-parallel (antiferromagnetism, AFM), or in other more exotic arrangements such as canted states, helical magnets, or spiral magnets.

To understand the magnetic data collected, we first must understand how to determine theoretical values so conclusions may be drawn from our observations. Magnetic moments associated with materials depend upon S (spin), L (angular momentum), J (coupling), and g (gyromagnetic ratio). Additionally, L is sufficiently quenched, and therefore J, in transition metal systems such that only the spin is critical to determining the theoretical magnetic moments:

$$\mu_s = g\sqrt{S(S+1)}\left[\frac{eh}{4\pi mc}\right] \qquad 1.1$$

μ_s is the spin only moment, g is the gyromagnetic ratio (g = 2.0023 for an electron), e is the elementary charge of an electron, h is Planks constant, m is the mass of an electron at rest, and c is the speed of light. As e, h, m, and c are all constants, the expression can be simplified by setting these equal to one Bohr magneton (1 μ_B) as shown in equation 1.2 and 1.3. It is important to remember that answers will be given in the effective number of Bohr magnetons:

$$\mu_B = \left[\frac{eh}{4\pi mc} \right] \tag{1.2}$$

$$\mu_s = g\sqrt{S(S+1)}\mu_B \tag{1.3}$$

The effective moment associated with a free electron is 1.73 μ_B.

The spin only approximation is not satisfactory to model the moments observed in lanthanide containing systems. Orbital angular momentum is critical and the coupling that arises between the orbital momentum and spin, J. The gyromagnetic ratio also deviates from that of a free electron as one must take in account S, L, and J:

$$g = 1 + \frac{J(J+1) + S(S+1) - L(L+1)}{2J(J+1)} \tag{1.4}$$

Additionally, the effective magnetic moment must reflect the coupling between the spin and orbital angular momentum:

$$\mu_{eff} = g\sqrt{J(J+1)}\mu_B \tag{1.5}$$

Returning paramagnetism, the spins may be influenced by temperature and applied field, but no ordered state develops at low temperature. Magnetization is linear at low field and is completely reversible. The molar magnetic susceptibility (χ_m) can easily be described by Curie type behavior:

$$\chi_m = \frac{C}{\mathrm{T}} \tag{1.6}$$

where C is the Curie constant and T is temperature. This relationship is valid at high temperature where thermal fluctuations dominate and nearest neighbor interactions can be ignored. The magnitude of χ_m sheds light on the magnetic state, as diamagnetic materials have small, negative values where paramagnetic materials have small, positive values of χ_m. A modification of the Curie law, equation 1.6, can be made to accommodate systems that favor magnetic ordering at low temperature:

$$\chi_m = \frac{C}{\mathrm{T} - \theta} \tag{1.7}$$

where θ is the Weiss temperature. Equation 1.7 is known as the Curie-Weiss Law, and the Weiss temperature describes the coupling between neighboring spins. A negative value for the Weiss temperature indicates AFM correlations and positive values indicate FM correlations. The spins in a ferromagnetic material align parallel to one another. Typically FM materials show large values of χ_m compared to a paramagnetic material and saturate when sufficiently below the Curie temperature (T_C), where AFM materials have comparable values of χ_m but decrease sharply at the Neel transition (T_N). The spins in an antiferromagnetic material align anti-parallel. Further corrections to compensate for background contributions to the susceptibility, such as temperature independent Van Vleck paramagnetism or diamagnetism, we can employ the modified Curie-Weiss expression:

$$\chi_m = \frac{C}{\mathrm{T} - \theta} + \chi_o \tag{1.8}$$

where χ_o describes the background contribution.

The topic of magnetism is as broad as it is deep and a thorough treatment not possible in the constraints of this introduction. As magnetism is a central property of the materials we study, the fundamentals of magnetism are critical and I defer the readers interested to *Basic Solid State Chemistry* (A. R. West)[5] and *Magnetism in Condensed Matter* (S. Blundell)[6].

1.2.3.2 Heat Capacity

Our search for new and exotic materials often revolves around a search for materials that exhibit an enhanced mass state at low temperature determined from heat capacity (HC) data. It is nontrivial to elucidate the exact nature of a compound at low temperature but rather important pieces of information can be gleaned from HC data that, when taken in their entirety, tells a story of competing and/or emergent phenomena. The collection of HC data itself is nontrivial, time consuming, and humbling for the experimentalist, as sample preparation can be exacting and it demands clean samples. In application, HC data can shed light on magnetic entropy (S_m), magnetic and/or structural transitions, the electronic contribution (Sommerfeld parameter, γ), the Debye temperature, and in some cases a magnon contribution.

The total HC at constant pressure of a metal is the sum of both the electronic and phonon contributions and can be written as:

$$C_p = \beta \mathrm{T}^3 + \gamma \mathrm{T} \qquad 1.9$$

where $\beta \mathrm{T}^3$ represents the phonon contribution and $\gamma \mathrm{T}$ the electronic contribution to the total HC y of the system. At sufficiently low temperatures the linear electronic contribution to HC becomes dominates, and it is useful to express the equation as:

$$\frac{C_p}{\mathrm{T}} = \beta \mathrm{T}^2 + \gamma \qquad 1.10$$

such that a plot of C/T vs. T^2 provides a linear relationship where β is the slope and γ is the intercept. Inspection of the equation reveals that the total HC is dominated by the phonon contribution and depending on the system, sufficiently low temperatures where the relationships become valid may be complicated by the magnetic transition of the lanthanide atom. Often we find it useful, assuming a magnetic transition is observed, to fit both above and below the transition temperature to extract values of γ. Judicious choice of fit ranges becomes critical.

To simplify the interpretation of the data, we find it useful to subtract the phonon contribution from the total HC, such that the remaining HC only describes the magnetic/electronic contribution. To subtract the phonon contribution two possible choices are available: 1) grow a non-magnetic analogue that is similar in electronic configuration and size (i.e. a nonmagnetic La derivative to subtract out the phonon contribution of a magnetic Ce species) or 2) estimate the phonon contribution from Equation 1.10 (phonon contribution = βT^3). When possible, it is preferred to grow a nonmagnetic analogue and measure the samples total HC for subtraction from the magnetic analogues total HC, resulting in C_m (electronic/magnetic heat capacity) as shown in Figure 1.3. Fitting data with the phonon contribution subtracted allows one to calculate S_m and the critical exponent associated with the magnon contributions.

At low temperature a heavy fermion shows a characteristic enhancement of its effective mass, observed by γ often being 10 - 100 fold larger than that of a typical metal ($\gamma > 100$ mJ/K^2-mol).[7-10] Fitting below a magnetic transition, the value of the Sommerfeld parameter is especially susceptible to artificial enhancement because of the transition, and often we report both the value above and below the transition. The Sommerfeld parameter is simply one data point in the grand scheme of classifying a compound as a heavy fermion since it can easily be compromised by poor phonon subtraction and structural/magnetic transitions. To better understand if the

observed γ value is truly reflective of a heavy fermion material, we look at the entire picture and ask a series of questions: Is γ enhanced? Do we recover less than the theoretical magnetic entropy? Is there Kondo behavior observed in the resistivity? Does it fit the Kadowaki Woods relationship?[11,12]

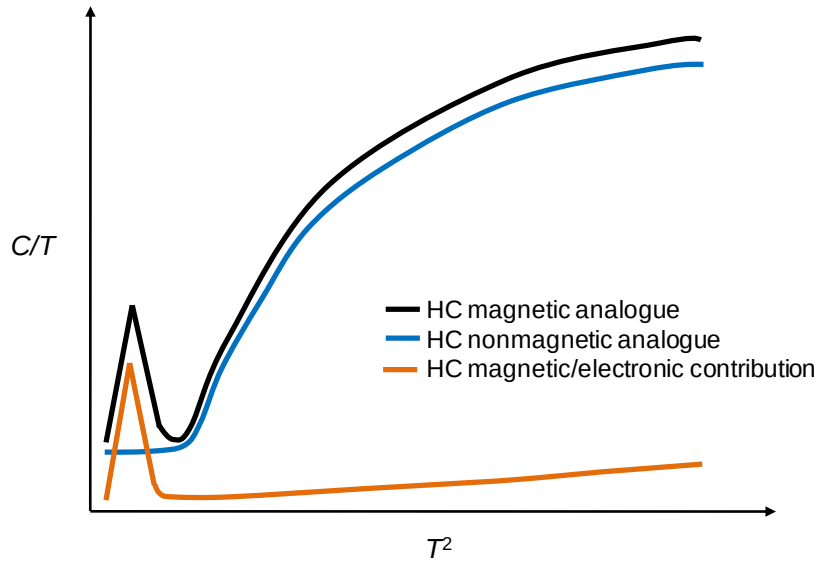

Figure 1.3 Arbitrarily scaled C/T as a function of T^2 plot illustrating the subtraction of magnetic (black line) and nonmagnetic (blue line) analogues, resulting in the magnetic/electronic (C_m) contributions to heat capacity (orange line).

The entropy associated with a magnetic transition can be quantified by:

$$S_m = R\ln(2J+1) \qquad 1.11$$

where R is the ideal gas constant and J is the angular momentum quantum number. This assumes no crystalline electric field effects and typically is used only to estimate the entropy associated with a Ce containing analogue. The calculated entropy assumes no external interaction of the *f* electrons. Since the enhancement of the effective mass associated with a heavy fermion directly stems from the interaction of the *f* electrons of the magnetic ion and the conduction electrons (Kondo behavior) we would expect a deviation from the theoretical entropy associated with a magnetic transition in the form of "missing" entropy. The entropy that is

associated with the interaction of the conduction and *f* electrons reduces the overall entropy associated with the magnetic transition. This is often expressed as some percentage of Rln2 and at what temperature Rln2 is recovered, for Ce-containing compounds. To experimentally determine the entropy associated with an observed magnetic transition the area found under the C_m/T vs T curve must be found:

$$S_m = \int_0^{T_m} \frac{C_m}{T} dT \qquad 1.12$$

over the range of the magnetic transition.

In some systems the exact nature of the magnetic ground state is difficult to elucidate. Magnetic transitions are easily observed in heat capacity data. Since C_m describes the magnetic/electronic contributions which can be fit to models derived from first principles of the form:

$$C_m \propto \mathrm{T}^n \qquad 1.12$$

where *n* is a critical exponent that describes the magnon contribution and is characteristic for each type of magnetic behavior. Understanding and the discussion of the critical exponents and their relation to the observed type of magnetism is outside the scope of this dissertation. For more specifics related to C_m or resistivity data and how it scales with the critical exponents associated with specific magnetic or transport behaviors, I defer to the thorough discussion by G. R. Stewart in a 2001 review *Non-Fermi-liquid behavior in d- and f-electron metals*.[13]

1.3 Grand Challenges

Growth of single crystalline material for structure and property investigations, either of fundamental value or for technological advances, is essential to quantitative elucidation of intrinsic properties. A recent report issued by the National Academy of Sciences (NAS) brings

to the forefront of discussion the basic need for a thriving community of crystal growers, which is diminishing throughout the United States. Currently programs on foreign soil lead the world in technological developments.[14] The current trajectory of condensed matter research in the United State has the country targeted to be dependent on other countries to develop and market new technologies for our future needs. The NAS report challenges the United States to reclaim the top position in crystalline materials research and development by promoting condensed matter research, in all aspects: growth, structural determination, property measurement, and training of endemic scientists to open a corridor for technological and scientific advancement. The NAS report outlined the following three grand challenges vital to a sustainable crystalline research effort in the United States: growth of crystalline material for new technologies, growth of crystalline material for energy applications, and using computations/theory to guide synthesis.

For the United States to lead the world again in new technologies, materials must be understood fundamentally through systematic studies of single crystals. Progression across or down the periodic table, and comparison of isostructural materials or sub-units, reveals trends in bonding, structure, local environments, disorder, … essentially the chemistry of a material. Couple this with fundamental investigation of the physical properties of a material, and with experience, a smart targeted synthesis is realized.

The NAS report issues, as the first grand challenge, an initiative for the development of new materials for information, communication, and technological applications. To do this judicious exploration of structures, sub-units, or motifs linked to a specific property of interest should be exploited. A prime example is low dimensionality and its link to high T_c superconductors ($YBa_2Cu_3O_{7-\delta}$). It is now thought that investigations concerning high T_c superconductors should focus on dimensionality, its limit, and phase space for doping.

Dimensionality is not only a concern for superconductivity, but 1 and 2 D magnetism and magnetic frustration as well. Identification of a structural motif, like layers, has great benefit in new materials development and discovery.

In line with the argument in the NAS report, small perturbations in low energy levels and the subsequent competition between internal forces via physical or chemical means leads to emergent behavior. This emergent behavior is collective in nature and independent of its parts. This behavior often defies our understanding of a state of matter and evolves from the complex inner-workings of crystalline material.

1.4 Our Group's Growth

Discovery of a new compound $CePdGa_6$ marks the beginning of a fledgling group. The initiative was growing isostructural analogues to the n = 1 members of the Ce_nMIn_{3n+2} (M = Co, Rh, or Ir; n = 1,2) family[15-20] and investigating the effects of Pd and Ga substitution. Ce_nMIn_{3n+2} compounds exist as layered materials that exhibit superconductivity, magnetism, and an enhanced-mass state. It was of curiosity how systematically adding one valence electron via the transition metal and manipulating the main group element (p orbital contribution) would influence the complex low temperature physical properties. This question was not answered but a structurally related, antiferromagnetic heavy fermion system was discovered. *Ln*$PdGa_6$ (*Ln* = La and Ce) orders first antiferromagnetically at 10 K with a subsequent ferromagnetic ordering at 5 K.[21] The magnetic contribution to heat capacity reveals a heavy mass state with $\gamma \sim 230$ mJ/(K^2 mol Ce). Shortly thereafter a plethora of compounds were grown, all structurally related to *Ln*$PdGa_6$: Ce_2PdGa_{10} is a paramagnetic Kondo compound with large magnetoresistance over 250 % at 2 K, and Ce_2PdGa_{12} shows a collinear to canted antiferromagnetic state with $T_N \sim 11$ K.[22,23]

The question of how a systematic change in constituents would alter the physical properties of an interesting motif did not receive a direct answer but a new interesting motif was readily found. The same question was posed when the group's focus changed from Pd to Ni and d^9 late transition metals like Cu or Ag. It is known that coordination preferences play a strong role in phase and structure stabilization. Yet the question lingers whether similar structural motifs can be found for Ni, Cu, and Ag gallides and aluminides. As with many questions the answers are complex. Ce_2MGa_{12} can be successfully stabilized for Ni and Cu. Reminiscent of Ce_2PdGa_{12} the Ni analogue has an antiferromagnetic transition $T_N \sim 10$ K with the La derivative showing large, non-saturating magnetoresistance of 216 % at 9 T. The Cu analogue is paramagnetic down to 2 K. Both compounds show enhanced mass behavior, similar to $CePdGa_6$, with Ce_2NiGa_{12} being a heavy fermion, $\gamma \sim 191$ mJ K^{-2} mol^{-1}.[24] In addition to the Cu and Ni derivatives of Ce_2MGa_{12}, other phases like $Ln(Cu,Ga)_{13-x}$ ($NaZn_{13}$ structure type), hexagonal $SmCu_4Al_8$ (isostructural to $SmZn_{11}$), and $Ln(Cu,Ga)_{12}$ ($ThMn_{12}$ structure type) were identified and characterized.[25,26] With the rich and promising phase space of *Ln*-Cu-Ga we became interested in the *Ln:* Cu aluminides and Ag gallides in hope to grow motifs similar to $CePdGa_6$, Ce_2PdGa_{10}, $CeMGa_{12}$ (M = Pd, Ni, and Cu), $Ln(Cu,Ga)_{13-x}$, and $Ln(Cu,Ga)_{12}$ and to understand how a systematic change from a 3 d^9 (Cu) to 4 d^9 (Ag) metal impacted the physical properties (Ga to Al).

The remaining sections give brief details on the exploration of the *Ln*-Cu-Al, *Ln*-Ag-Al-Si, and *Ln*-Cu-Al-Si phase space and summarize important details of each as they relate to the *Grand Challenges*.

1.4.1 *Ln*(Cu,Al)$_{12}$ (*Ln* = Ce, Pr, Sm, Yb, and Y) and *Ln*(Cu,Ga)$_{12}$ (*Ln* = Y, Gd-Er, and Yb)

During the investigation of the *Ln*(Cu,Ga)$_{13}$ phase it was observed that only the large lanthanides would form the $NaZn_{13}$ structure type, where as the smaller rare earths formed the $ThMn_{12}$ structure type.[26,27] Investigation of the Pr(Cu,Ga)$_{13}$ compound led to the observation that the material showed an enhanced-mass state. With our systematic approach it was of interest to see if the Al-containing analogues were isostructural, and if so, do similarities exist in their physical properties. During exploration of the *Ln*-Cu-Al system, the $NaZn_{13}$ structure could not be stabilized via flux growth, where the $ThMn_{12}$ structure was stable for all lanthanides.

Single crystals of *Ln*(Cu,Al)$_{12}$ and *Ln*(Cu,Ga)$_{12}$ compounds (*Ln* = Y, Ce-Nd, Sm, Gd-Ho, and Yb for Al and *Ln* = Y, Gd-Er, Yb for Ga) have been grown by flux-growth methods and characterized by single crystal X-ray diffraction, complemented by microprobe analysis, magnetic susceptibility, resistivity and heat capacity measurements.[27] *Ln*(Cu,Ga)$_{12}$ and *Ln*(Cu,Al)$_{12}$ of the $ThMn_{12}$ structure type crystallize in the tetragonal *I*4/*mmm* space group with lattice parameters $a \sim 8.59$ Å and $c \sim 5.15$ Å and $a \sim 8.75$Å and $c \sim 5.13$ Å for Ga and Al containing compounds, respectively. For aluminum-containing compounds, magnetic susceptibility data shows Curie paramagnetism in the Ce and Pr analogue down to 50 K with no magnetic ordering down to 3 K, whereas the Yb analogue shows a temperature-independent Pauli paramagnetism. Sm(Cu,Al)$_{12}$ orders antiferromagnetically at $T_N \sim 5$ K, and interestingly, exhibits Curie- Weiss behavior down to 10 K with no Van Vleck contribution to the susceptibility. Specific heat data show that Ce(Cu,Al)$_{12}$ is a heavy fermion antiferromagnet with $T_N \sim 2$ K and with an electronic specific heat coefficient γ_0 as large as 390 mJ/K^2 mol. In addition, this is the first report of Pr(Cu,Al)$_{12}$ and Sm(Cu,Al)12 showing an enhanced mass (~ 80 mJ/K^2 mol and 120 mJ/K^{2}mol). For the Ga containing analogues, the magnetic susceptibility

data also show the expected Curie-Weiss behavior from Gd to Er, with the Yb analogue being once again a Pauli paramagnet. Antiferromagnetic transition temperatures range from 12.5 K, 13.5 K, 6.7 K, to 3.4 K for Gd, Tb, Dy, and Er, respectively. Metallic behavior is observed down to 3 K for all Ga and Al analogues. A large positive magnetoresistance up to 150 % at 9 T is also observed for $Dy(Cu,Ga)_{12}$. The structure, magnetic, and transport properties of these compounds will be discussed in depth in Chapter 2.

1.4.2 *Ln*(Ag,Al,Si)$_2$ (*Ln* = Ce and Gd)

Much of the *Ln*: Cu:Al phase space has previously been explored. With a large body of pre-existing knowledge for this phase space, it was of interest if isostructural *Ln*:Ag:Al phases could be stabilized. The potential to understand the differences in bonding and coordination preferences between Cu and Ag in *Ln* and Al networks is indispensible for solid state chemists. An ultimate goal for the solid state community is to have the synthetic footing found in organic synthesis labs. To do so requires an intimate understanding of the bonding and coordination preferences in specific environments. Unfortunately the subsequent work did not result in the isolation of isostructural phases, but equally, it did result in a very interesting, 4 component pseudo-binary; opening a new door for future materials exploration.

Single crystals of *Ln*(Ag,Al,Si)$_2$ (*Ln* = Ce and Gd) have been grown by flux-growth methods and characterized by single crystal X-ray diffraction, magnetic susceptibility, resistivity and heat capacity measurements.[28] *Ln*(Ag,Al,Si)$_2$, of the $ThSi_2$ structure type, crystallize in the tetragonal $I4_1/amd$ space group with lattice parameters $a \sim 4.2$ Å and $c \sim 14.4$ Å. Magnetic susceptibility data shows Curie-Weiss paramagnetism in the Ce and Gd analogues down to 80 and 50 K, respectively. The Ce analogue undergoes a ferromagnetic transition at 11 K in both the $H \parallel ab$ and $H \parallel c$ planes with the Gd analogue undergoing an antiferromagnetic transition at 24

K for H$\|c$ and is paramagnetic down to 3 K for H$\|ab$. Specific heat data reveal that $Ce(Ag,Al,Si)_2$ is a heavy fermion ferromagnet with two magnetic transitions T_{C1} ~ 10.8 and T_{C1} ~ 8.8 K. and with an electronic specific heat coefficient γ_0 as large as ~ 170 mJ/K^2 mol. In the related phases, $CeSi_{1.70}$, double magnetic transitions were observed and attributed to an antiferromagnetic modulation of the spins, as observed in neutron scattering experiments. Analysis of the heat capacity data below T_{C2} and its critical exponent dependence revealed either helical or 2D antiferromagnetic magnon contributions. Additionally, analysis of resistivity data below 8.8 K shows a T^2 dependence, typical of a fermi liquid, but more importantly it showed the absence of a $T^{5/2}$ dependence, ruling out helical magnon contributions. This reinforces the observation of an antiferromagnetic modulation in $CeSi_{1.70}$. The structure, magnetic, and transport properties of these compounds will be discussed in depth in Chapter 3.

1.4.3 *Ln*$Cu_2(Al,Si)_5$ (*Ln* = La and Ce)

While exploring the *Ln*-Cu-Al phase space in a more *Ln* and Cu rich growth, serendipitous discovery of small single crystals of *Ln*$Cu_2(Al,Si)_5$ (*Ln* = La and Ce) occured. Initial attempts to repeat this synthesis resulted in isolation of a $BaAl_4$ type phase ($CeCuAl_3$). Elemental analysis revealed the presence of Si and a synthetic strategy was found to once again grow *Ln*$Cu_2(Al,Si)_5$ (*Ln* = La and Ce). *Ln*$Cu_2(Al,Si)_5$ (*Ln* = La and Ce) could not be isolated as a single phase, and single crystals grew from the surface of a $BaAl_4$ type impurity ($CeCuAl_{3-x}Si_x$). This may be expected in part to the similarity in the $BaAl_4$ and $SrAu_2Ga_5$ structure types.[29] Mechanical separation was unsuccessful, and conditions were found to synthesis phase-pure polycrystalline samples from arc melt and annealing conditions.

Single crystals of *Ln*$Cu_2(Al,Si)_5$ (*Ln* = La and Ce) crystallize in the Sr_2AuGa_5 structure type, space group *P*4/*mmm* (No. 123), with lattice parameters of *a* = 4.2040(15) Å and c =

7.925(4) Å, and the Ce, Cu, M, and N (M = Al/Cu and N = Al/Si) atoms occupy the 1*a*, 1*b*, 2*h*, and 4*i* Wyckoff positions, respectively. Polycrystalline samples were used for magnetic measurements. Magnetic susceptibility measurements show Curie-Weiss like behavior at temperature higher than 200 K. Below 200 K curvature is observed in the inverse susceptibility, consistent with crystal electric field effects. $CeCu_2(Al,Si)_5$ remains paramagnetic down to 2.25 K. A somewhat smaller effective moment is recovered, 2.19 μ_B/mol Ce, but is consistent with previous reports for the $CePd_{1.5}Al_{5.5}$ phase.[30] Preliminary resistivity measurements show Kondo-like behavior. This, coupled with the rich heavy fermion behavior in related phases, offers hope that $CeCu_2(Al,Si)_5$ will be a new heavy fermion compound. The structure, magnetic, and transport properties of these compounds will be discussed in depth in Chapter 4.

1.5 References

(1) Canfield, P.C. and Fisk, Z., Growth of single crystals from metallic fluxes. *Philos. Mag. B* **1992,** *65*, 1117-1123.

(2) Cullity, B.D., "Elements of X-ray diffraction." Addison-Wesley Pub. Co., Reading, Mass., 1978.

(3) Stout, G.H. and Jensen, L.H., "X-ray structure determination: A practical guide." Macmillan, New York, 1968.

(4) Stout, G.H. and Jensen, L.H., "X-ray structure determination: A practical guide." Wiley, New York, 1989.

(5) West, A.R., "Basic solid state chemistry." John Wiley & Sons, New York, 1999.

(6) Blundell, S., "Magnetism in condensed matter." Oxford University Press, Oxford ; New York, 2001.

(7) Stewart, G.R., Heavy-fermion systems. *Rev. Mod. Phys.* **1984,** *56*, 755-785.

(8) Fisk, Z., Sarrao, J.L., Smith, J.L., and Thompson, J.D., The physics and chemistry of heavy fermions. *Proc. Natl. Acad. Sci. U.S.A.* **1995,** *92*, 6663.

(9) Fisk, Z., A whiff of chemistry in heavy electron physics. *Science* **2007,** *318*, 1559-1560.

(10) Thomas, E.L., Millican, J.N., Okudzeto, E.K., and Chan, J.Y., Crystal growth and the search for highly correlated intermetallics. *Comment. Inorg. Chem.* **2006,** *27*, 1 - 39.

(11) Kadowaki, K. and Woods, S.B., Universal relationship of the resistivity and specific heat in heavy-Fermion compounds. *Solid State Commun.* **1986,** *58*, 507-509.

(12) Jacko, A.C., Fjaerestad, T.O., and Powell, B.J., A unified explanation of the Kadowaki–Woods ratio in strongly correlated metals. *Nature Physics* **2009,** *5*, 422-425.

(13) Stewart, G.R., Non-Fermi-liquid behavior in d- and f-electron metals. *Rev. Mod. Phys.* **2001,** *73*, 797.

(14) *Frontiers in crystalline matter: From discovery to technology*, The National Academies Press: Washington DC, **2009**, ISBN: 0-309-13801-9.

(15) Hegger, H., Petrovic, C., Moshopoulou, E.G., Hundley, M.F., Sarrao, J.L., Fisk, Z., and Thompson, J.D., Pressure-induced superconductivity in quasi-2D $CeRhIn_5$. *Phys. Rev. Let.* **2000,** *84*, 4986.

(16) Macaluso, R.T., Sarrao, J.L., Moreno, N.O., Pagliuso, P.G., Thompson, J.D., Fronczek, F.R., Hundley, M.F., Malinowski, A., and Chan, J.Y., Single-crystal growth of Ln_2MIn_8 (Ln = La, Ce; M = Rh, Ir): implications for the heavy-fermion ground state. *Chem. Mater.* **2003,** *15*, 1394-1398.

(17) Moshopoulou, E.G., Fisk, Z., Sarrao, J.L., and Thompson, J.D., Crystal growth and intergrowth structure of the new heavy fermion materials $CeIrIn_5$ and $CeRhIn_5$. *J. Solid State Chem.* **2001,** *158*, 25-33.

(18) Moshopoulou, E.G., Sarrao, J.L., Pagliuso, P.G., Moreno, N.O., Thompson, J.D., Fisk, Z., and Ibberson, R.M., Comparison of the crystal structure of the heavy-fermion materials $CeCoIn_5$, $CeRhIn_5$ and $CeIrIn_5$. *Appl. Phys. A-Mater.* **2002,** *74*, s895-s897.

(19) Petrovic, C., Pagliuso, P.G., Hundley, M.F., Movshovich, R., Sarrao, J.L., Thompson, J.D., Fisk, Z., and Monthoux, P., Heavy-fermion superconductivity in $CeCoIn_5$ at 2.3 K. *J. Phys. Condens. Mat.* **2001,** *13*, L337.

(20) Petrovic, C., Movshovich, R., Jaime, M., Pagliuso, P.G., Hundley, M.F., Sarrao, J.L., Fisk, Z., and Thompson, J.D., A new heavy-fermion superconductor $CeIrIn_5$: A relative of the cuprates? *Europhys. Lett.* **2001,** *53*, 354.

(21) Macaluso, R.T., Nakatsuji, S., Lee, H., Fisk, Z., Moldovan, M., Young, D.P., and Chan, J.Y., Synthesis, structure, and magnetism of a new heavy-fermion antiferromagnet, $CePdGa_6$. *J. Solid State Chem.* **2003,** *174*, 296-301.

(22) Macaluso, R.T., Millican, J.N., Nakatsuji, S., Lee, H.-O., Carter, B., Moreno, N.O., Fisk, Z., and Chan, J.Y., A comparison of the structure and localized magnetism in Ce_2PdGa_{12} with the heavy fermion $CePdGa_6$. *J. Solid State Chem.* **2005,** *178*, 3547-3553.

(23) Millican, J.N., Macaluso, R.T., Young, D.P., Moldovan, M., and Chan, J.Y., Synthesis, structure, and physical properties of Ce_2PdGa_{10}. *J. Solid State Chem.* **2004,** *177*, 4695-4700.

(24) Cho, J.Y., Millican, J.N., Capan, C., Sokolov, D.A., Moldovan, M., Karki, A.B., Young, D.P., Aronson, M.C., and Chan, J.Y., Crystal growth, structure, and physical properties of Ln_2MGa_{12} (Ln = La, Ce; M = Ni, Cu). *Chem. Mater.* **2008,** *20*, 6116-6123.

(25) Cho, J.Y., Capan, C., Young, D.P., and Chan, J.Y., Crystal growth, structure, and physical properties of $SmCu_4Ga_8$. *Inorg. Chem.* **2008,** *47*, 2472-2476.

(26) Cho, J.Y., Thomas, E.L., Nambu, Y., Capan, C., Karki, A.B., Young, D.P., Kuga, K., Nakatsuji, S., and Chan, J.Y., Crystal growth, structure, and physical properties of $Ln(Cu,Ga)_{13-x}$ (Ln = La-Nd, Eu; x ~ 0.2). *Chem. Mater.* **2009,** *21*, 3072-3078.

(27) Drake, B.L., Capan, C., Cho, J.Y., Nambu, Y., Kuga, K., Xiong, Y.M., Karki, A.B., Nakatsuji, S., Adams, P.W., Young, D.P., and Chan, J.Y., Crystal growth, structure, and physical properties of $Ln(Cu,Al)_{12}$ (Ln = Y, Ce, Pr, Sm, and Yb) and $Ln(Cu,Ga)_{12}$ (Ln = Y, Gd-Er, and Yb). *J. Phys. Condens. Mat.* **2010,** *22*, 066001.

(28) Drake, B.L., Kangas, M.J., Capan, C., Haldolaarachchige, N., Xiong, Y.M., Adams, P.W., Young, D.P., and Chan, J.Y., Crystal growth, structure, and physical properties of $Ln(Ag,Al,Si)_2$ (Ln = Ce and Gd). *J Phys. Condens. Mat.* **2010,** *22*, 426002.

(29) Gout, D., Benbow, E., Gourdon, O., and Miller, G.J., Composition-structure relationships in polar intermetallics: experimental and theoretical studies of $LaNi_{1+x}Al_{6-x}$ (x = 0.44). *Inorg. Chem.* **2004,** *43*, 4604-4609.

(30) Tobash, P.H., Ronning, F., Thompson, J.D., Bobev, S., and Bauer, E.D., Magnetic order and heavy fermion behavior in $CePd_{1-x}Al_{6-x}$: Synthesis, structure, and physical properties. *J. Solid State Chem.* **2010,** *183*, 707-711.

CHAPTER 2. CRYSTAL GROWTH, STRUCTURE, AND PHYSICAL PROPERTIES OF *Ln*(Cu,Al)$_{12}$ (*Ln* = Y, Ce, Pr, Sm, and Yb)*

2.1 Introduction

Pseudo-binary lanthanide intermetallic compounds (*Ln*-*T*-*X* where *Ln* = lanthanide, *T* = transition metal, and *X* = main group element) adopting the $ThMn_{12}$ structure type [1,2] have been extensively studied and show a variety of interesting physical properties including magnetism and superconductivity.[3-12] This tetragonal phase (*I*4/*mmm*) consists of a lanthanide, transition metal, and main group element occupying the 2*a* (4/*mmm*), 8*f* (*2*/*m*), 8*i* (*m2m*), and 8*j* (*m2m*) Wyckoff sites. It is of merit to note that the 8*i* and 8*j* position are jointly occupied by *T* and *X* when *X* = Ga and for *X* = Al only 8*j* is jointly occupied. Growth of the pseudo-binary lanthanide analogues in this structure type is considerably stabilized with the addition of the third element, as only binary Mn and Zn lanthanide derivatives have been shown to crystallize in this structure type.[13-16]

The magnetic ordering at low temperatures due to long-range lanthanide interactions has been reported in several compounds where *M* = Cr, or Cu and *X* = Al. $CeCr_4Al_8$ exhibits an enhanced Sommerfeld coefficient of specific heat, $\gamma \sim 62$ mJmol^{-1}K^{-1} and does not magnetically order down to 1.5 K.[17] $GdCr_4Al_8$ and $ErCr_4Al_8$ show antiferromagnetic (AFM) ordering around 8 K and 14 K, respectively.[18,19] Similarly, $CeCu_4Al_8$ shows heavy-fermion behavior with $\gamma \sim 300$ mJmol^{-1}K^{-1}.[20] Reported more recently, $CeCu_{4+x}Al_{8-x}$ ($0 < x < 0.55$) shows heavy-fermion behavior ($\gamma \sim 200$ mJmol^{-1}K^{-1}) with antiferromagnetic ordering at 5.8 K, which was not previously observed and was reported to be paramagnetic down to 4.1 K.[19,21-23] $HoCu_4Al_8$ and

*Reprinted by permission of Journal of Physics: Condensed Matter: Drake, B.L., Capan, C., Cho, J.Y., Nambu, Y., Kuga, K., Xiong, Y.M., Karki, A.B., Nakatsuji, S., Adams, P.W., Young, D.P., and Chan, J.Y., Crystal growth, structure, and physical properties of Ln(Cu,Al)12 (Ln = Y, Ce, Pr, Sm, and Yb) and Ln(Cu,Ga)12 (Ln = Y, Gd-Er, and Yb). J. Phys. Condens. Mat. 2010, 22, 066001.

$ErCu_4Al_8$ compounds have been shown to order antiferromagnetically at 5.5 K and 6 K,respectively, which is due to the ordering of the lanthanide sublattice, with a second report of $HoCu_4Al_8$ ordering at 7 K.[17-19,24]

Addition of magnetic transition metals like Fe presents possibilities for magnetic ordering due to transition metal interactions and long range lanthanide interactions, respectively.[10,25-28] For example, $ErFe_4Al_8$ shows two magnetic transitions, 25 K and 111 K corresponding to the ordering of the Er and Fe sublattice, respectively.[26] In addition, negative magnetoresistance in the range of -1.8 % to -20.1 % has been found in several of the $R Fe_4Al_8$ compounds (*R* = Sc, Y, Ce, Yb, and Lu).[6]

We have grown $Ln(Cu,Al)_{12}$ analogues (*Ln* = Y, Ce-Nd, Sm, Gd-Ho, and Yb) Al flux growth techniques. To the best of our knowledge, there has not been a systematic study of the $ThMn_{12}$ structure in the *Ln*-Cu-Ga system. During exploration of the *Ln*-Cu-Al system, high quality single crystals were grown that upon further study are not in agreement with some previously published results. Here, we report the crystal growth, magnetism, and transport properties of $Ln(Cu,Al)_{12}$ compounds (*Ln* = Y, Ce, Pr, Sm, and Yb).

2.2 Experimental

2.2.1 Synthesis

Single crystals of $Ln(Cu,Al)_{12}$ (*Ln* = Y, Ce-Nd, Sm, Gd-Ho and Yb (note that *Ln* = Ce-Nd, Sm, Gd-Ho, Yb, and Y have been grown for $Ln(Cu,Al)_{12}$ but only the properties of Ce, Pr, Sm, Yb, and Y will be reported) were grown in the presence of excess flux. *Ln* (3N, chunks, Alfa Aesar), Cu (5N, powder, Alfa Aesar), and Al (5N, pellets, Alfa Aesar) were loaded, respectively, into an alumina crucible with a reaction ratio of 1:9:20. The crucibles were placed into a fused silica tube and the contents were evacuated and sealed. The vessel was loaded into a

Table 2.1 Crystallographic Parameters for $Ln(Cu,Al)_{12}$

Formula	$Ce(Cu,Al)_{12}$	$Pr(Cu,Al)_{12}$	$Sm(Cu,Al)_{12}$	$Yb(Cu,Al)_{12}$	$Y(Cu,Ga)_{12}$
a (Å)	8.813(3)	8.792(6)	8.749(2)	8.721(3)	8.704 (3)
c (Å)	5.16002)	5.156(3)	5.146(2)	5.118(2)	5.131(2)
V (Å)	400.8(2)	398.6(4)	393.9(2)	389.3(2)	388.7(2)
Z	2	2	2	2	2
Crystal system	Tetragonal	Tetragonal	Tetragonal	Tetragonal	Tetragonal
Space group	I4/mmm	I4/mmm	I4/mmm	I4/mmm	I4/mmm
θ range (°)	3.27-30.02	3.28-29.95	3.29-29.94	3.30-29.72	3.31-28.61
μ (mm^{-1})	18.424	19.015	21.075	25.657	18.961
Data collection					
Measured reflections	531	465	487	479	476
Independent reflections	196	190	191	190	169
Reflections with $I>2\sigma(I)$	195	188	188	184	161
R_{int}	0.0581	0.0359	0.0471	0.0304	0.0525
h	-12→12	-12→12	-12→12	-12→12	-11→11
k	-8→8	-8→8	-8→8	-8→8	-7→8
l	-7→5	-6→5	-7→4	-7→4	-6→6
Refinement					
$^{a}R_1[F^2>2\sigma(F^2)]$	0.0292	0.0262	0.021	0.0237	0.0289
$^{b}wR_2(F^2)$	0.0679	0.0624	0.0509	0.0542	0.0715
Reflections	196	190	191	190	169
Parameters	17	17	17	17	17
$\Delta\rho_{max}$ ($eÅ^{-3}$)	2.293	1.239	1.487	2.928	1.088
$\Delta\rho_{min}$ ($eÅ^{-3}$)	-1.688	-1.904	-1.69	-1.836	-0.845

$^{a}R_1 = \sum\|F_o| - |F_c\| / \sum|F_o|$, $^{b}wR_2 = [\sum[w(F_o^2 - F_c^2)]/\sum[w(F_o^2)^2]]^{1/2}$

$w = 1/[\sigma^2(F_o^2) + (0.0328P)^2 + 1.7521P$, $w = 1/[\sigma^2(F_o^2) + (0.0252P)^2 + 1.7135P$, $w = 1/[\sigma^2(F_o^2) + (0.0085P)^2 + 0.6996P$,

$w = 1/[\sigma^2(F_o^2) + (0.0241P)^2 + 1.1008P$, $w = 1/[\sigma^2(F_o^2) + (0.0390P)^2 + 0.0000P$, for Ce, Pr, Sm, Yb and Y respectively

furnace and heated to a dwell temperature of 1100 °C for 10 h at 200 °C/h. Samples were slowly cooled to 720 °C at a rate of 4 °C/h at which they were centrifuged to separate crystals from the Al flux. In attempts to increase the crystal size, Yb samples were cooled at slower ramp down temperatures (0.5-1 °C/h). Final dwell times were varied from hours to days, and it was observed that crystal size increase with dwell time. In addition, it was clearly observed with different dwell times a differing amount of Cu was substituted into the Al site. For Yb samples, crystal size was maximized from a short dwell time not following the general trend for the other analogues. This is possibly due to the high vapor pressure of Yb. In all growths, silver metallic

crystals were retrieved via etching in NaOH (6M) until excess aluminum was removed and subsequently cleaned with 30% HNO_3, retrieving flux-free single crystals which were observed to be air stable.

2.2.2 Single Crystal X-ray Diffraction, Powder X-ray Diffraction, and Elemental Analysis

The crystals of $Ln(Cu,Al)_{12}$ were cut to suitable sizes for data collection (≤ 0.05 mm^3) and mounted onto a glass fiber using epoxy. They were then positioned onto the goniometer of a Nonius KappaCCD diffractometer equipped with Mo K_α radiation (λ = 0.71073 Å). Data collection was carried out up to θ = 30.0° at 298 K. Further crystallographic parameters for $Ln(Cu,Al)_{12}$ (Ln = Y, Ce, Pr, Sm and Yb) are provided in Table 2.1. Direct methods were used to solve the structure. SHELXL97 [29] was used to refine the structural model and data were corrected with extinction coefficients and refined with anisotropic displacement parameters. Refinement assuming a fully occupied formula led to convergence with very small final difference residual peaks. Selected interatomic distances are presented in Table 2.2, and atomic positions and displacement are provided in Table 2.3. To determine the composition of $Ln(Cu,Al)_{12}$, electron probe microanalysis was performed using a JEOL JSM-5060 scanning electron microscope equipped with an energy dispersive spectrometer. The accelerating voltage was 15 kV with beam to sample distance of 20 mm. An average of 5-7 scans was performed on each single crystal. The results are provided in Table 2.4. After taking account of elemental analysis results, the structures of $Ln(Cu,Al)_{12}$ (Ln = Y, Ce, Pr, Sm and Yb) were carefully checked for a mixed occupancy on all Cu and Al sites, and refinements of single crystal X-ray diffraction data suggest that the 8*j* site in $Ln(Cu,Al)_{12}$ is occupied statistically by Cu and Al. The resulting structural models showed similar stoichiometry for *Ln*:Cu:Al to the result of elemental

analysis. For simplicity, we will discuss the compounds as *Ln*(Cu,Al)$_{12}$ where (*Ln* = Y, Ce, Pr, Sm, and Yb for Al).

For all growths, ground single crystal samples were characterized by X-ray powder diffraction to confirm phase purity with a Bruker AXS D8 Advance Diffractometer.

Table 2.2 Selected Interatomic Distances for *Ln*(Cu,Al)$_{12}$ (Å)

	Ce(Cu,Al)$_{12}$	Pr(Cu,Al)$_{12}$	Sm(Cu,Al)$_{12}$	Yb(Cu,Al)$_{12}$	Y(Cu,Al)$_{12}$
Ln environment					
*Ln*1-Al1(x8)	3.073(2)	3.062(2)	3. 0384(2)	3. 016(2)	3.020(2)
*Ln*1-*M*0(x8)	3.2427(10)	3.2352(10)	3.2201(11)	3.2017(14)	3.2040(10)
*Ln*1-Cu1(x4)	3.3723(10)	3.3651(10)	3.3501(5)	3.3383(7)	3.3340(10)
Cu environment					
Cu1-Cu1(x2)	2.5800(10)	2.5780(10)	2.5730(10)	2.5590(10)	2.5655(10)
Cu1-Al1(x4)	2.6972(7)	2.6906(7)	2.6765(7)	2.6626(10)	2.6632(7)
Cu1-*M*0(x4)	2.5643(2)	2.5597(2)	2.5499(5)	2.5409(7)	2.5389(2)

*M*0 = Al or Cu

2.2.3 Physical Properties

Magnetic data was collected using a Quantum Design Physical Property Measurement System (PPMS). The temperature-dependent susceptibility data was measured under zero-field cooled (ZFC) conditions from 2-3 K to 285-300 K under an applied field of 0.1 T. Field-dependent magnetization data were measured at 3 K with field up to 9 T. The electrical resistivity and magnetoresistance (MR) were measured by the standard four-probe AC technique. The heat capacity was measured by the standard adiabatic heat pulse relaxation technique down to 0.4 K.

2.3 Results and Discussion

2.3.1 Structure

The $ThMn_{12}$ structure type has been well studied and has been shown to crystallize with a general formula of *Ln*(TM,X)$_{12}$, *Ln* = rare earth, TM = transition metal, X= main group element.[15] Herein, Ce(Cu,Al)$_{12}$ will be discussed as a general structural model for the series of

rare earth aluminides reported in this document, as only unit cell parameters such as the *a* or *c* unit cell lengths change due to lanthanide contraction. This pseudo-binary crystallizes in the tetragonal I4/*mmm* space group with the *Ln*, Cu, Al, and *M*0 (*M*0(8*j*) - Cu/Al) occupying 2*a*, 8*f*, 8*i*, and 8*j* respectively. It was found that statistical disorder is observed on the 8*j* site for Al containing compounds. The degree of statistical disorder depends on the reaction ratio, dwell times, and the lanthanide.

Table 2.3 Atomic Positions and Thermal Parameters for $Ln(Cu,Al)_{12}$

Atom	Wyckoff position	*x*	*y*	*z*	U_{eq} (Å^2)[a]
Ce	2*a*	0	0	0	0.0048(4)
Cu	8*f*	1/4	1/4	1/4	0.0091(4)
Al	8*i*	0.3483(3)	0	0	0.0059(8)
*M*0	8*j*	0.2771(2)	1/2	0	0.0135(10)
Pr	2*a*	0	0	0	0.0026(3)
Cu	8*f*	1/4	1/4	1/4	0.0067(4)
Al	8*i*	0.3483(2)	0	0	0.0052(8)
*M*0	8*j*	0.27769(18)	1/2	0	0.0105(9)
Sm	2*a*	0	0	0	0.0043(3)
Cu	8*f*	1/4	1/4	1/4	0.0085(3)
Al	8*i*	0.34729(18)	0	0	0.0064(7)
*M*0	8*j*	0.27870(14)	1/2	0	0.0156(7)
Yb	2*a*	0	0	0	0.0030(3)
Cu	8*f*	1/4	1/4	1/4	0.0064(4)
Al	8*i*	0.3458(3)	0	0	0.0048(9)
*M*0	8*j*	0.2794(2)	1/2	0	0.0144(10)
Y	2*a*	0	0	0	0.0057(5)
Cu	8*f*	1/4	1/4	1/4	0.0097(5)
Al	8*i*	0.3470(3)	0	0	0.0070(11)
*M*0	8*j*	0.2795(2)	1/2	0.00	0.0165(9)

[a] U_{eq} is defined as one-third of the trace of the orthogonalized U_{ij} tensor.
*M*0 = Cu and Al

Figure 2.1a illustrates the *Ln* (*Ln* = Ce-Nd, Sm, Gd-Yb) polyhedral environment; each polyhedron is comprised of 8 Cu atoms (medium yellow spheres), 4 Al atoms (small green spheres, identified as *M*1 in Ga analogues), and 8 *M*0 atoms (small purple spheres, identified as

*M*2 in Ga analogues). The Ce environment is similar to the one of $SmCu_4Ga_8$ (hexagonal), which belongs to the family of $CaCu_5$ structure type. *M*0 atoms are face sharing atoms in the polyhedron around the Ce atom (large powder blue spheres), in which the Ce polyhedron are corner sharing through Cu atoms. The polyhedron is comprised of 2 perpendicular six member rings which are coordinated about the Ce atom. Each ring is composed of 2 Al and 4 *M*0 atoms. The rectangular prism of Cu atoms is situated so 2 Cu positions set at ~ 45 degrees between the two perpendicular 6 member rings, essentially bi-capping the structure as shown in the Figure 2.1b. The face sharing 8*j* sites are the location of mixing in the ternary phase. These sites (Table 2.3), which the bond distances are listed in Table 2.2, show that this *M*0 position is at an intermediate distance when compared to the Cu and Al bond lengths, giving rise to the potential for statistical disorder on this 8*j* site.

Table 2.4 Composition as obtained from Electron Probe Microanalysis

	$Ce(Cu,Al)_{12}$	$Pr(Cu,Al)_{12}$	$Sm(Cu,Al)_{12}$	$Yb(Cu,Al)_{12}$
(Cu:Al)[a]	4.46(4):7.54(4)	4.65(4):7.35(4)	4.75(5):7.25(5)	4.77(8):7.23(8)

[a] Composition is normalized to lanthanide.

Figure 2.2a and 2.2b show the structural relationship between $ThMn_{12}$ and $CaCu_5$ structure-type [30] (Hereafter, $ThMn_{12}$ and $CaCu_5$ are represented as RT_{12} and RT_5, respectively for clarity). The relationship of lattice parameters has previously been described as the following: $aRT_{12} \approx \sqrt{3}aRT_5 \approx 2cRT_5$; $cRT_{12} \approx aRT_5 \approx aRT_{12}/\sqrt{3}$.[31,32] The transformation from RT_5 to RT_{12} structure is caused by systematic substitution of a pair of *T* atoms for *R* atom along the *c*-axis from the parental RT_5 structure. This can be described as equation; $2(RT_5) - R + 2T$ (a pair of *T*s) $\rightarrow RT_{12}$.[33,34] The crystallographic sites between the hexagonal *P*6/*mmm* RT_5 and tetragonal *I*4/*mmm* RT_{12} are shown in Figure 2.2*a*-*c*.

2.3.2 Physical Properties of *Ln*(Cu,Al)$_{12}$ (*Ln* = Ce, Pr, Sm, Yb, and Y)

Figures 2.3 – 2.5 show the temperature dependence of the magnetic susceptibility of single crystal of *Ln*(Cu,Al)$_{12}$ (*Ln* = Ce, Pr, Sm) measured at an applied field of 0.1 Tesla and the field dependence of magnetization at 3 K. The magnetic susceptibility of all three compounds was fitted to a Curie-Weiss equation of the following form: $\chi(T) = \chi_0 + C/(T - \theta)$, where C represents the Curie constant and θ is the Weiss temperature in the paramagnetic state, and where χ_0 is a constant positive background. The effective moments obtained from C were compared to the calculated values using $\mu_{eff} = g_J(J(J+1))^{1/2}$, they are both summarized in Table 2.5.

The temperature-dependent magnetic susceptibility of Ce(Cu,Al)$_{12}$ in an applied field of 0.1 T is shown in Figure 2.3a. The material is paramagnetic down to 3 K with no magnetic transition. The effective moment (35 – 253 K) of the Ce^{3+} ion was determined to be 2.63 μ_B which is close the calculated effective moment of 2.54 μ_B. A negative Weiss constant, θ = -106.6 K, indicates strong antiferromagnetic correlations. The field-dependent magnetization is presented in Figure 2.3b for Ce(Cu,Al)$_{12}$ at 3 K and shows no saturation up to 9 T.

Figure 2.4a shows the temperature-dependent magnetic susceptibility of Pr(Cu,Al)$_{12}$, measured with the magnetic field of 0.1T parallel to c-axis (H ∥ *c*) and perpendicular to it (H ∥ *ab*). Pr(Cu,Al)$_{12}$, as with the Ce analogue, is paramagnetic down to 3 K for both field orientations. The effective moment determined from Curie Weiss equation for the Pr^{3+} ion (20 - 200 K), was found to be 3.26 μ_B for H ∥ *ab* and 3.78 μ_B for H ∥ *c*. Both values agree well with the calculated effective moment for Pr^{3+} of 3.54 μ_B. The Weiss temperature for Pr(Cu,Al)$_{12}$ was found to be θ = -36.5 K and -49.9 K for H ∥ *ab* and H ∥ *c*, respectively, indicating weakly anisotropic antiferromagnetic interactions. The smaller value of θ in Pr(Cu,Al)$_{12}$, as compared to the Ce analogue, also implies weaker antiferromagnetic coupling. Figure 2.4b shows the field-

dependent magnetization at 3 K in both the H ∥ *ab* and H ∥ *c* directions. A downward curvature is observed at ~ 2 T, more dramatically in H ∥ *ab*, yet no saturation is observed up to 9 T supporting the negative values of the Weiss constant.

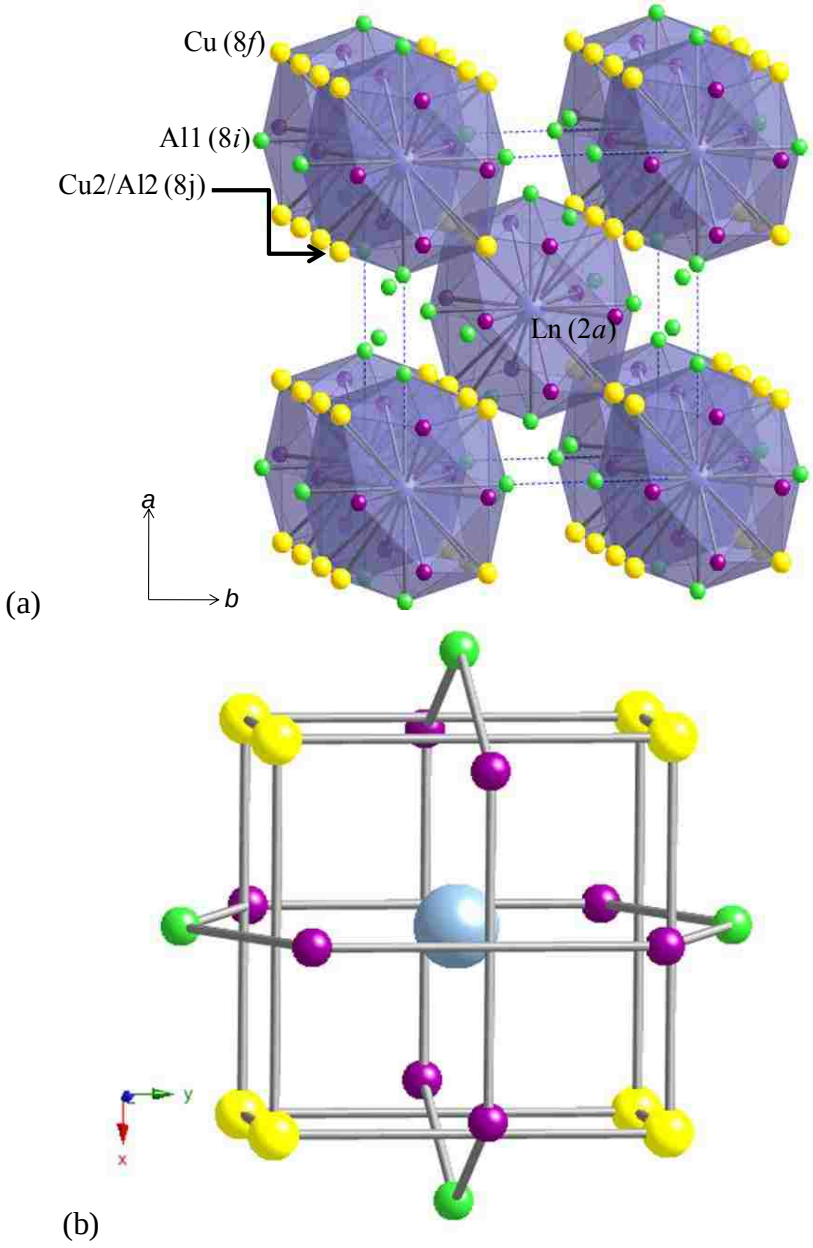

Figure 2.1a and 2.1b The crystal structure of $Ce(Cu,Al)_{12}$ is shown in (a), where the Ce(2*a*) atoms are represented with large metallic blue spheres; Cu (8*f*) atoms are denoted as medium yellow spheres, Al (8*i*) atoms are denoted with small green spheres, and the *M*0 (8*j*) position is denoted with small purple spheres. Dashed lines are used to show the unit cell. The local (b) Ce environment is shown depicting the two perpendicular six member rings with the square prismatic array of Cu atoms.

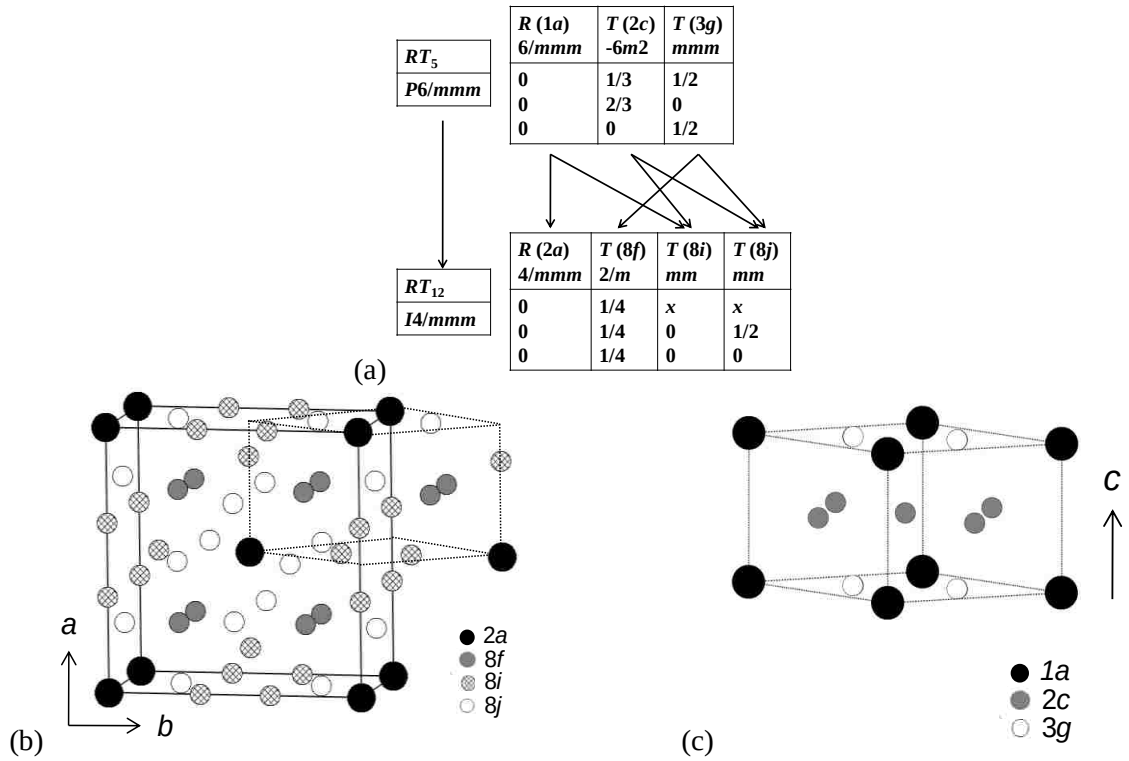

Figure 2.2a, 2.2b, and 2.2c (a) The relationship between RT_{12} and RT_5 as adapted from Ref. 34. The unit cell of (b) RT_{12}, in which the RT_5 unit cell is marked by solid lines. The original (c) unit cell of RT_5 is shown for comparison.

Temperature-dependent magnetic susceptibility of $Sm(Cu,Al)_{12}$ is shown in Figure 2.5a, in an applied field of 0.1 T. $Sm(Cu,Al)_{12}$ has an antiferromagnetic transition at $T_N \sim 5$ K. The effective moment for the Sm^{3+} ion above 10 K, from Curie Weiss equation, was found to be 0.81 μ_B which is close to the calculated effective moment of 0.71 μ_B. The Weiss temperature for $Sm(Cu,Al)_{12}$ was found to be θ = -26.7 K. It is worth noting that the inverse susceptibility remains linear down to 10 K which is unusual for a Sm analogue. Deviations from Curie-Weiss behavior in Sm compounds are generally attributed to Van Vleck paramagnetism. The absence of Van Vleck contribution in $Sm(Cu,Al)_{12}$ is likely due to the spherical environment of Sm^{3+} which minimizes the crystal electric field splitting. Figure 2.5b shows the field-dependent magnetization at 3 K. The magnetization is linear with no sign of saturation in the field measured, up to 9 T, as expected for an antiferromagnetic material.

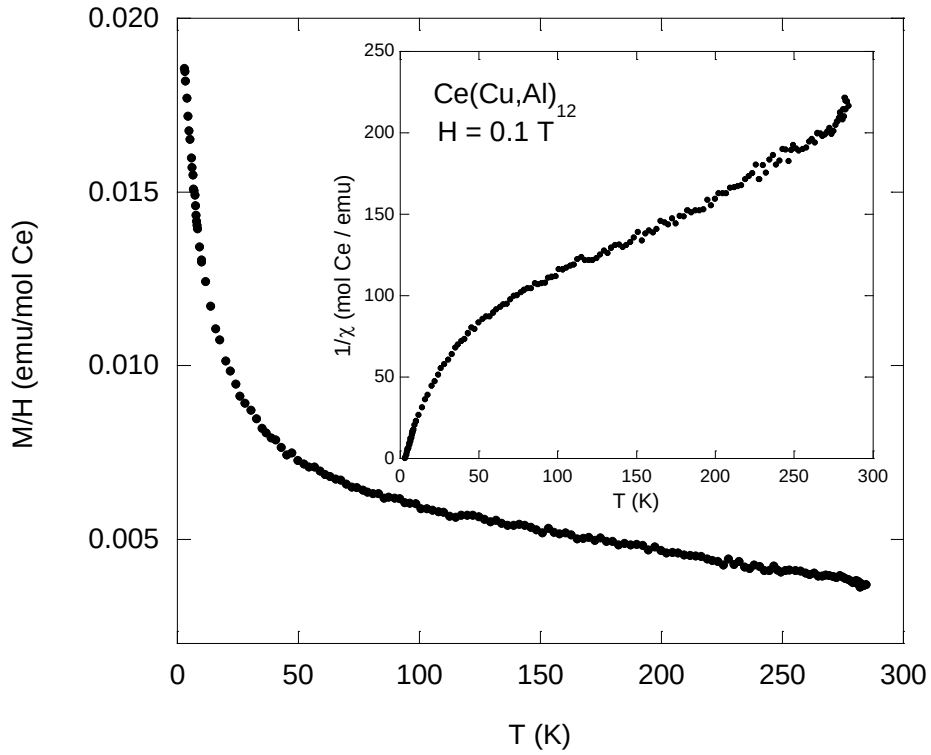

(a)

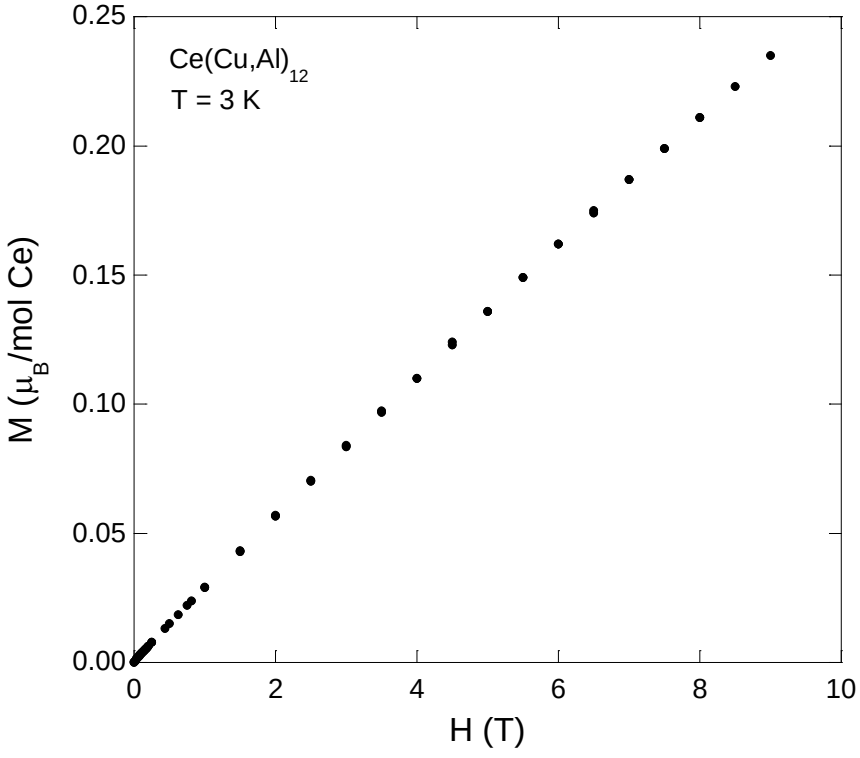

(b)

Figure 2.3a and 2.3b (a) Magnetic susceptibility (emu/mol Ce) of $Ce(Cu,Al)_{12}$ vs temperature. The inset shows the inverse magnetic susceptibility. (b) Magnetization of $Ce(Cu,Al)_{12}$ as a function of field at 3 K.

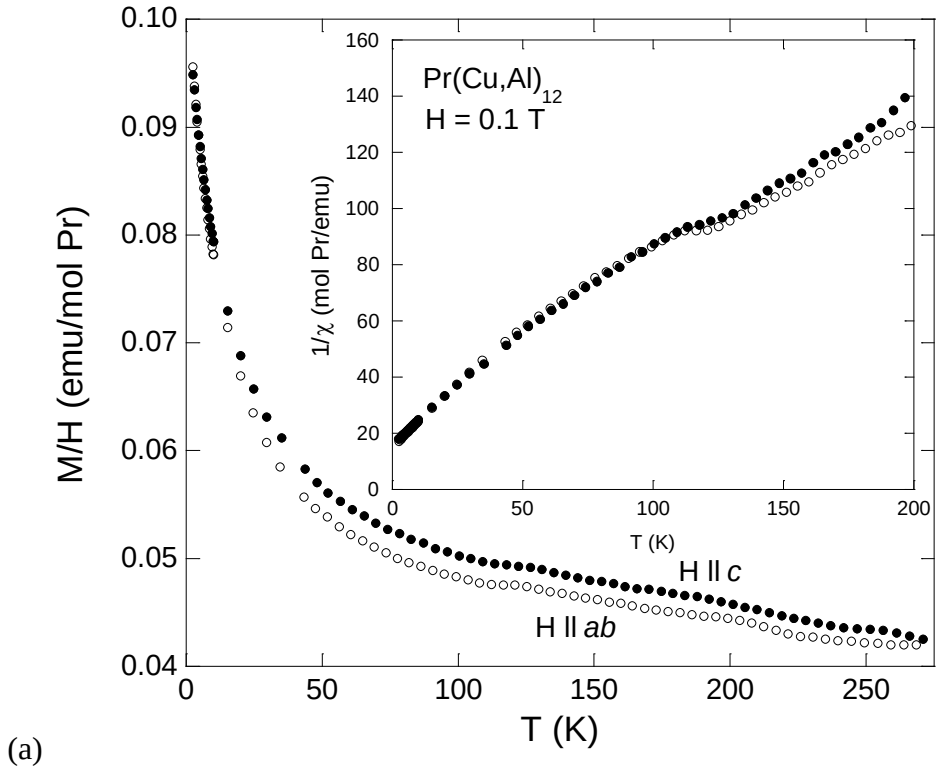

(a)

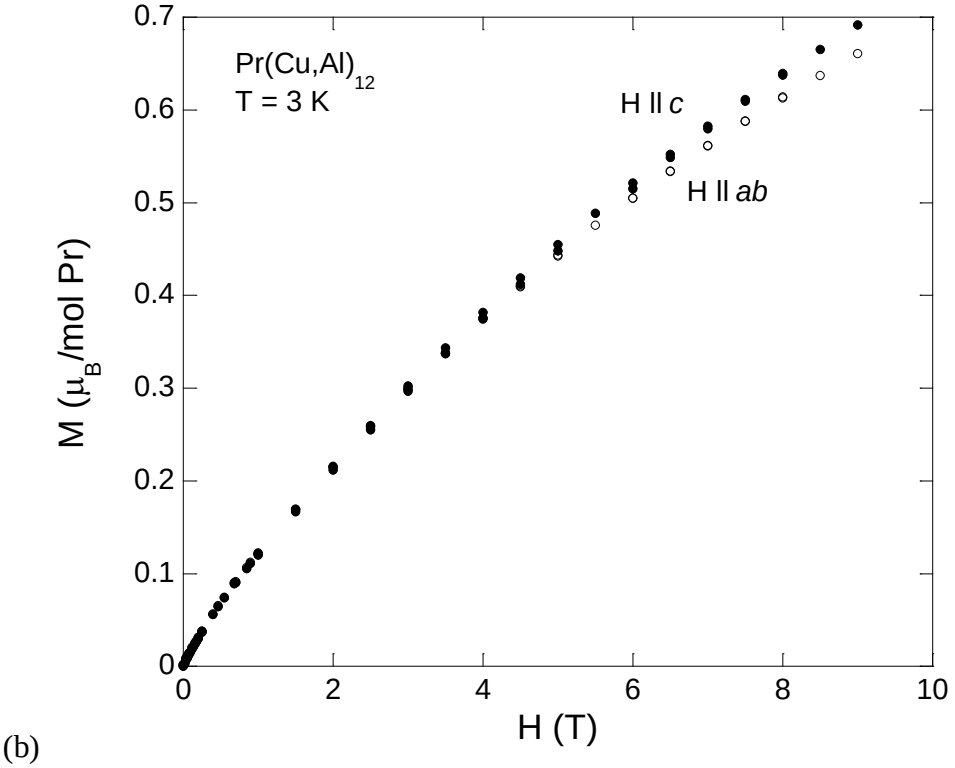

(b)

Figure 2.4a and 2.4b (a) Magnetic susceptibility (emu/mol Pr) of $Pr(Cu,Al)_{12}$ as a function of temperature is shown. The inset shows the inverse magnetic susceptibility. (b) Magnetization of $Pr(Cu,Al)_{12}$ as a function of field.

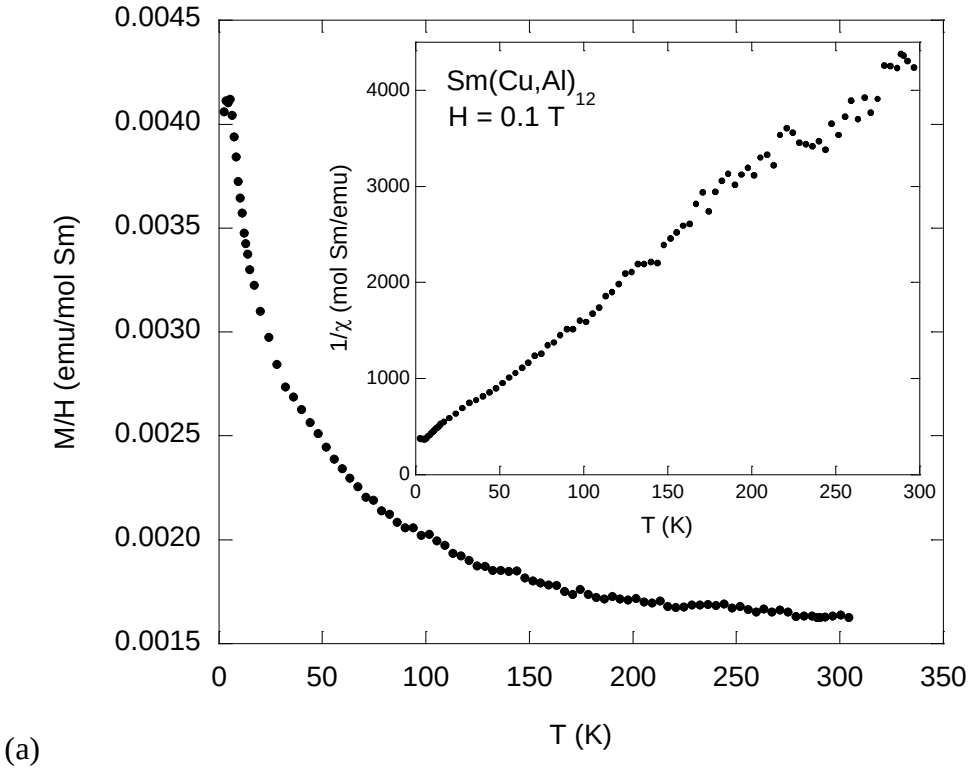

(a)

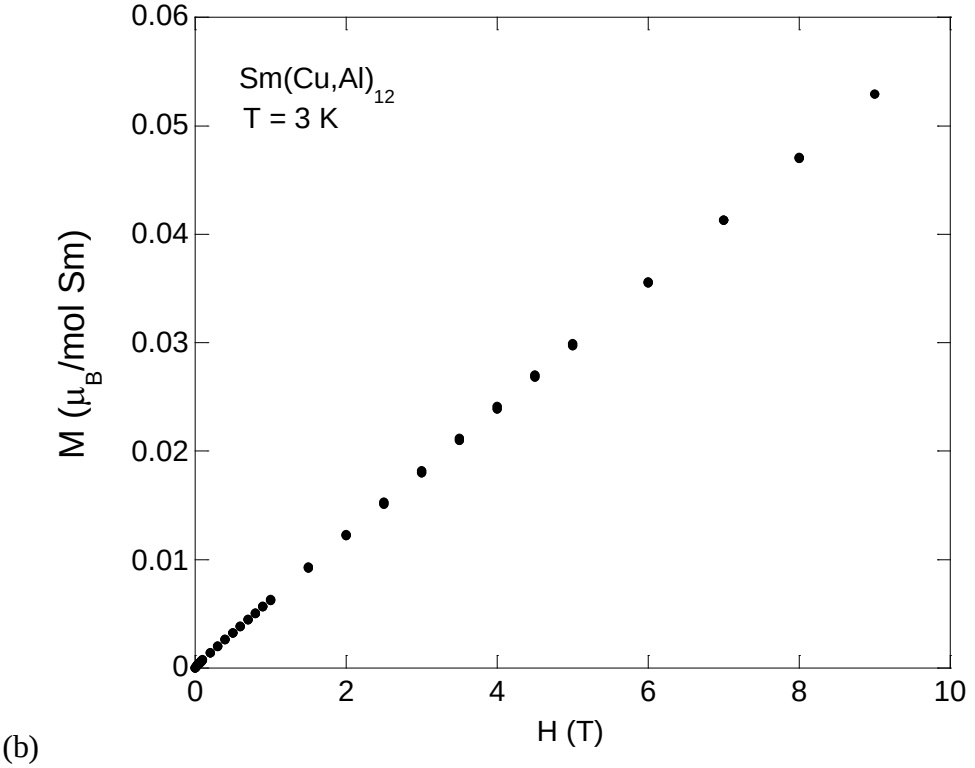

(b)

Figure 2.5a and 2.5b (a) Magnetic susceptibility (emu/mol Sm) of $Sm(Cu,Al)_{12}$ as a function of temperature is shown. The inset shows the inverse magnetic susceptibility. (b) Magnetization of $Sm(Cu,Al)_{12}$ as a function of field.

Table 2.5 Magnetic Properties of $Ln(Cu,Al)_{12}$ (Ln = Y, Ce, Pr, Sm, and Yb)

	C	θ	μ_{calc} (μ_B)	μ_{eff} (μ_B)	Fit range (K)	de Gennes factor $[(g-1)^2J(J+1)]$	Ordering T_N (K)
$Y(Cu,Al)_{12}$	-	-	-	-	-		PPM[a]
$Ce(Cu,Al)_{12}$	0.869	-106.6	2.49	2.63	35-253	0.18	PM[c]
$Pr(Cu,Al)_{12}$	1.786	-49.9	3.54	3.78	20-200	0.80	PM (H ‖ c)
	1.333	-36.4	3.54	3.26	20-200		PM (H ‖ ab)
$Sm(Cu,Al)_{12}$	0.082	-26.7	0.71	0.81	10-300	4.46	AFM[b] 4.8
$Yb(Cu,Al)_{12}$	-	-	-	-	-		PPM

[a]Pauli Paramagnetic. [b]Antiferromagnetic. [c]Paramagnetic.

The Curie Weiss parameters and the observed and calculated effective moment values are summarized in Table 2.5. These findings are in contrast to some previous reports which show $PrCu_4Al_8$ and $SmCu_4Al_8$ to order antiferromagnetically with T_N = ~15 K and ~25 K.[19] Multiple attempts to grow these materials on stoichiometry were unsuccessful. It is still unclear as to the source of the 15 K and 25 K Néel temperature in the previously reported powder samples as the magnetic susceptibility, magnetization, resistivity, magnetoresistance, and heat capacity of single crystals was measured here with magnetic susceptibility for $Pr(Cu,Al)_{12}$ measured H ‖ *c* and H ‖ *ab* showing no ordering down to 3 K and little magnetic anisotropy.

The magnetic susceptibility is positive for both $Y(Cu,Al)_{12}$ and $Yb(Cu,Al)_{12}$ and temperature independent, which we attribute to Pauli paramagnetism (not shown). The magnitude of χ_0=2.9E-3 emu/mol found in $Yb(Cu,Al)_{12}$ is consistent with the Pauli susceptibility, χ_{PPM}=1.092 E-3 emu/mol , determined from the experimental electronic specific heat coefficient γ_0=11 mJ/K^2 mol, using the Wilson ratio $R = (\pi^2 k_B^2/g^2 J(J+1) \mu_B^2) \chi_{PPM}/\gamma_0 = 1$. It is also close to the values of χ_0= 1.79 E-3 emu/mol and 1.36 E-3 emu/mol obtained in the Ce and Sm analogues respectively. The absence of Curie-Weiss behavior in $Yb(Cu,Al)_{12}$ is a strong indication that the valence of Yb is close to 2+, a conclusion also supported by the analysis of the lattice volume evolution across the Ln series. As can be seen in Table 2.1, the $Yb(Cu,Al)_{12}$ analogue shows deviation from a Yb^{3+} ion in the lanthanide contraction indicating at least partial

occupancy of Yb^{2+}. One would expect for a full occupation of Yb^{2+} ion that the volume of the unit cell would be similar to that of a Sm^{3+} ion. With the existence of Yb^{2+} ions in the crystal lattice this effectively acts to magnetically dilute the system such that the Pauli paramagnetism is observed.

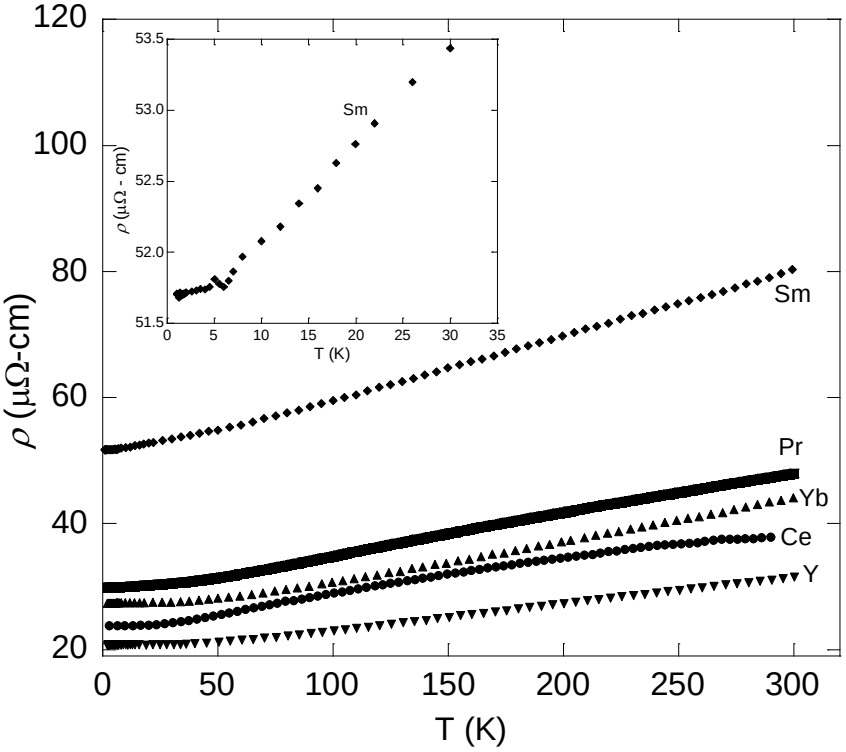

Figure 2.6 Normalized electrical resistivity of $Ln(Cu,Al)_{12}$ (*Ln* = Ce, Pr, Sm, Yb, and Y) as a function of temperature is shown. Inset shows blow up of low temperature resistivity of $Sm(Cu,Al)_{12}$.

The electrical resistivity as a function of temperature of single crystals of $Ln(Cu,Al)_{12}$ (*Ln* = Ce, Pr, Sm, Yb, and Y) is shown in Figure 2.6. These compounds show metallic behavior with residual resistivity ratio (RRR) values of 3.0, 1.6, 1.6, 2.1, and 1.5 for Ce, Pr, Sm, Yb, and Y analogues, respectively. No anomalous behavior is observed for Pr, Yb, and Y. $Ce(Cu,Al)_{12}$ shows deviations from an expected linear resistivity which may be attributed to some Kondo like behavior from the screening of conduction electrons. Figure 6 inset is a blow up of the low temperature data for $Sm(Cu.Al)_{12}$. A small kink is observed at ~ 5 K, coinciding with the AFM

transition at ~ 5 K observed in the magnetic susceptibility data. The resistivity saturates below 5 K with no indication of a reduced spin disorder scattering.

Heat capacity data was collected on *Ln*$(Cu,Al)_{12}$ where *Ln* = Y, Ce, Pr, Sm, and Yb. The $Y(Cu,Al)_{12}$ analogue was used to subtract the phonon contribution to heat capacity in the Ce, Pr, and Sm compounds. Attempts were made to grow the La derivative, but all synthetic attempts result in the formation of $La(Cu,Al)_{13}$, a cubic phase with the $NaZn_{13}$ structure. Figure 2.7a and 2.7b shows the plots of C_p vs T and C_p/T vs. T. In the latter case the data provided have had the phonon contribution to heat capacity, as determined by $Y(Cu,Al)_{12}$, subtracted.

It is clear in Figure 2.7a and 2.7b, $Ce(Cu,Al)_{12}$ shows a transition at ~ 2 K. Magnetic susceptibility data was collected down to 3 K. In consideration of the negative θ_W value, it is thought that the transition in heat capacity data is an antiferromagnetic ordering at ~ 2 K. With the absence of antiferromagnetic ordering in the magnetic susceptibility data and the absence of an anomaly in heat capacity, the previous report of T_N = 5.8 K is not supported in single crystal physical property measurements.[21] In addition, analysis of the low temperature portion of the heat capacity shows $Ce(Cu,Al)_{12}$ is a heavy fermion, with a Sommerfeld coefficient , obtained from a linear fit of C_p/T vs T^2 for T < 1 K, of $\gamma \sim 390$ mJ/K^2 mol Ce, corresponding to a mass enhancement of 39 compared to the non-magnetic Yb analog. This is also supported by the fact that the entropy at 2 K is only 0.35 R ln2, the full magnetic entropy S_{mag}= R ln2 being recovered only at 20K. The missing entropy is likely the result of the Kondo screening of the Ce3+ moments at low temperatures. The temperature dependence of the resistivity also suggests the presence of Kondo screening (see Fig. 2.6). The partial recovery of the magnetic entropy at 2 K reinforces that the large γ value retrieved from the low temperature fit is a signature of a heavy fermion, which is in agreement with earlier reports.[21,22,35]

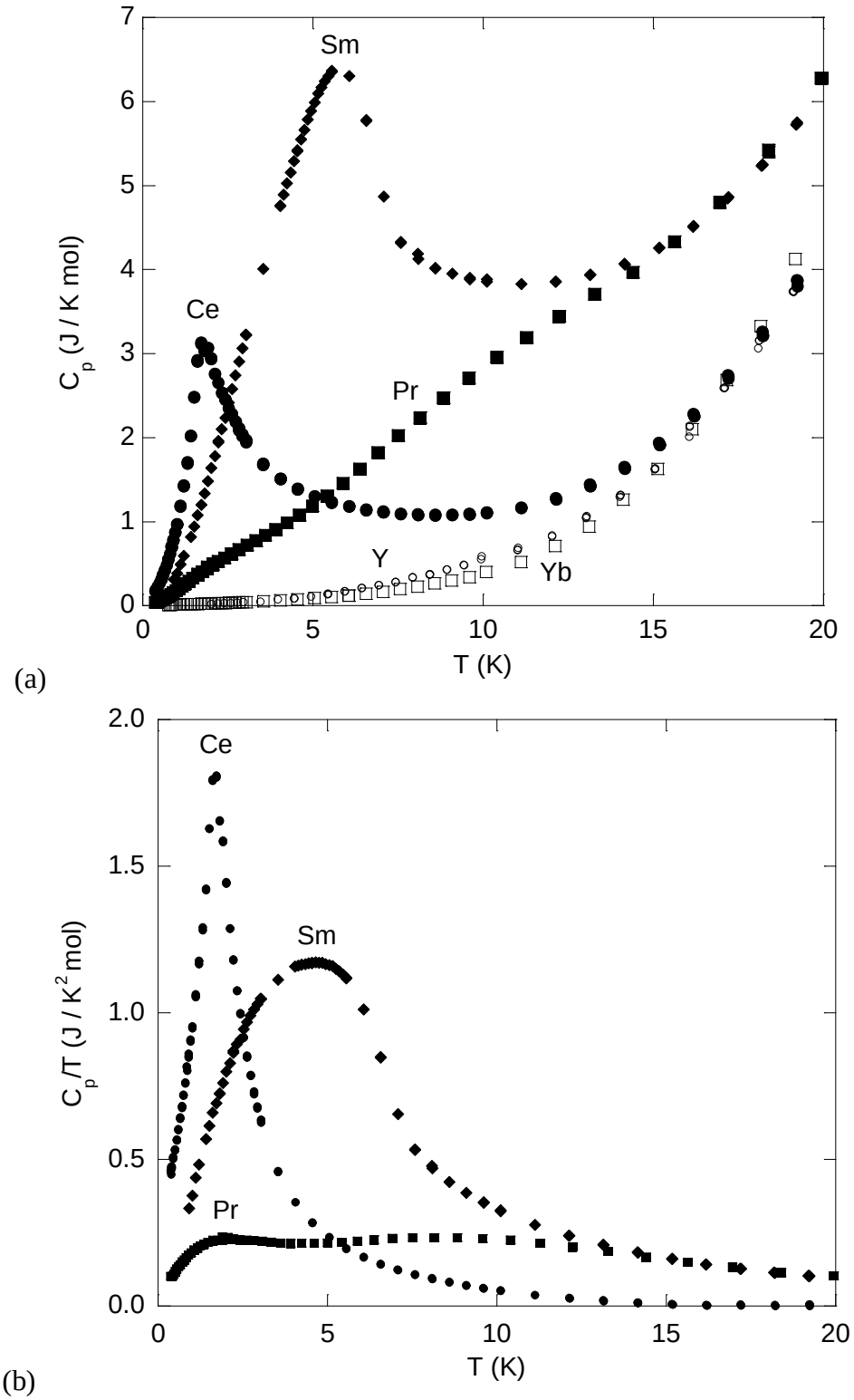

Figure 2.7a and 2.7b (a) Heat capacity vs temperature for $Ln(Cu,Al)_{12}$ (*Ln* = Y, Ce, Pr, Sm, and Yb. Inset of (a) shows a zoom of the low temperature heat capacity. (b) Electronic heat capacity C_p/T as a function of temperature.

Heat capacity data for $Pr(Cu,Al)_{12}$ and $Sm(Cu,Al)_{12}$ is also presented in Figures 2.7a and 2.7b. $Pr(Cu,Al)_{12}$ shows two broad peaks in the low temperature range, T_{anom} ~ 1.9 K and 8.8 K A two level Schottky formula does not give a satisfactory fit of the broad peak at 8.8 K. Nevertheless, this feature might correspond to a multi-level Schottky anomaly, since there is no indication of magnetic ordering in the susceptibility data at this temperature. For second peak at the lower temperature, we cannot rule out the possibility of an antiferromagnetic transition, since the susceptibility has only been measured down to 3 K. From the fit of the linear low temperature regime of $Pr(Cu,Al)_{12}$ heat capacity data, C_p/T vs T^2 for $T < 0.7$ K, a rather large electronic specific heat coefficient is obtained, γ = ~80 mJ/K^2 mol Pr. This value shows a mass enhancement of a factor of 8 as compared to the non-magnetic Yb analogue. For the Sm analogue, a broad peak can be seen in Figures 2.7a and 2.7b at ~ 5 K, coinciding with the antiferromagnetic transition observed in the magnetic susceptibility data. In addition, fits of the low temperature regime of C_p yields γ ~ 130 mJ/K^2 mol Sm. Heat capacity data was collected only down to 0.9 K in this compound. The entropy recovered at 5 K is R ln2. It remains unclear if this represents the full magnetic entropy, as one would expect R ln(2J + 1)= R Ln6 for Sm^{3+} in the absence of crystal field splitting. Based on the spherical environment and the absence of Van Vleck interactions, it could be asserted that the splitting is negligible and the entropy does follow R ln(2J + 1). Following this assumption, only 39% of the expected full magnetic entropy (R ln6) is recovered at the transition (with C/T integrated from 1 K to 7 K), possibly due to the Kondo screening. It is unclear at this time if $Sm(Cu,Al)_{12}$ is a heavy electron system or the Sommerfeld coefficient is large due to the transition.

Overall, the Curie-Weiss temperatures obey the expected scaling as a function of the de Gennes factor $(g - 1)^2 J(J + 1)$ for $Ln(Cu,Ga)_{12}$ analogues, Figure 2.8. In contrast, $Ln(Cu,Al)_{12}$

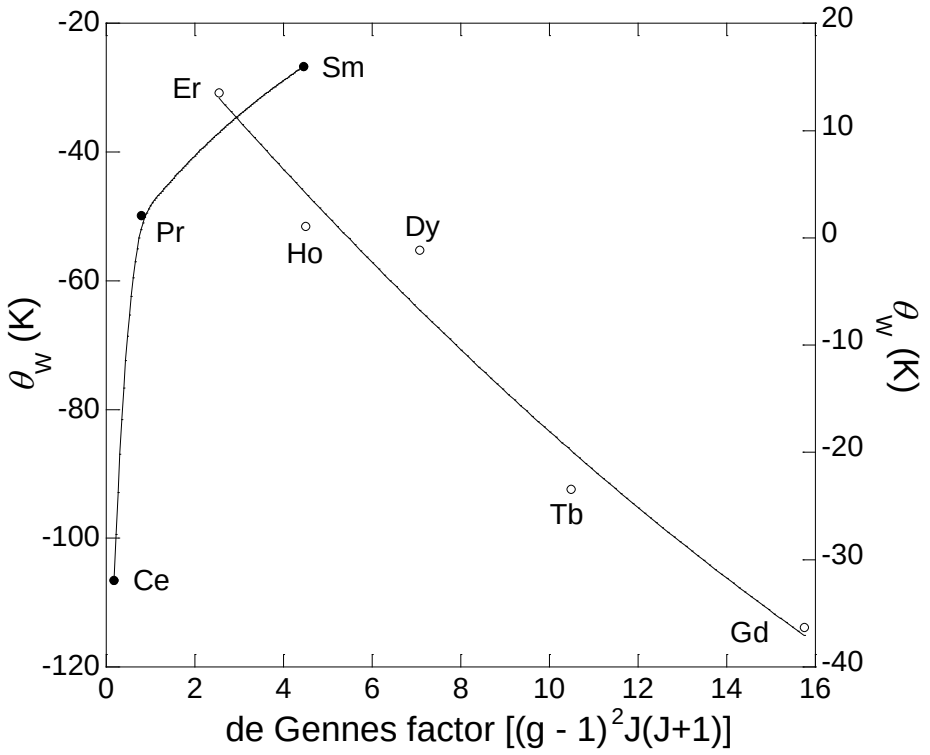

Figure 2.8 Curie-Weiss temperature (K) as a function of de Gennes factor. Closed circles correspond to *Ln*(Cu,Al)$_{12}$ and open circles to *Ln*(Cu,Ga)$_{12}$.

doesn't scale to de Gennes factor, attributed to frustration. The Ce analogue shows large a Weiss temperature of -106.6 K, whereas the T_N is only 2 K, the large difference between the two may be indicative of magnetic frustration or may be attributed to the Kondo effect. It is noteworthy that the two systems, *Ln*(Cu,Ga)$_{12}$ and *Ln*(Cu,Al)$_{12}$, despite being isoelectronic, Al and Ga being in the same column of the periodic table, have so widely different magnetic properties.

In conclusion, we have reported structural and physical properties of single crystals of *Ln*(Cu,Al)$_{12}$ (*Ln* = Y, Ce, Pr, Sm, and Yb) adopting the $ThMn_{12}$ structure-type. Crystallographic refinements of single crystal X-ray diffraction data of *Ln*(Cu,Al)$_{12}$ (*Ln* = Y, Ce, Pr, Sm, and Yb) suggest that 8*j* site is occupied statistically by Cu and Al. Sm(Cu,Al)$_{12}$ exhibits an antiferromagnetic transition at 5 K. In addition, Ce(Cu,Al)$_{12}$ shows heavy fermion characteristics, with Pr(Cu,Al)$_{12}$ and Sm(Cu,Al)$_{12}$ showing enhanced mass behavior.

2.4 References

(1) Florio, J.V., Rundle, R.E., and Snow, A.I., Compounds of thorium with transition metals. The thorium-manganese system. *Acta Crystallogr.* **1952,** *5*, 449-457.

(2) Gladishevskii, E.I., Kripyakevich, P.I., Teslvuk, M.Y., Zarechnyuk, O.S., and Kuz'ma, Y.B., Crystal structure of some intermetallic compounds. *Kristallografiya* **1961,** *6*, 267-268.

(3) Christides, C., Kostikas, A., Zouganelis, G., Psyharis, V., Kou, X.C., and Grossinger, R., Spin-glass-like magnetic properties for rare earth (*R*)-iron-molybdenum ($RFe_{10}Mo_2$) compounds (*R* = yttrium or lutetium) with the $ThMn_{12}$-type structure. *Phys. Rev. B* **1993,** *47*, 11220-11229.

(4) Coldea, M., Neumann, M., Lutkehoff, S., Mahl, S., and Coldea, R., Spin and valence fluctuations in $CeMn_4Al_8$ and $CeMn_6Al_6$. *J. Alloys Compd.* **1998,** *278*, 72-79.

(5) Dmitriev, V.M., Stepien-Damm, J., Suski, W., Talik, E., and Prentslau, N.N., Possible coexistence of antiferromagnetism, spin-glass, and superconductivity in $ScFe_4Al_8$ and YFe_4Al_8 single crystals. *Phys. Status Solidi C* **2004,** *1*, 1824-1827.

(6) Dmitriev, V.M., Terekhov, A.V., Suski, W., Ishchenko, L.A., Cwik, J., Palewski, T., Kotur, B.Y., and Talik, E., Negative magnetoresistivity of the RM_4Al_8 (*R* = Sc, Y, Ce, Yb, Lu; M=Cr, Mn, Fe) ternaries with the $ThMn_{12}$-type crystal structure. *J. Alloys Compd.* **2008,** *452*, 217-224.

(7) Gottwick, U., Held, R., Sparn, G., Steglich, F., Vey, K., Assmus, W., Rietschel, H., Stewart, G.R., and Giorgi, A.L., Seebeck coefficient of heavy fermion compounds. *J. Magn. Magn. Mater.* **1987,** *63-64*, 341-343.

(8) Kotur, B.Y., Palasyuk, A.M., Bauer, E., Michor, H., and Hilscher, G., Uncommon conductivity of *R*-Mn-Al (*R* = Gd, Tb) ternary compounds. *J. Phys. Condens. Mat.* **2001,** *13*, 9421-9431.

(9) Leavey, C.J., Rainford, B.D., Stewart, J.R., and Adroja, D.T., Spin gaps in pseudo-one-dimensional RMn_4Al_8 compounds (*R* = Y, Ce and La). *J. Magn. Magn. Mater.* **2007,** *310*, 1041-1043.

(10) Moze, O., Caciuffo, R., Li, H.S., Hu, B.P., Coey, J.M.D., Osborn, R., and Taylor, A.D., Observation of intermultiplet transitions in samarium-iron-titanium ($SmFe_{11}Ti$) by inelastic magnetic neutron scattering. *Phys. Rev. B* **1990,** *42*, 1940-1943.

(11) Paci, B., Caciuffo, R., Amoretti, G., Moze, O., Buschow, K.H.J., and Murani, A.P., Neutron scattering determination of the crystal field parameters in $ErCu_4Al_8$ and $ErFe_4Al_8$ intermetallics. *Solid State Commun.* **1995,** *94*, 489-493.

(12) Yamasaki, T., Matsui, K., Nakamura, H., and Shiga, M., Nearly antiferromagnetic metal with linear spin chains: $LaMn_4Al_8$. *Solid State Commun.* **2001,** *119*, 415-418.

(13) Gladyshevskii, E.I., Kripyakevich, P.I., Cherkashin, E.E., Zarechnyuk, O.S., Zalutskii, I.I., and Evdokimenko, V.I., Crystal structure of the intermetallic compounds of the rare-earth elements. *Redkozem. Elementy* **1963,** 67.

(14) Landelli, A. and Palenzona, A., Atomic size of rare earths in intermetallic compounds. MX compounds of CsCl type. *J. Less-Common Met.* **1965,** *9*, 1-6.

(15) Suski, W., Karl A. Gschneidner, Jr., and LeRoy, E., "Chapter 149 The ThMn12-Type compounds of rare earths and actinides: Structure, magnetic and related properties." Elsevier, Amsterdam, 1996.

(16) Wang, F.E. and Gilfrich, J.V., The crystal structures of $LuMn_5$ and the RMn_{12} compounds (where *R* is Gd, Tb, Dy, Ho, Er, and Tm). *Acta Crystallogr.* **1966,** *21*, 476-481.

(17) Hagmusa, I.H., Klaasse, J.C.P., Bruck, E., de Boer, F.R., and Buschow, K.H.J., A specific-heat study of RCr_4Al_8 compounds (*R* = La, Ce, Pr, Gd, Er). *J. Alloys Compd.* **2001,** *314*, 37-41.

(18) Baio, G., Moze, O., Amoretti, G., Sonntag, R., Stusser, N., and Buschow, K.H.J., Neutron diffraction study of RMn_4Al_8 (*R* = Nd, Dy, Ho, Er), $ErCr_4Al_8$, and $ErCu_4Al_8$. *Z. Phys. B - Con. Mat.* **1997,** *102*, 449-453.

(19) Felner, I. and Nowik, I., Magnetism and hyperfine interactions of iron-57, europium-151, gadolinium-155, dysprosium-161, erbium-166, and ytterbium-170 in RM_4Al_8 compounds, (*R* = rare earth or yttrium, M = chromium, manganese, iron, copper). *J. Phys. Chem. Solids* **1979,** *40*, 1035-1044.

(20) Rauchschwalbe, U., Gottwick, U., Ahlheim, U., Mayer, H.M., and Steglich, F., Investigation of new lanthanum-, cerium- and uranium-based ternary intermetallics. *J. Less-Common Met.* **1985,** *111*, 265-275.

(21) Ido, H., Nishioka, T., and Kontani, M., Magnetic properties of $ThMn_{12}$-type $CeCu_4Al_8$ and related Ce-compounds: Heat-treatment effects. *J. Magn. Magn. Mater.* **1998,** *177-181*, 385-386.

(22) Kontani, M., Hamada, M., Mizukoshi, T., and Mukai, H., NMR/NQR and specific heat studies on the $ThMn_{12}$-type $CeCu_{4+x}Al_{8-x}$ system. *Physica B* **2000,** *284-288*, 1267-1268.

(23) Oe, K., Kobayashi, R., Nishioka, T., Kato, H., Matsumura, M., and Kodama, K., Single crystal growth and low temperature magnetic properties of the Ce-Cu-Al ternary system *J. Phys.: Conf. Ser.* **2009,** *150*, 042146.

(24) Lue, C.S., Su, T.H., and Lai, W.J., Antiferromagnetism in the new $ThMn_{12}$-type compound $HoCu_4Al_8$. *J. Magn. Magn. Mater.* **2006,** *304*, e445-e447.

(25) Buschow, K.H.J., Permanent magnet materials based on tetragonal rare earth compounds of the type $RFe_{12-x}M_x$. *J. Magn. Magn. Mater.* **1991,** *100*, 79-89.

(26) Caciuffo, R., Amoretti, G., Buschow, K.H.J., Moze, O., Murani, A.P., and Paci, B., Neutron spectroscopy studies of the crystal-field interaction in RET_4Al_8 compounds (*RE* = Tb, Ho, or Er; T = Mn, Fe or Cu). *J. Phys.: Condens. Matter* **1995,** *7*, 7981-7989.

(27) De Boer, F.R., Ying-Kai, H., De Mooij, D.B., and Buschow, K.H.J., Magnetic properties of a series of novel ternary intermetallics ($RFe_{10}V_2$). *J. Less-Common Met.* **1987,** *135*, 199-204.

(28) De Mooij, D.B. and Buschow, K.H.J., Some novel ternary thorium-manganese ($ThMn_{12}$)-type compounds. *J. Less-Common Met.* **1988,** *136*, 207-215.

(29) Sheldrick, G.M., A short history of shelX. *Acta Crystallogr. A* **2008,** *A64*, 112-122.

(30) Haucke, W., The crystal structure of $CaZn_5$ and $CaCu_5$. *Z. Anorg. Allg. Chem.* **1940,** *244*, 17-22.

(31) Hu, B.P., Li, H.S., and Coey, J.M.D., Relationship between thorium-manganese ($ThMn_{12}$) and thorium-nickel (Th_2Ni_{17}) structure types in the yttrium-iron-titanium ($YFe_{11-x}Ti_x$) alloy series. *J. Appl. Phys.* **1990,** *67*, 4838-4840.

(32) Mason, J.T., Harsha, K.S., and Chiotti, P., Crystal structure of a samarium-zinc compound with approximate composition $SmZn_{11}$. *Acta Crystallogr. B* **1970,** *26*, 356-361.

(33) Bessais, L. and Djega-Mariadassou, C., Structure and magnetic properties of nanocrystalline $Sm(Fe_{1-x}Co_x)_{11}Ti$ ($x \leq 2$). *Phys. Rev. B* **2001,** *63*, 054412.

(34) Yang, Y., Sun, H., Kong, L., Yang, J., Ding, Y., Zhang, B., Ye, C., Jin, L., and Zhou, H., Neutron diffraction study of yttrium-titanium-iron ($Y(Ti,Fe)_{12}$). *J. Appl. Phys.* **1988,** *64*, 5968-5970.

(35) Rauchschwalbe, U., Gottwick, U., Ahlheim, U., Mayer, H.M., and Steglich, F., Investigation of new lanthanum-, cerium- and uranium-based ternary intermetallics. *J. Less-Common Met.* **1985,** *111*, 265-275.

CHAPTER 3. CRYSTAL GROWTH, STRUCTURE, AND PHYSICAL PROPERTIES OF *Ln*(Ag,Al,Si)$_2$ (*Ln* = Ce and Gd)[1]

3.1 Introduction

Complex, competing, and emergent phenomena can often be found in intermetallic compounds of Ce and Yb such as superconductivity, heavy fermion behavior, and mixed valency.[2-7] The vast majority of Ce containing compounds exists as the Ce^{3+} ion ordering antiferromagnetically at sufficiently low temperatures. Rarer are ferromagnetic and ferrimagnetic ordering Ce intermetallic compounds such as $CeAl_{1.02}Si_{0.98}$, $CeAu_{0.28}Ge_{1.72}$, $CeAg_{1-x}Ni_xSb_2$, Ce_5Pb_3O, and $CeAgAl_3$.[8-12]

Lanthanide di-silicides and di-germanides binary compounds and lanthanide pseudo-binary aluminum or transition metal di-silicides and di-germanides that adopt the polar intermetallic α - $ThSi_2$ structure type have been well studied. The α - $ThSi_2$ structure type has a narrow width of formation with Al substitution of x = 0.9 – 1.2, higher Al content shifts phase stability to the AlB_2 structure type.[13-15] Ce derivatives of the α - $ThSi_2$ structure type show a range of transport behaviors: metallic resistivity for $CeAl_{1.02}Si_{0.98}$, metallic resistivity with an upturn at ~ 30 K for $CeAl_{1.2}Si_{0.8}$, and $CeSi_{2-x}$ where the electrical transport is sensitive to the Si deficiency.[8,9,13,15-18] This structure type has garnered much interest due to the dense Kondo behavior observed in $CeSi_{2-x}$.[17,18] In most cases the $CeAl_xSi_{2-x}$ derivatives are ferromagnetic with some derivatives eliciting an enhanced Sommerfeld parameter.[9,18] The magnetic and transport properties of $CeSi_2$ and its related alumosilicide phases are extremely sensitive to composition as $CeSi_{2-x}$ for x > 1.85 is nonmagnetic down to 0.1 K and elicits heavy fermion behavior, but for

---

Reprinted by permission of Journal of Physics: Condensed Matter: Drake, B.L., Kangas, M.J., Capan, C., Haldolaarachchige, N., Xiong, Y.M., Adams, P.W., Young, D.P., and Chan, J.Y., Crystal growth, structure, and physical properties of Ln(Ag,Al,Si)2 (Ln = Ce and Gd). J Phys. Condens. Mat. 2010, 22, 426002.

$x < 1.85$ the compound orders ferromagnetically at 10 K.[19,20] Ferromagnetic order appears to be common in the α - $ThSi_2$ structure, both $CeGe_2$ and $CeSi_2$ become ferromagnetic for a variety of dopants.[13,21-24]

While working on compounds in the *Ln*-Ag-Al phase space (*Ln* = Ce and Gd) and searching for highly disordered Ag/Al compounds, we have grown pseudo-binaries of the α - $ThSi_2$ structure type. It was quickly understood that small amounts of silicon were contaminating the reactions from the silica wool used as a centrifuge filtering medium. Experimental conditions were found in which Si could be introduced in a controlled manner, as Ag substitution into the alumosilicide has not been previously observed. In order to understand the sensitivity of this system to its elemental components, it was of interest how Ag substitution would impact the magnetic and transport properties of a $4f^1$ and $4f^7$ system. Herein, we report the structural, magnetic, and transport properties for CeM_2 and GdM_2 (M = Ag, Al, and Si).

3.2 Experimental

3.2.1 Synthesis

Single crystals of *Ln*$(Ag,Al,Si)_2$ (*Ln* = Ce and Gd) were grown in the presence of excess Al flux.[25] *Ln* (3N, chunks, Alfa Aesar), Ag (3N, powder, Alfa Aesar), and Al (5N, pellets, Alfa Aesar) and Si (5N, powder, Alfa Aesar) were used as received and loaded into an alumina crucible with a reaction ratio of 1:1:10:1.2 for *Ln*:Ag:Al:Si respectively. Rare earth elements are stored in vacuum desiccators to prevent oxidation (0.1 mmHg). The crucibles were placed into a fused silica tube and the contents were evacuated (0.05 – 0.07 mmHg) and sealed. The charged vessel was loaded into a furnace and heated to a dwell temperature of 1200 °C for 72 h at 250 °C/h. Samples were slowly cooled to 1000 °C with a rate of 2 °C/h at which the cooling rate was doubled to 4 °C/h to a dwell temperature of 720 °C upon which the samples were centrifuged to

separate crystals from the Al flux. Final dwell times were varied from hours to days, and no correlation of crystal size and dwell time could be made. In addition, nominal starting concentrations of 1:1:10:1.2 remain constant. In all growths, silver metallic crystals were retrieved via etching in NaOH (1-3 M) until excess aluminum was removed and subsequently cleaned with 10% HNO_3, retrieving flux-free single crystals which were observed to be air stable. Crystal morphology is best described as more block-like for Ce with Gd forming pristine thin blades as can be seen in Figure 3.1. It was found that statistical disorder is observed on the 8*e* site for Ag, Al, and Si. The degree of statistical disorder does not appear to depend on the reaction ratio or dwell times as several experiments were attempted with differing amounts of Ag, all resulting ~5 % substitution onto the 8*e* position.

3.2.2 X-ray Diffraction and Elemental Analysis

Crystals of CeM_2 and GdM_2 were cut to suitable sizes for data collection ($\leq$ 0.05 mm x 0.05 mm x 0.05 mm) and mounted onto a glass fiber using epoxy. They were then positioned onto the goniometer of a Nonius KappaCCD diffractometer equipped with Mo K_α radiation (λ = 0.71073 Å). Further crystallographic parameters for $Ln(Ag,Al,Si)_2$ (Ln = Ce and Gd) and are provided in Table 3.1. Direct methods were used to solve the structure. SIR97 was employed to give a starting model and SHELXL97 used to refine the structural model and data were corrected with extinction coefficients and refined with anisotropic displacement parameters.[26,27] Refinement assuming a full Si occupancy ($LnSi_2$) led to a structural model with large atomic displacement parameters associated with the Si position. Selected interatomic distances are presented in Table 3.2, and atomic positions and displacement are provided in Table 3.3. These tables reflect the structural model obtained after mixing the occupancy of the 8*e* position. To determine the composition of CeM_2 and GdM_2, elemental analysis was performed using a

Hitachi S-3600N Variable Pressure scanning electron microscope equipped with an energy dispersive spectrometer. The accelerating voltage was 15 kV with beam to sample distance of 15 mm. An average of 15-20 scans was performed on each single crystal. The results are provided in Table 3.4. Inspection of single crystals using a scanning electron microscope revealed the crystals contained *Ln*, Ag, Al, and Si. Subsequently, the single crystal models were checked for mixed occupancy of Ag, Al, and Si on the 8*e* position in ratios similar to those found via SEM. Atomic displacement parameters behavior improved and the structural model led to convergence with very small final difference residual peaks.

Table 3.1 Crystallographic Parameters for $Ln(Ag,Al,Si)_2$ (*Ln* = Ce and Gd)

Formula	$Ce(Ag,Al,Si)_2$	$Gd(Ag,Al,Si)_2$
a (Å)	4.2450(15)	4.1230(15)
c (Å)	14.440(2)	14.401(5)
V (Å^3)	260.21(13)	244.80(15)
Z	4	4
Crystal system	Tetragonal	Tetragonal
Space group	$I4_1/amd$	$I4_1/amd$
θ range (°)	5.01-29.90	5.14-29.83
μ (mm^{-1})	19.001	28.704
Data collection		
Measured reflections	301	272
Independent reflections	119	114
Reflections with $I>2\sigma(I)$	108	104
R_{int}	0.0281	0.0374
h	-5 – 5	-5 – 5
k	-4 – 4	-4 – 4
l	-18 – 19	-20– 15
Refinement		
[a]$R_1[F^2>2\sigma(F^2)]$	0.0312	0.0187
[b]$wR_2(F^2)$	0.0755	0.0442
Reflections	119	114
Parameters	8	8
GOOF	1.388	1.106
Extinction	0.097(13)	0.045(4)
$\Delta\rho_{max}$ (eÅ^{-3})	2.022	2.360
$\Delta\rho_{min}$ (eÅ^{-3})	-2.340	-1.017

[a]$R_1=\sum\| |F_o| - |F_c| \| / \sum |F_o|$, [b]$wR_2 = [\sum[w(F_o^2 - F_c^2)]/\sum[w(F_o^2)^2]]^{1/2}$
$w = 1/[\sigma^2(F_o^2)+(0.0351P)^2 + 0.8966P]$ for Ce
$w = 1/[\sigma^2(F_o^2)+(0.0197P)^2 + 0.0000P]$ for Gd

For all growths, ground single crystal samples were characterized by powder X-ray diffraction to confirm phase purity and sample homogeneity with a Bruker AXS D8 Advance Diffractometer. CeM_2 and GdM_2 (M = Ag, Al, and Si) were determined to be phase pure with no visible evidence of inclusions by powder X-ray diffraction.

Table 3.2 Selected Interatomic Distances for *Ln*$(Ag,Al,Si)_2$ (*Ln* = Ce and Gd) (Å)

		Ce$(Ag,Al,Si)_2$	Gd$(Ag,Al,Si)_2$
Ln – *Ln* (Å)	(x4)	4.1878(6)	4.1230(15)
	(x4)	4.2450(15)	4.1487(11)
Ln – *M* (Å)	(x4)	3.208(3)	3.1689(18)
	(x8)	3.2344(16)	3.1502(14)
M – *M* (Å)	(x1)	2.409(7)	2.387(6)
	(x2)	2.439(4)	2.392(3)

M = Ag, Al, and Si

Table 3.3 Atomic Positions and Thermal Parameters for *Ln*$(Ag,Al,Si)_2$ (*Ln* = Ce and Gd)

Atom	Wyckoff position	x	y	z	$U_{eq}(Å^2)$[a]
Ce	4*a*	0	1/4	3/8	0.0111(7)
M[b]	8*e*	0	1/4	0.7916(2)	0.0168(8)
Gd	4*a*	0	1/4	3/8	0.0083(4)
M	8*e*	0	1/4	0.7921(2)	0.0156(5)

[a]U_{eq} is defined as 1/3 of the trace of the orthogonalized U_{ij} tensor.
[b]M = Ag, Al, and Si (relative concentrations listed in Table 4)

In all cases, a crystal was selected and a fragment cleaved for single crystal X-ray diffraction experiments. SEM data was then collected on the remaining single crystal. This crystal was then cleaned using acetone and hexanes to remove any carbon tape residue. Physical property measurements (heat capacity, magnetization, and resistivity) were done on the same crystal.

3.2.3 Physical Properties

Magnetic data was collected using a Quantum Design Physical Property Measurement System (PPMS). The temperature-dependent susceptibility data was measured under zero-field

cooled (ZFC) conditions between 3 K to 285 K for CeM_2 and GdM_2 under an applied field of 0.1 T and 0.05 T for CeM_2 and 0.1 T for GdM_2. Field-dependent magnetization data were measured at 3 K with applied fields up to 9 T. The electrical resistivity measurements were measured on single crystals by the standard four-probe AC technique. The heat capacity was measured by the standard adiabatic heat pulse relaxation technique down to 0.4 K.

Table 3.4 Composition as Obtained from Energy Dispersive X-ray Spectroscopy

	$Ce(Ag,Al,Si)_2$	$Gd(Ag,Al,Si)_2$
Ln[a]	1.00(3)	1.00(6)
Ag	0.15(1)	0.09(1)
Al	0.85(3)	0.81(4)
Si	1.02(2)	1.05(3)
Ln:M[b]	1:2.02(4)	1:1.95(6)

[a] Composition is normalized to lanthanide.
[b] M = Ag, Al, and Si

3.3 Results and Discussion

3.3.1 Structure

The α - $ThSi_2$ structure type has been shown to crystallize with a general formula of $Ln(X,Y)_2$, *Ln* = lanthanide, X = main group or transition metal, Y = Si or Ge. Herein, CeM_2 (M = Ag, Al, and Si) will be discussed as a general structural model for both analogue reported herein, as only unit cell parameters such as the *a* or *c* unit cell lengths and interatomic connections change due to lanthanide contraction. The pseudo-binary LnM_2 crystallizes in the tetragonal $I4_1/amd$ space group with the *Ln* and M (M = Ag, Al, and Si) atoms occupying the 4*a* and 8*e* Wyckoff position, respectively.

The α - $ThSi_2$ structure for CeM_2 (M = Ag, Al, and Si) is shown in Figure 3.2. The structure consists of open three dimensional network created by the M sublattice (2*mm*, orange spheres) with the interstitials occupied by Cerium atoms ($\bar{4}m2$, light blue spheres). Two polyhedral environments arise from the lanthanide and M atoms local environments. As shown in Figure 3.2b, the Ce atoms occupy the center of a 12 coordinate polyhedron best described as a

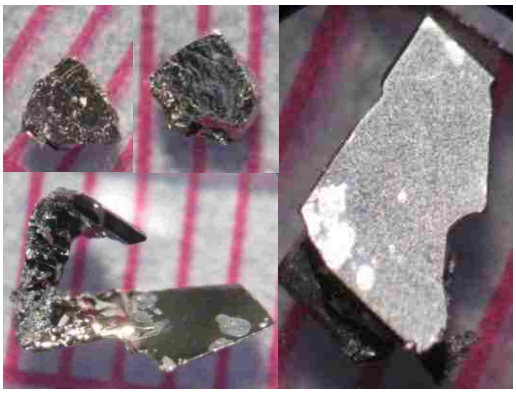

Figure 3.1 Image of un-etched single crystals retrieved from Al flux (grey spots on surface). Two upper left images show the more block-like morphology of the single crystals of CeM_2, with the lower left and right image depicting the blade morphology of GdM_2 single crystals. Each graduation marks 1 mm.

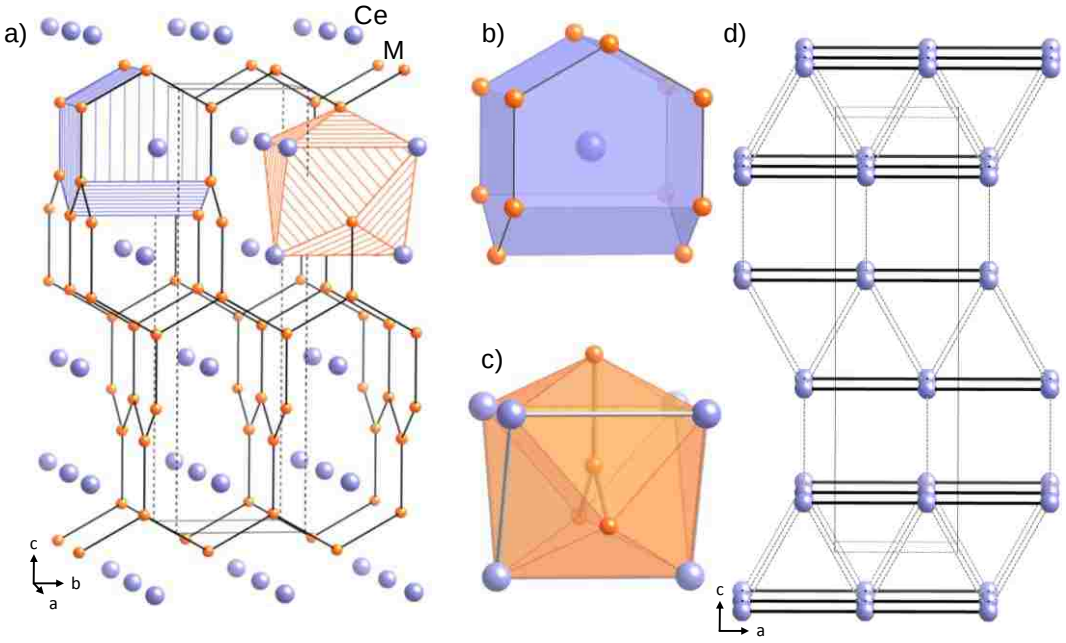

Figure 3.2 The crystal structure of CeM_2 (M = Ag, Al, and Si) is shown. (a) Ce (4*a*) atoms are represented with large light blue spheres; Ag, Al, and Si (8*e*) atoms are denoted as small orange spheres. Dashed lines show the unit cell. The local Ce environment is shown first in (a) as a blue striped polyhedron and again in (b) as a translucent blue polyhedron depicting the local 12 coordinate Ce environment. The local M environment is first illustrated in (a) as an orange striped polyhedron and again in (c) as a translucent orange polyhedron depicting the 9 coordinate tricapped trigonal prismatic M environment. (d) The Ce sublattice is shown slightly above the *ab* plane showing the square planar layers of Ce along the *c* axis and the triangular prismatic layers in the *ab* plane.

rectangular prism capped on opposite faces with triangular prisms orthogonal with respect to the other, to give the full symmetry of D_{2d} "anti-house prismatic." These prisms pack in a face sharing arrangement such that they are completely space filling throughout the lattice. Figure 3.2c shows the local M environment. As illustrated, M atoms occupy the centers of a tricapped trigonal prism. The Ce atoms are located on the corners of the trigonal prism, with other M atoms capping the 3 equatorial faces. It is important to note that the M atom at the center of the tricapped trigonal prism is the capping atom of an adjacent trigonal prism. *M* to *M* contacts range from 2.409(2) – 2.439(4) Å for the Ce analogue which are longer, as would be expected due to Ag substitutions, than $CeSi_2$ (Si – Si, 2.297 – 2.381Å) and agree well with what is observed for $CeAl_{1.2}Si_{0.8}$ (Si/Al – Si/Al, 2.383(4) – 2.501(2) Å) and $YbAg_{0.28}Si_{1.72}$ (Ag/Si – Ag/Si, 2.3463(16) – 2.3664(8) Å).[14,28,29] Nearest connection to Ce range from 4.1878(6) – 4.2450(15) Å and agree well with $CeAl_{1.2}Si_{0.8}$ (Ce – Ce, 4.2581(2) – 4.2741(1) Å) and are longer due to Ag and Al substitution than those found in $CeSi_2$ (Ce – Ce, 4.036 – 4.156 Å).[14,29]

3.3.2 Physical Properties

Figures 3.3a and 3.4a show the temperature dependent molar magnetic susceptibility (χ_m) of $Ln(Ag,Al,Si)_2$ (*Ln* = Ce and Gd) with an applied field of 0.1 T with the inset of Figure 3.3a depicting χ_m with an applied field of 0.05 T for CeM_2. Field dependent magnetization data are shown in Figures 3.3b and 3.4b with T = 3 K. Both Ce and Gd were fit with a modified Curie-Weiss equation of the form: $\chi(T) = \chi_0 + C/(T - \theta)$ where C is the Curie constant, θ_W is the Weiss temperature, and χ_0 is a constant representative of background contribution to magnetic susceptibility. In all cases the modified Curie-Weiss equation was fit over the linear region of $1/\chi_m$. Table 3.5 gives a summary of the fit range, C, θ, T_c/T_N, μ_{eff} and μ_B. When making reference to the applied field and its direction relative to the *ab* plane and/or c axis, crystals grew

in a block-like/blades morphology and directions were assigned as the *ab* plane being ∥ to the face of the blade and the c axis being ⊥ to the blades face.

3.3.2.1 Magnetic Susceptibility of $Ce(Ag,Al,Si)_2$

Figure 3.3a shows the temperature dependent molar magnetic susceptibility of CeM_2 down to 3 K with H∥*c* and H∥*ab*. CeM_2 undergoes a ferromagnetic transition at ~11 K with no other transition down to 3 K with H = 0.1 T. The right axis of Figure 3.3a corresponds to the inverse molar magnetic susceptibility ($1/\chi_m(T)$). Temperatures above 80 K for H∥*c* or H∥*ab* exhibit paramagnetic behavior consistent with Curie-Weiss law. Fitting above these temperatures with a modified Curie-Weiss equation resulted in θ_W = -16.5 and -28.9 K for H∥*c* and H∥*ab* respectively. Negative Weiss temperatures and ferromagnetic ordering have been reported previously for the related $CeSi_{1.70}$, CeAlSi, $Ce_yLa_{1-y}Si_2$ and $CeAl_{1.2}Si_{0.8}$ phases.[13,18,22] The recovered magnetic moment of 2.60 and 2.29 μ_B/mol Ce for H∥*c* and H∥*ab* respectively, are in close agreement with the calculated moment of 2.54 μ_B/mol for a free Ce^{3+} ion. Data between 11 K < T < 80 K for H∥*c* and H∥*ab*, deviation from Curie-Weiss law is observed due to crystal electric field splitting of the J = 5/2 ground state for a Ce^{3+} atom. At T = 11 K for H∥*ab* and H∥*c* a sudden and large change in slope in the molar magnetic susceptibility data is observed indicating a ferromagnetic transition. Inspection of the molar magnetic susceptibility for H∥*ab* and an applied field of 0.05 T, a second transition is observed in the susceptibility data at ~ 9 K. It is important to note that the larger values of χ_m at low temperature for H = 0.05 T over that of H = 0.1 T would be expected due to the onset of saturation at applied fields ≥ 0.1 T with H = 0.05 T being close to the inflection point in the magnetization data. The transition at ~ 9 K will be discussed in more detail later in this manuscript.

Figure 3.3b shows the field dependent magnetization of CeM_2 at 3 K for applied fields $H \| c$ and $H \| ab$. Strong field dependent magnetization is observed at low applied fields in both $H \| c$ and $H \| ab$ but quickly saturates above 0.1 T, indicative of a soft ferromagnetic state. Small hysteresis is observed with $H \| ab$ and small asymmetric hysteresis observed for $H \| c$. It is important to note that hysteresis is present in both directions of the magnetization, with the negative quadrant being much less hysteretic than the positive quadrant for applied fields parallel to the *c* axis. This feature in the magnetization data for $Ce(M)_2$ has been observed in multiple measurements. With the magnetization data being measured within the ferromagnetic regime, the expected saturated magnetic moment of 2.14 μ_B/mol, for a Ce^{3+} ion, is not recovered with $H \| c$ or $H \| ab$, only obtaining a maximum value of 0.68 and 0.85 μ_B/mol at 9 T respectively. The reduced moment is consistent with a J = 5/2 moment split by a tetragonal crystal electric field (μ_{sat} = 0.71 μ_B/mol Ce) which is in agreement with deviations from Curie Weiss law in the molar magnetic susceptibility, similar to $CeAu_{0.28}Ge_{1.72}$.[9]

3.3.2.2 Magnetic Susceptibility of $Gd(Ag,Al,Si)_2$

Figure 3.4a shows the temperature dependent magnetic susceptibility of GdM_2 down to 3 K with $H \| c$ and $H \| ab$. GdM_2 undergoes an antiferromagnetic transition at ~ 24 K with no other transition down to 3 K for $H \| c$. The effect of ~ 0.1 mole of Ag is rather dramatic as the antiferromagnetic transition is suppressed from 32 K for $Gd(Al,Si)_2$ to 24 K for $Gd(Ag,Al,Si)_2$ [8]. The inset of Figure 3.4a shows inverse molar magnetic susceptibility ($1/\chi_m(T)$). Temperatures above 50 K for $H \| c$ or $H \| ab$ exhibit paramagnetic behavior consistent with Curie-Weiss law. Fitting above these temperatures with a modified Curie-Weiss equation resulted in θ_W = -88.7 and -75.6 K for $H \| c$ and $H \| ab$ respectively, and a recovered magnetic moment of 8.46 and 7.96 μ_B/mol for $H \| c$ and $H \| ab$ respectively, which are in agreement with the calculated moment of

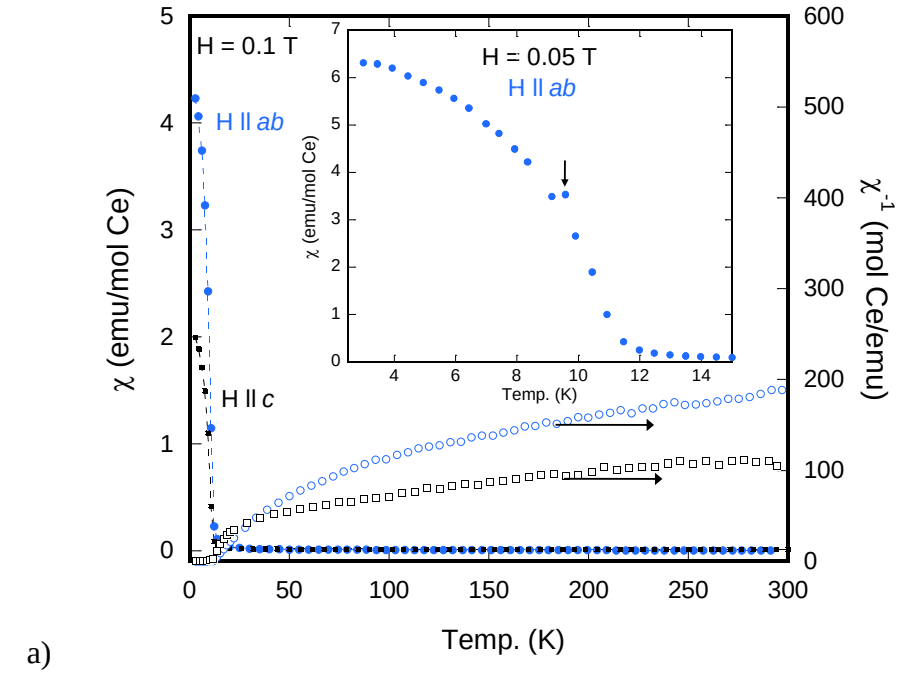

a)

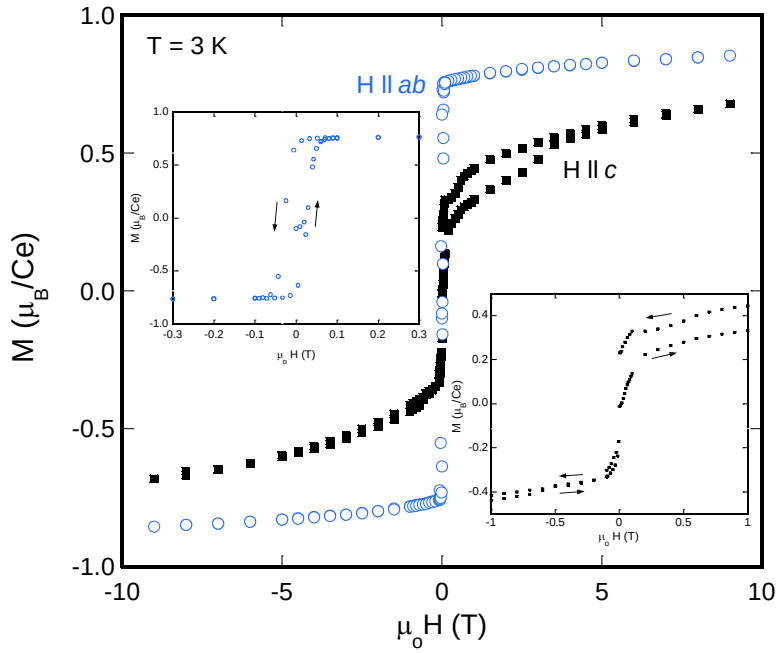

b)

Figure 3.3a and 3.3b (a) Anisotropic molar magnetic susceptibility, closed blue circles H $\|$ *ab* and closed black squares H $\|$ *c*, χ_m = M/H (emu/mol), of CeM_2 as a function of temperature measured under an applied field of 0.1 T on the left axis, and inverse molar magnetic susceptibility, open blue circles H $\|$ *ab* and open black squares H $\|$ *c*, χ_m^{-1} = H/M (mol/emu) as a function of temperature on the right axis. The inset shows the molar magnetic susceptibility of CeM_2 with H $\|$ *ab* = 0.05 T. (b) Magnetization of CeM_2 as a function of applied field at 3 K, open blue circle correspond to H $\|$ *ab* and closed black squares correspond to H $\|$ *c*. The insets are enlargements of the magnetization data.

7.94 μ_B/mol for a Gd^{3+} ion. The Weiss temperature is 3 fold larger than T_N with H$\|$c, but is not large enough to be considered frustrated. Frustration values ($|\theta_W|/T_N$) of 2-5 are considered typical for an antiferromagnetic system,[30] and as can be seen in Figure 3.2d no triangular lattice is observed down the *c* axis. Saturation at T < 24 K of the molar magnetic susceptibility for H$\|$*c* can be best explained such that the applied field is perpendicular to the spin direction. More simply stated that the spin associated with the Gd atoms most likely are located in the *ab* plane. The absence of magnetic ordering with the applied field parallel to the *ab* plane in the molar magnetic susceptibility data suggests that the triangular prismatic arrangement of Gd atoms prevent antiferromagnetic ordering due to frustration. As shown in Figure 3.2d, viewing the lanthanide environment down the *c* axis one only encounters square planar arrangements of Gd atoms which would allow antiferromagnetism to exist without frustration, while viewing in the *ab* plane the shifts in these square planar arrangements with respect to the other creates a trigonal prismatic arrangement of Gd atoms giving rise to frustration and paramagnetism down to 3 K for data with H$\|$*ab* supported by the molar magnetic susceptibility. As can be seen in Figure 3.4a, H$\|$*ab* magnetic susceptibility shows a small shoulder at 24 K corresponding to an antiferromagnetic transition with an upturn at 20 K remaining down to 3 K. The observed shoulder is most likely due to imperfect alignment in the magnetic field and GdM_2 is paramagnetic down to 3 K with H$\|$*ab*. The Weiss temperature for H$\|$*ab* is on the same scale as H$\|$*c* but GdM_2 remains paramagnetic down to 3 K giving rise to the possibility that GdM_2 is magnetically frustrated when H$\|$*ab*. The absences of a magnetic transition when H$\|$*ab* down to 3 K gives rise to frustration values $\geq$ 25, well within the frustrated classification.

Figure 3.4b shows the field-dependent magnetization at 3 K with H$\|$*ab* and H$\|$*c*. No saturation is observed up to 9 T for H$\|$*c* as expected for an antiferromagnetic system. Small

curvature in the magnetization data can be seen for applied fields parallel to the *ab* plane, consistent with the assertion of paramagnetism at 3 K.

Table 3.5 Magnetic Properties of *Ln*(Ag,Al,Si)$_2$ (*Ln* = Ce and Gd)

	C	θ	μ_{calc} (μ_B)	μ_{eff} (μ_B)	Fit range (K)	Ordering, T_c/T_N (K)
Ce(Ag,Al,Si)$_2$	0.849	-16.5	2.54	2.60	80-270	FM[a], 11 (H$\|c$)
	0.662	-28.9	2.54	2.29	80-270	FM[a], 11 (H$\|ab$)
Gd(Ag,Al,Si)$_2$	8.966	-88.7	7.94	8.46	50-285	AFM[b], 24 (H$\|c$)
	7.9203	-75.6	7.94	7.96	50-285	PM[c] (H$\|ab$)

[a] ferromagnetic, [b] antiferromagnetic, [c] paramagnetic

3.3.2.3 Transport Properties: *Ln*(Ag,Al,Si)$_2$ (Ln = Ce and Gd)

Heat capacity data and entropy for CeM_2 are shown in Figures 3.5a and 3.5b. As can be seen in Figure 3.5a, a sharp increase observed with the first maximum, $T_{C1,}$ at 10.8 K and a second, T_{C2}, at 8.8 K. These transitions agree well with the ferromagnetic transition at 11 K as observed in the molar magnetic susceptibility and the second transition at ~ 9 K, inset of Figure 3.3a, in the molar magnetic susceptibility with H = 0.05 T. The double transition in heat capacity has been observed in $CeSi_{1.70}$ which corresponds to two magnetic transitions, a ferromagnetic ordering and a subsequent small antiferromagnetic modulation as determined by neutron diffraction.[18,31,32] Phonon contribution to heat capacity (C_{phonon}) was approximated by a linear fit to C_p/T vs. T^2 over the range of 18 – 35 K, as LaM_2 could not be grown with Ag disorder. Close analysis of the low temperature specific heat for 3D ferromagnetic magnons ($T^{3/2}$ dependence), 2D antiferromagnetic or helical magnons (T^2 dependence), or 3D antiferromagnetic magnons (T^3 dependence) are shown in Figures 3.6a – 3.6c respectively. The low temperature specific heat data shows that the data is most consistent with 2D antiferromagnetic or helical magnons as the low temperature heat capacity ($C - C_{phonon}$) data

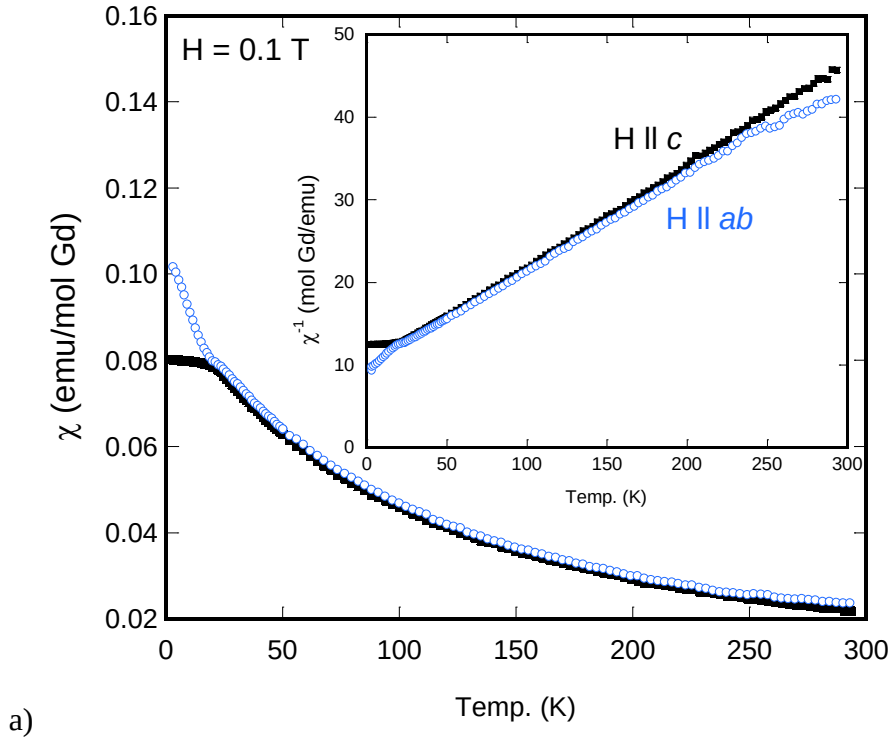

a)

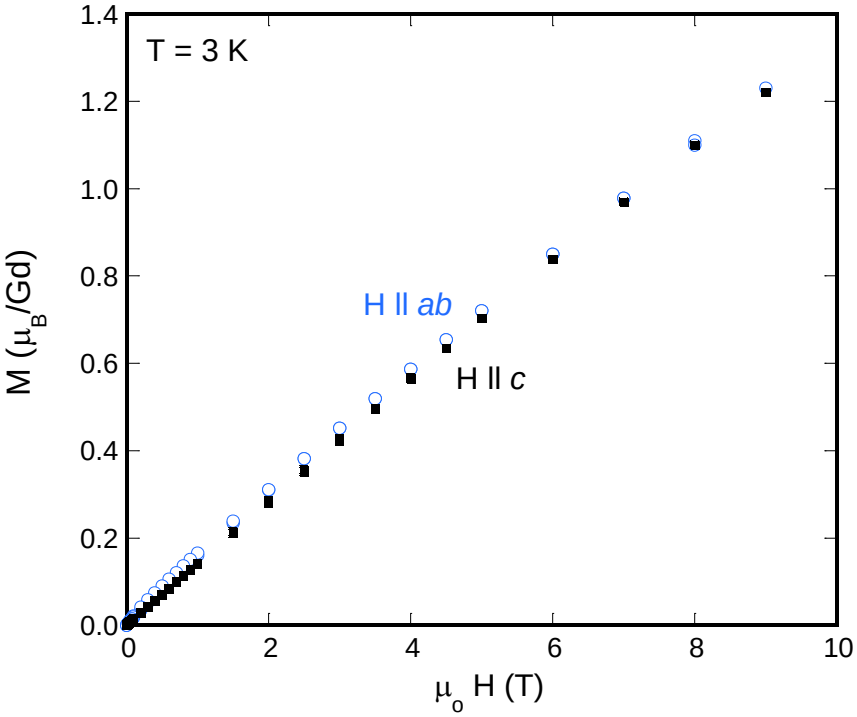

b)

Figure 3.4a and 3.4b (a) Anisotropic molar magnetic susceptibility, χ_m = M/H (emu/mol), of GdM_2 as a function of temperature measured under an applied field of 0.1 T. The inset shows the inverse molar magnetic susceptibility of GdM_2. (b) Magnetization of GdM_2 as a function of applied field at 3 K. Open blue circles correspond to H$\|ab$ and closed black squares correspond to H$\|c$ for both χ_m and magnetization.

scales linearly as a function of T^2, shown in Figure 3.6b. It is possible to differentiate between helical and 2D antiferromagnetic magnons as helical magnons scale linearly in resistivity as $T^{5/2}$. As can be seen in Figure 3.7a, resistivity does not scale linearly as a function of $T^{5/2}$, refuting helimagnons contribution and supporting 2D antiferromagnetic magnon contributions below T_{C2} and electron-electron scattering with an enhanced A term in resistivity due to Kondo coupling. With negative Weiss constants, a T^2 dependence of resistivity and specific heat, and a two transitions evident in specific heat and molar magnetic susceptibility with H = 0.05 T, T_{C2} is attributed to an antiferromagnetic transition. The Sommerfeld coefficient in the ordered state, irrespective of the power law used, for the T = 0 extrapolation gives a zero intercept for $C - C_{phonon}$ vs. T^n, therefore a γ value cannot be estimated in the ordered state by extrapolation. However, we can estimate the γ contribution to the specific heat in the ordered state from the Kadowaki Woods ratio $1x10^{-5}$ $\mu\Omega$-cm $K^2mol^2mJ^{-2} = A/\gamma^2$, where A is the coefficient of the T^2 term in resistivity ($\rho = \rho_0 + AT^2$) and γ is the Sommerfeld parameter.[33] As can be seen in Figure 3.7a, A = 0.2774 at H = 0 T (2 K < T < 11 K). This gives a γ in the ordered state of ~ 167 mJ/K^2-mol f.u. Extrapolation to T = 0 above T_c in the paramagnetic state over the range of 18 K < T < 35 K we find γ = 12.6 mJ/K^2-mol. This indicates that in the paramagnetic state the carriers are not heavy, supported by the fact that most of the entropy is recovered by 11 K. The 13 fold enhancement of the Sommerfeld coefficient in the ordered state over that found in the paramagnetic state is indicative of mass enhancement. The Debye temperature was found to be 342 K, consistent with the saturation in heat capacity. As can be seen in Figure 3.5b at 10.8 K the recovered entropy is ~ 0.79Rln2 with Rln2 recovered at T > 20 K. We see no evidence for short range order above T_c and the recovered effective moments agree well with a Ce^{3+} ion.

Therefore, the reduced entropy can be accounted for by the Kondo effect, which is reinforced by the resistivity measurements, and the enhanced mass behavior at low temperatures.

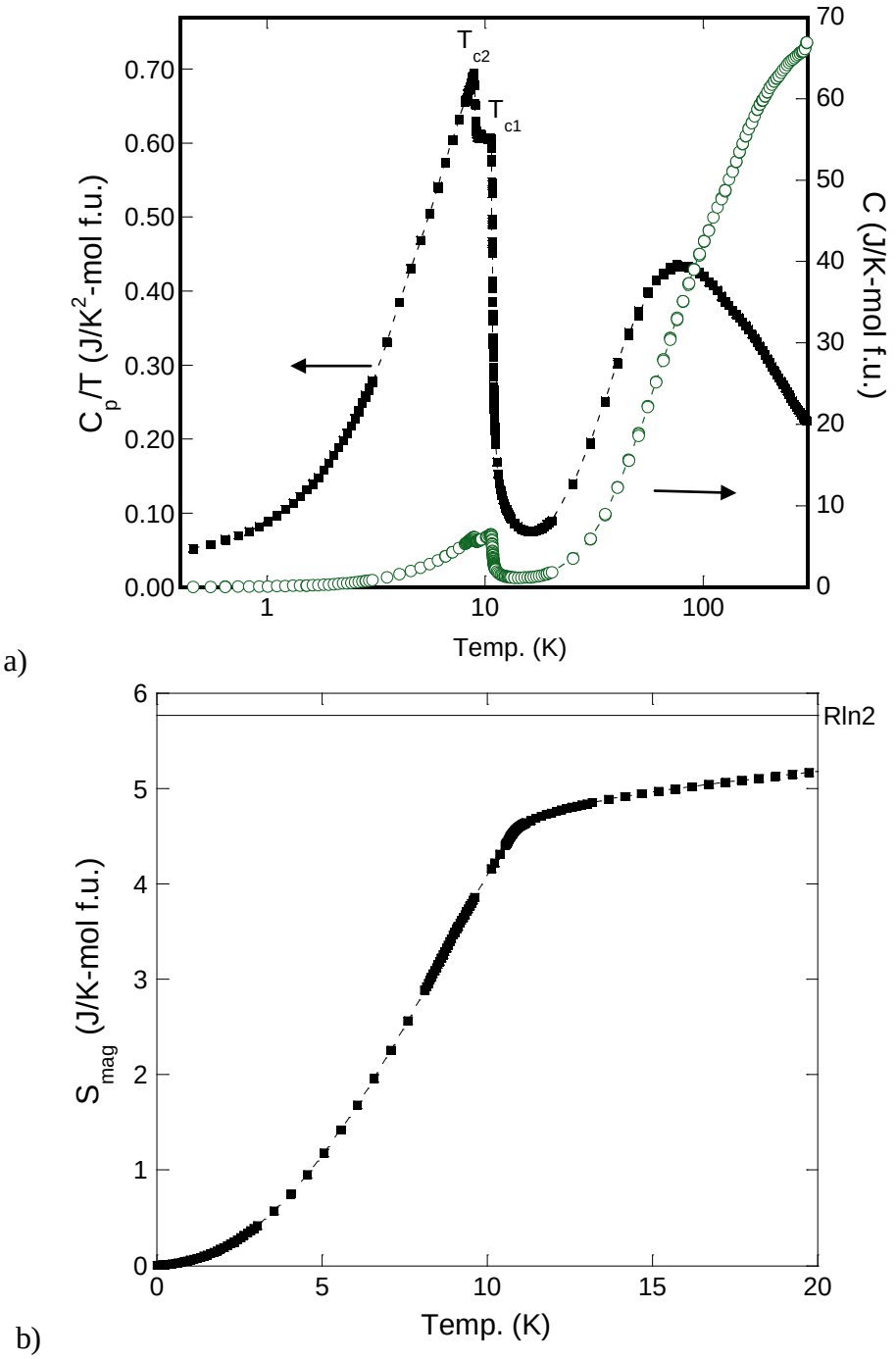

Figure 3.5a and 3.5b (a) C_p/T as a function of T (K) (closed black squares) for CeM_2 and heat capacity as a function of temperature (open green circles). (b) S_{mag} as a function of temperature for CeM_2 with Rln2 shown as a solid black line.

The electrical resistivity as a function of temperature for CeM_2 and GdM_2 are shown in Figure 3.7b and 3.7c respectively, with the resistivity of CeM_2 being measured at 0 and 9 T for $I \| ab$ and H = 0 T for $I \| c$. For CeM_2 metallic behavior is observed down to 50 K for $I \| ab$ and 30 K for $I \| c$ where a minimum is observed. Resistivity from 11 K < T < 50 K for H = 0 T and 9 T with $I \| ab$, and 15 K < T < 30 K for H = 0 T, $I \| c$, increases with decreasing temperature reaching a maximum value at the magnetic ordering temperature. The broad features above the minimum in the resistivity data and the upturn below the minimum is consistent with Kondo behavior or increased scattering due to site disorder. A linear fit from the minimum to the magnetic transition in the resistivity (11 K < T < 50 K for H = 0 T and $I \| ab$) scales linearly with the lnT, reinforcing Kondo behavior. This observation is not that surprising as most related analogues in the α - $ThSi_2$ structure type exhibit Kondo behavior. At 11 K for H = 0 T with $I \| ab$ and $I \| c$ and at 15 K for H = 9 T with $I \| ab$ a sudden decrease is observed down to the 2 K. The peak in resistivity data for CeM_2 at 11 K (15 K for H = 9 T with $I \| ab$) coincides with the ferromagnetic transition in the molar magnetic susceptibility and a sudden drop in resistivity due to reduced spin disorder scattering is observed. As can be seen in Figure 3.7a, the T^2 behavior (2 K < T < 11 K) in resistivity corresponds to electron-electron scattering, consistent with the enhanced Sommerfeld coefficient.

In a similar fashion GdM_2 shows metallic behavior with a minimum and upturn at 32 K, a result of increased scattering due to site disorder. At 24 K for GdM_2 a kink in resistivity is observed which corresponds to the onset of antiferromagnetism in agreement with the molar magnetic susceptibility. The sudden drop in resistivity, again, is due to the reduction in spin disorder scattering. In both analogues the RRR values are close to 1, providing insight to the intrinsic Ag, Al, and Si disorder throughout the lattice.

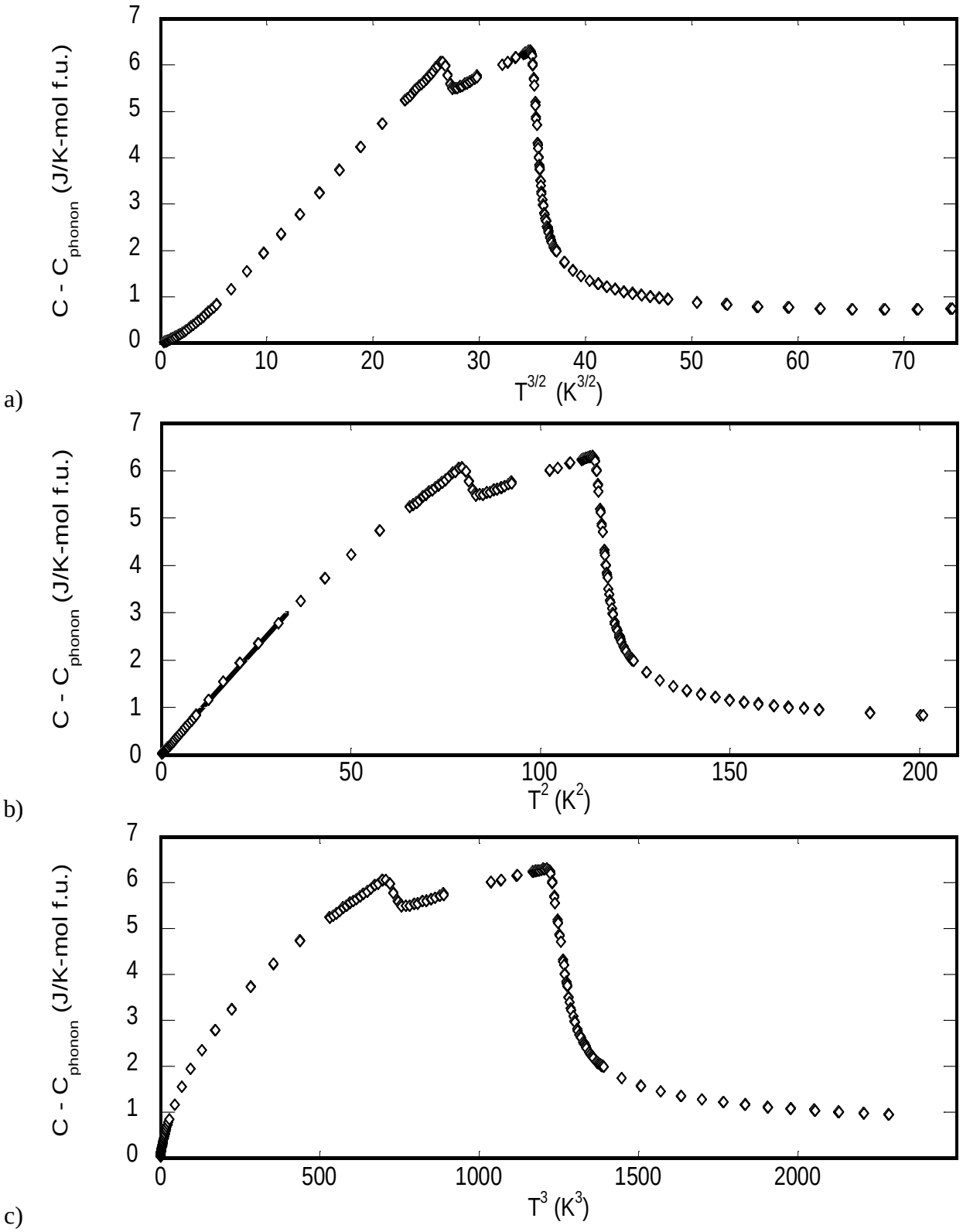

Figure 3.6a – 3.6c $C - C_{phonon}$ as a function of a) $T^{3/2}$ ($K^{3/2}$), b) T^2 (K^2), and c) T^3 (K^3) for CeM_2.

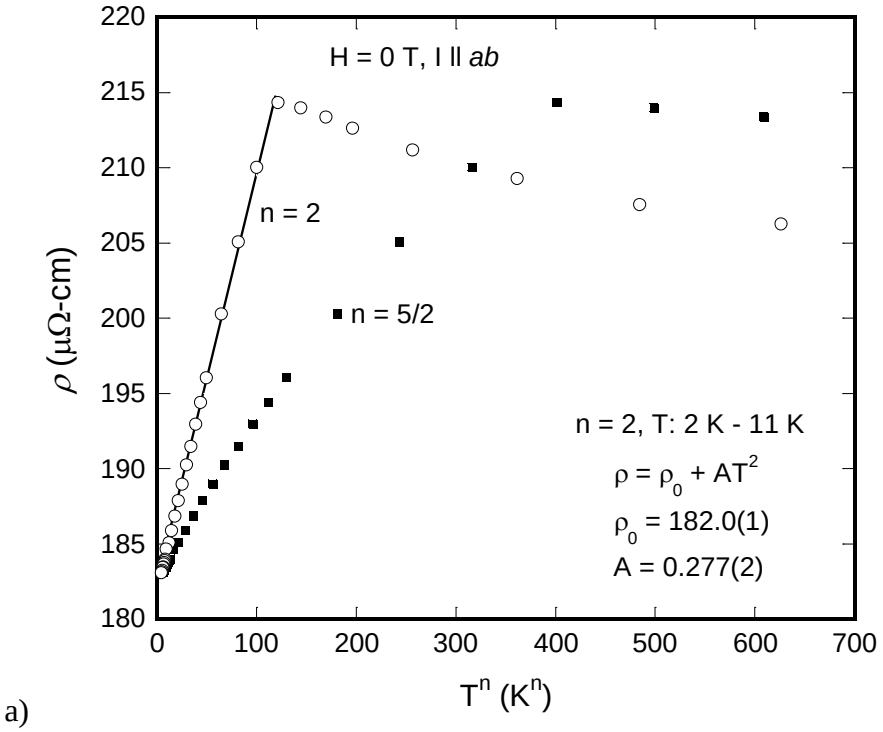

a)

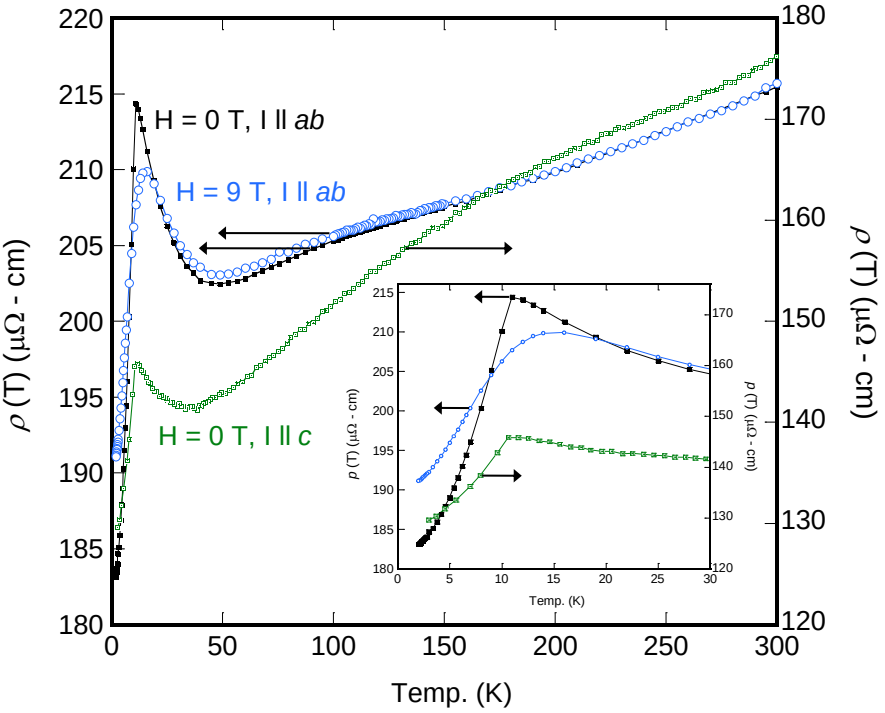

b)

Figure 3.7a – 3.7c (a) Electrical resistivity of CeM_2 as a function of T^n where n = 2 (open circles) and 5/2 (closed squares). (b) Electrical resistivity of $Ce(M)_2$ with an applied field of 0 T (closed black square) and 9 T (open blue circles) as a function of temperature for I ‖ *ab* and resistivity for H = 0 T with I ‖ *c* (open green squares). The inset is an enlarged view of the low temperature resistivity. (c) Electrical resistivity of $Gd(M)_2$ with the low temperature region expanded in the inset.

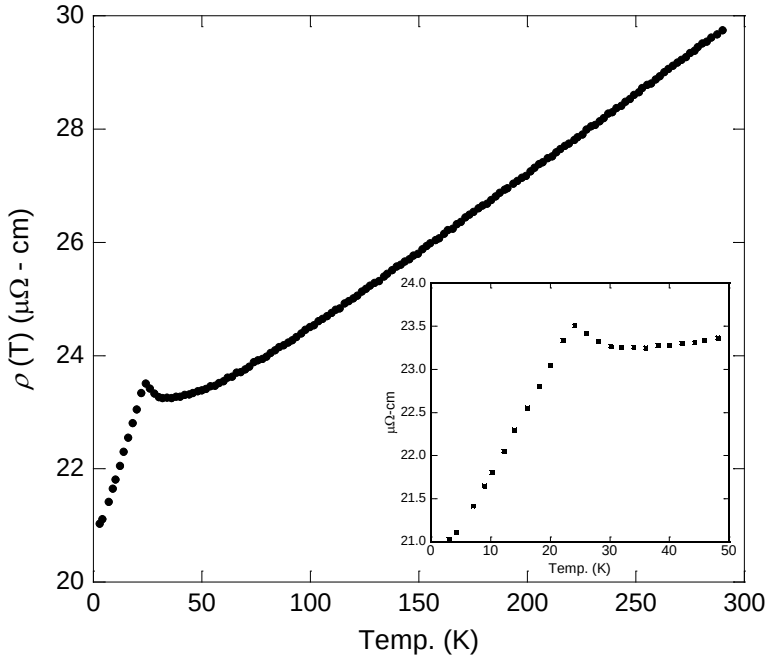

c)

(Figure 3.7 continued)

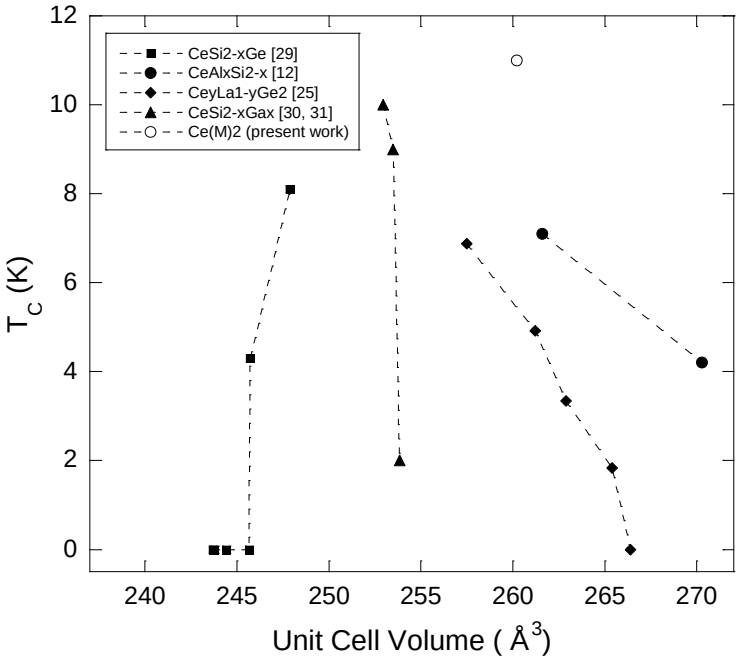

Figure 3.8 T_C (K) as a function of unit cell volume (Å^3) for $CeSi_{2-x}Ge_x$ (closed squares) [21], $CeAl_xSi_{2-x}$ (closed circles) [13], $Ce_yLa_{1-y}Si_2$ (closed diamonds) [22], $CeSi_{2-x}Ga_x$ (closed triangles) [23,24], and $Ce(M)_2$ (open circle).

Single crystals of $Ce(Ag,Al,Si)_2$ and $Gd(Ag,Al,Si)_2$ were grown by the flux growth technique. The crystals were characterized by single crystal X-ray diffraction and composition

determined by SEM/EDXS. We have shown that CeM_2 orders ferromagnetically at 11 K with a second antiferromagnetic transition at 9 K. In addition, the transport behavior of CeM_2 is consistent with Kondo interactions and specific heat measurements reveal an enhanced Sommerfeld coefficient ($\gamma_0 \sim 53$ mJ/K^2-mol in the ordered state). In an attempt to understand the amplitude of the T_C in this structure type, a plot of T_C vs. unit cell volume was compiled from $CeSi_{2-x}Ge_x$ [21], $CeAl_xSi_{2-x,}$ [13] $Ce_yLa_{1-y}Si_{2,}$ [22] and $CeSi_{2-x}Ga_x$ [23,24] as shown in Figure 3.8. Curiously, there is no universal dependence of T_C on unit cell volume. It would be expected that the distance between Ce nearest neighbors is what determines T_C, which is not the case in the α - $ThSi_2$ structure type. This suggests that although we have a local moment ordering, the ordering temperature is not just determined by Ce – Ce distances but is extremely sensitive to the electronic structure. Additionally, GdM_2 orders antiferromagnetically at 24 K, with a minimum in the resistivity at 32 K. The antiferromagnetic ordering temperature for GdM_2 was suppressed by 8 K over the related $GdAl_{0.98}Si_{1.02}$ phase[8] and we have presented the possibility of frustration due to the triangular rare-earth lattice along the *ab* plane.

3.4 References

(1) Drake, B.L., Kangas, M.J., Capan, C., Haldolaarachchige, N., Xiong, Y.M., Adams, P.W., Young, D.P., and Chan, J.Y., Crystal growth, structure, and physical properties of $Ln(Ag,Al,Si)_2$ (Ln = Ce and Gd). *J Phys. Condens. Mat.* **2010,** *22*, 426002.

(2) Petrovic, C., Movshovich, R., Jaime, M., Pagliuso, P.G., Hundley, M.F., Sarrao, J.L., Fisk, Z., and Thompson, J.D., A new heavy-fermion superconductor $CeIrIn_5$: A relative of the cuprates? *Europhys. Lett.* **2001,** *53*, 354.

(3) Petrovic, C., Pagliuso, P.G., Hundley, M.F., Movshovich, R., Sarrao, J.L., Thompson, J.D., Fisk, Z., and Monthoux, P., Heavy-fermion superconductivity in $CeCoIn_5$ at 2.3 K. *J. Phys. Condens. Mat.* **2001,** *13*, L337.

(4) Bauer, E., Pillmayr, N., Gratz, E., Gignoux, D., Schmitt, D., Winzer, K., and Kohlmann, J., $CeCu_4Ga$: A high γ heavy fermion compound. *J. Magn. Magn. Mater.* **1988,** *71*, 311-317.

(5) Macaluso, R.T., Nakatsuji, S., Lee, H., Fisk, Z., Moldovan, M., Young, D.P., and Chan, J.Y., Synthesis, structure, and magnetism of a new heavy-fermion antiferromagnet, $CePdGa_6$. *J. Solid State Chem.* **2003,** *174*, 296-301.

(6) Kishimoto, Y., Kawasaki, Y., and Ohno, T., Mixed valence state in Ce and Yb compounds studied by magnetic susceptibility. *Phys. Lett. A* **2003,** *317*, 308-314.

(7) Fisk Z, Sarrao J L, Smith J L, and Thompson J D, The physics and chemistry of heavy fermions. *Proc. Natl. Acad. Sci. U. S. A.* **1995,** *92*, 6663-6667.

(8) Bobev, S., Tobash, P.H., Fritsch, V., Thompson, J.D., Hundley, M.F., Sarrao, J.L., and Fisk, Z., Ternary rare-earth alumo-silicides-single-crystal growth from Al flux, structural and physical properties. *J. Solid State Chem.* **2005,** *178*, 2091-2103.

(9) Sebastian, C.P. and Kanatzidis, M.G., Ferromagnetic ordering in $ThSi_2$ type $CeAu_{0.28}Ge_{1.72}$. *J. Solid State Chem.* **2010,** *183*, 878-882.

(10) Popescu, B., Birsan, A., Galatanu, A., Royanian, E., Hilscher, G., and Bauer, E., Physical properties of the new ferromagnetic Kondo system $CeAg_{1-x}Ni_xSb_2$. *J. Optoelectron. Adv. M.* **2008,** *10*, 1625-1629.

(11) Macaluso, R.T., Moreno, N.O., Fisk, Z., Thompson, J.D., and Chan, J.Y., Structure and magnetism of Ce_5Pb_3O. *Chem. Mater.* **2004,** *16*, 1560-1563.

(12) Muranaka, T. and Akimitsu, J., Thermodynamic properties of ferromagnetic Ce-compound, $CeAgAl_3$. *Physica C* **2007,** *460-462*, 688-690.

(13) Dhar, S.K. and Pattalwar, S.M., Structural and magnetic properties of $CeAl_xSi_{2-x}$ and $CeAl_xGe_{2-x}$ alloys. *J. Magn. Magn. Mater.* **1996,** *152*, 22-26.

(14) Flandorfer, H., Kaczorowski, D., Gröbner, J., Rogl, P., Wouters, R., Godart, C., and Kostikas, A., The systems Ce-Al-(Si, Ge): phase equilibria and physical properties. *J. Solid State Chem.* **1998,** *137*, 191-205.

(15) Jung, M.H., Park, S.H., Kim, H.C., and Kwon, Y.S., Magnetism of the new rare-earth intermetallic compounds $RAl_{0.9}Si_{1.1}$ (R=Ce,Pr,Gd). *J. Magn. Magn. Mater.* **2004,** *272-276*, E431-E432.

(16) Pukas, S., Lutsyshyn, Y., Manyako, M., and Gladyshevskii, E., Crystal structures of the RAlSi and RAlGe compounds. *J. Alloy Compd.* **2004,** *367*, 162-166.

(17) Pierre, J., Laborde, O., Houssay, E., Rouault, A., Senateur, J.P., and Madar, R., Anisotropy of the magnetic and electrical properties of $CeSi_x$. *J. Phys. Condens. Mat.* **1990,** *2*, 431.

(18) Sato N, Mori H, Satoh T, Miura T, and Takei H, Thermal, electrical and magnetic properties of the ferromagnetic dense Kondo system. *J. Phys. Soc. Japan* **1988,** *57*, 1384.

(19) Yashima, H., Mori, H., Satoh, T., and Kohn, K., Ferromagnetic dense Kondo behavior of Ce-Si system. *Solid State Commun.* **1982,** *43*, 193-197.

(20) Yashima, H. and Satoh, T., Nonmagnetic-magnetic transition in Ce-Si system. *Solid State Commun.* **1982,** *41*, 723-727.

(21) Lahiouel, R., Galera, R.M., Pierre, J., and Siaud, E., Crossover between fermi liquid behaviour and magnetic order in $CeSi_{2-x}G_x$ System. *Solid State Commun.* **1986,** *58*, 815-817.

(22) Mori H, Yashima H, and Sato N, A newdense Kondo system: $Ce_yLa_{1-y}Ge_2$. Resistivity, specific heat, and susceptibility studies. *J. Low Temp. Phys.* **1985,** *58*, 513-531.

(23) Moshchalkov, V.V., Petrenko, O.V., and Zalyayutdinov, M.K., The new kondo lattice compounds: $CeSi_{2-x}Ga_x$. *Physica B* **1990,** *163*, 395-397.

(24) Priolkar, K.R., Rao, M.N., Prabhu, R.B., Sarode, P.R., Paranjpe, S.K., Raj, P., and Sathyamoorthy, A., Spin dynamics of $CeSi_{2-x}Ga_x$, $0.7< x < 1.3$. *J. Magn. Magn. Mater.* **1998,** *185*, 375-378.

(25) Canfield, P.C. and Fisk, Z., Growth of single crystals from metallic fluxes. *Philos. Mag. B* **1992,** *65*, 1117-1123.

(26) Altomare, A., Burla, M.C., Camalli, M., Luca, G.L., Gaicovazzo, C., Guagliardi, A., Moliterni, A.G.G., Polidori, G., and Spagna, R., SIR97: a new tool for crystal structure determination and refinement. *J. Appl. Cryst.* **1999,** *32*, 115.

(27) Sheldrick, G.M., A short history of SHELX. *Acta Crystallogr. A* **2008,** *64*, 112-122.

(28) Brauer, G. and Haag, H., Über darstellung und kristallstruktur der disilicide von einigen metallen der seltenen erden. *Z. Anorg. Allg. Chem.* **1952,** *267*, 198-212.

(29) Bobev, S. and Bauer, E.D., $YbAg_xSi_{2-x}$ [x = 0.28(1)] with the tetragonal α-$ThSi_2$ structure type. *Acta Crystallogr. E* **2005,** *61*, i96-i98.

(30) Greedan, J.E., Geometrically frustrated magnetic materials. *J. Mater. Chem.* **2001,** *11*, 37-53.

(31) Sato, N., Kohgi, M., Satoh, T., Ishikawa, Y., Hiroyoshi, H., and Takei, H., Magnetic states of the Kondo lattice $CeSi_{1.70}$. *J. Magn. Magn. Mater.* **1985,** *52*, 360-362.

(32) Shaheen, S.A. and Mendoza, W.A., Origin of multiple magnetic transitions in $CeSi_x$ systems. *Phys. Rev. B* **1999,** *60*, 9501.

(33) Kadowaki, K. and Woods, S.B., Universal relationship of the resistivity and specific heat in heavy-Fermion compounds. *Solid State Commun.* **1986,** *58*, 507-509.

CHAPTER 4. CRYSTAL GROWTH, STRUCTURE, AND PHYSICAL PROPERTIES OF *Ln*$Cu_2(Al,Si)_5$ (*Ln* =La and Ce)

4.1 Introduction

An important family of compounds are the magnetic, heavy fermion superconducting Ce_nMIn_{3n+2} (*M* = Co, Rh, or Ir, n = 1 or 2) phases.[1-6] It was of interest if single crystals of an isostructural phase could be stabilized for Pd derivatives and how the addition of one valence electron would perturb the ground state of the Ce_nMIn_{3n+2} family. An isostructural derivative was not found, however a new compound was observed. $CePdGa_6$ ($\gamma > 230$ mJ/K^{2}mol, $T_N = 5$ K), an antiferromagnetic heavy fermion, was grown from excess Ga flux and crystallizes with the $SrAu_2Ga_5$ structure type.[7-9] Additionally, a structurally similar antiferromagnetic phase, Ce_2PdGa_{12}, was grown ($\gamma > 70$ mJ/K^{2}mol, $T_N = 11$ K) and is isostructural to Sm_2NiGa_{12}.[7,10] The observation of two new antiferromagnetic phases with enhanced mass behavior resulted in exploration of both the Ni and Cu containing phases. Judicious exploration of this phase space resulted in stabilization of Ln_2MGa_{12} (*Ln* = La – Nd and *M* = Ni or Cu).[11,12] Later *Ln*'s are formed for α – *Ln*$NiGa_4$ (Y, Gd – Yb), *β* – *Ln*$Ni_{1-x}Ga_4$ (*Ln* = Tb - Er), $SmCu_4Ga_{12}$, and *Ln*$(Cu,Ga)_{12}$ (*Ln* = Y, Gd – Er, and Yb).[13-16] In any case, Ni or Cu derivatives of $CePdGa_6$ were not observed.

Exploration of similar phase space with Al flux resulted in the isolation of $LaNi_{1+x}Al_{6-x}$ and more recently $CePd_{1-x}Al_{6-x}$.[17,18] The disorder in these compounds is observed on the 2*h* Wyckoff position, the same site observed to disorder in the parent phase $SrAu_2Ga_5$. Band structure calculations from DFT calculations reveal the stabilization of this structure may arise from the optimization of Al – Al and Al – Ni contacts in $LaNi_{1+x}Al_{6-x}$ and valence electron count of 19.68 electron/f.u.[17]. This is in good agreement with $CePd_{1-x}Al_{6-x}$ (~ 19.5 e-/f.u.), $CePdGa_6$ (~ 21 e-/f.u.), and $SrAu_2Ga_5$ (~ 19 e-/f.u.).[8,9,18]

While working on compounds in the *Ln*-Cu-Al phase space (*Ln* = La and Ce), searching for highly disordered Cu/Al compounds, we have grown pseudo-ternaries of the $SrAu_2Ga_5$ structure type. This work is motivated by the observation of mass enhancement, γ, in a plethora of disordered compounds recently reported by our group.[11,16,19,20] Here in we report the crystal growth, both single crystal and polycrystalline, magnetic, and transport properties of a new derivative of the $SrAu_2Ga_5$ structure type, $LnCu_2(Al,Si)_5$ (*Ln* = La and Ce).

4.2 Experimental

4.2.1. Synthesis

Single crystals of $CeCu_2(Al,Si)_5$ were first grown in the presence of excess Al flux.[21] *Ln* (Alfa Aesar, 3N, chunks), Cu (Alfa Aesar, 3N, powder), and Al (Alfa Aesar, 5N, pellets) were used as received and loaded into an alumina crucible with a reaction ratio of 1:1:10 for *Ln*:Cu:Al respectively. Rare earth elements are stored in vacuum desiccators to prevent oxidation (0.1 mmHg). The crucibles were placed into a fused silica tube with silica wool used as a filtering medium and the contents were evacuated (0.05 – 0.07 mmHg) and sealed. The charged vessel was loaded into a furnace and heated to a dwell temperature of 1200 °C for 72 h at 250 °C/h. Samples were slowly cooled to 1000 °C with a rate of 2 °C/h at which the cooling rate was doubled to 4 °C/h to a dwell temperature of 720 °C upon which the samples were centrifuged to separate crystals from the Al flux. Subsequent attempts to repeat this growth failed, resulting in the growth of $CeCuAl_3$ crystallizing in the $BaAl_4$ structure type. Close investigation of the composition via SEM/EDS revealed the presence of Si. No silicon was added for the initial reaction. Silicon was introduced into the reaction either from the fused silica tube or more likely the silica wool filtering material at high temperature. Subsequent growths were carried out with the following reaction ratios: 1:2:0.1:10, 1:2:0.5:10, and 1:2:2:10 for Ce:Cu:Si:Al, Si (Alfa

Aesar, 5N, powder), which resulted in the successful growth of $CeCu_2(Al,Si)_5$ and a $BaAl_4$ type impurity ($Ce(Cu,Al,Si)_4$), $CeCu_2(Al,Si)_5$ and a $BaAl_4$ type impurity, and a $BaAl_4$ type impurity for each reaction ratio respectively. The presence of both phases, $CeCu_2(Al,Si)_5$ and the $BaAl_4$ type phase, were confirmed by both X-ray powder diffraction and single crystal X-ray diffraction. The stabilization of a phase adopting the $BaAl_4$ type phase maybe expected due to the structural similarities between the $SrAu_2Ga_5$ and $BaAl_4$ structure types.[17] Attempts were made to mechanically separate the phases though both form plate-like crystals, the $BaAl_4$ type impurity formed a larger and thicker plate. Specifically $CeCu_2(Al,Si)_5$ grow as thin sub-mm plate protruding from the surface of the $BaAl_4$ type impurity. The mechanical separation did result in small amounts of the impurity phase remaining on the small single crystals of $CeCu_2(Al,Si)_5$. The reaction ratio 1:2:0.1:10 and 1:2:0.5:10 were very similar but with the smaller amount of Si present larger plate-like single crystals of $CeCu_2(Al,Si)_6$ were isolated (< 0.5 mm). $CeCu_2(Al,Si)_5$ could only be isolated with Si present, all attempts to grow $CeCu_2Al_5$ failed indicating that the presence of Si is critical to the phase stabilization.

Multiple attempts to grow the La analogue were completed and synthesis was realized under the following conditions: La (3N, chunks, Alfa Aesar), Cu (3N, powder, Alfa Aesar), Si (5N, powder, Alfa Aesar), and Al (5N, pellets, Alfa Aesar) loaded into an alumina crucible with a reaction ratio of 1:2:1:4, respectively. The sample was heated to 1150 °C at 300 °C/hr for 24 hrs. The sample was cooled to 720 °C at a cooling rate of 4 °C/hr upon which the sample was centrifuged to cool. Small (< 0.5 mm) crystals were isolated. Once again the $BaAl_4$ structure type impurity was observed.

In all growths, silver metallic crystals were retrieved via etching in NaOH (1-3 M) until excess aluminum was removed and subsequently cleaned with 10% HNO_3, retrieving flux-free

single crystals which were observed to be air stable. Crystal morphology is best described as plate-like for La and Ce.

In light of the presence of the $BaAl_4$ type impurity remaining on the small single crystals of $LnCu_2(Al,Si)_5$ (*Ln* = La and Ce) and the inability to avoid the impurity phase, a stoichiometric sample was prepared via arc-melt. The *Ln*-Cu-Al constituents (same purities as mentioned previously) were first melted and the button turned and melted with Si pieces (5N, pieces, Alfa Aesar). Each button was subsequently flipped 3 times to ensure homogeneity. Mass loss for the La and Ce analogues was 0.17% and 0.01% respectively. X-ray powder diffraction again indicated the presence of both $LnCu_2(Al,Si)_5$ (*Ln* = La and Ce) and the $BaAl_4$ type impurity. The samples were annealed at 750 °C for 3 weeks. Powder X-ray diffraction indicated phase purity of $LnCu_2(Al,Si)_5$ (*Ln* = La and Ce). To ensure the purity, data were collected at Argonne's Advanced Photon Source using the 11-BM-B high resolution, high throughput powder diffractometer. Results will be discussed further in the results and discussion section. Attempts to grow $LnCu_2(Al,Si)_5$ sans Si with the above annealing step resulted in the formation of $ThMn_{12}$ type and $BaAl_4$ type impurities, again indicating Si is critical to phase stabilization.

4.2.2. X-ray Diffraction and Elemental Analysis

Crystals of $LaCu_2(Al,Si)_5$ and $CeCu_2(Al,Si)_5$ were cut to suitable sizes for data collection ($\leq$ 0.05 mm x 0.05 mm x 0.05 mm) and mounted onto a glass fiber using epoxy. They were then positioned onto the goniometer of a Nonius KappaCCD diffractometer equipped with Mo K_α radiation (λ = 0.71073 Å). Further crystallographic parameters for $LnCu_2(Al,Si)_5$ (Ln = La and Ce) are provided in Table 4.1. Direct methods were used to solve the structure. SIR97 was employed to give a starting model and SHELXL97 used to refine the structural model and data were corrected with extinction coefficients and refined with anisotropic displacement

parameters.[22,23] Based on lattice parameters and the initial refinements, our initial structural model was found to be isostructural to $CePdGa_6$ and crystallize in the $SrAu_2Ga_5$ structure type.[8,9] However, refinement of the 2*h* Wyckoff position assuming full main group element occupancy (Al), as observed in $CePdGa_6$, resulted in a model with an abnormally small atomic displacement parameter (ADP) for the 2*h* position. Selected interatomic distances are presented in Table 4.2, and atomic positions and displacement are provided in Table 4.3. These tables reflect the structural model obtained after mixing the occupancy of the 2*h* and 4*i* positions.

Table 4.1 Crystallographic Parameters for $LaCu_2(Al,Si)_5$ and $CeCu_2(Al,Si)_5$

Formula	$LaCu_2(Al,Si)_5$	$CeCu_2(Al,Si)_5$
a (Å)	4.221(2)	4.2040(15)
c (Å)	7.916(3)	7.925(4)
V (Å^3)	141.04(11)	140.06(10)
Z	1	1
Crystal system	tetragonal	tetragonal
Space group	*P*4/*mmm*	*P*4/*mmm*
θ range (°)	2.546-31.507	2.57-34.97
μ (mm^{-1})	15.589	16.197
Data collection		
Measured reflections	475	303
Independent reflections	178	211
Reflections with $I>2\sigma(I)$	178	205
R_{int}	0.0159	0.0136
h	-6 – 6	0 – 6
k	-4 – 4	-4 – 4
l	-11 – 11	0 – 12
Refinement		
[a]$R_1[F^2>2\sigma(F^2)]$	0.0232	0.0153
[b]$wR_2(F^2)$	0.0619	0.0378
Parameters	13	13
GOOF	1.456	1.266
Extinction	0.254(19)	0.085(5)
$\Delta\rho_{max}$ (eÅ^{-3})	1.156	1.069
$\Delta\rho_{min}$ (eÅ^{-3})	-2.607	-0.768

[a]$R_1=\sum\|F_o\|-|F_c\|/\sum|F_o|$, [b]$wR_2 = [\sum[w(F_o^2 - F_c^2)]/\sum[w(F_o^2)^2]]^{1/2}$
$w = 1/[\sigma^2(F_o^2)+(0.0344P)^2 + 0.1307P]$ and $w = 1/[\sigma^2(F_o^2)+(0.0181P)^2 + 0.2080P]$ for La and Ce respectively

Table 4.2 Selected Interatomic Distances for $LaCu_2(Al,Si)_5$ and $CeCu_2(Al,Si)_5$ (Å)

	$LaCu_2(Al,Si)_5$	$CeCu_2(Al,Si)_5$
Ce - M rectangular prisms		
Ce – *M* (x8)	3.2082(14)	3.1942(11)
M – *M* (*c*-axis, x4)	2.353(2)	2.337(2)
M – *M* (*ab*-plane, x4)	4.221(2)	4.2040(15)
Cu - N rectangular prisms		
Cu – *N* (x8)	2.5137(12)	2.5114(9)
N – *N* (*c*-axis, x4)	2.731(3)	2.749(2)
N – *N* (*ab*-plane, x4)	2.9847(14)	2.9727(11)

M = Cu/Al and *N* = Al/Si

Table 4.3 Atomic Positions and Thermal Parameters for *Ln*$Cu_2(Al,Si)_5$ (*Ln* = La, Ce)

Atom	Wyckoff position	*x*	*y*	*z*	Occupancy	U_{eq}(Å^2)[a]
La	1*a*	0	0	0	1.00	0.0050(3)
Cu	1*b*	0	0	½	1.00	0.0068(3)
Cu/Al (*M*)	2*h*	½	½	0.14862(14)	0.5/0.5	0.0056(3)
Al/Si (*N*)	4*i*	0	½	0.32749(17)	0.75/0.25	0.0086(4)
Ce	1*a*	0	0	0	1.00	0.00526(14)
Cu	1*b*	0	0	½	1.00	0.00639(18)
Cu/Al (*M*)	2*h*	½	½	0.14747(10)	0.5/0.5	0.00616(18)
Al/Si (*N*)	4*i*	0	½	0.32658(12)	0.75/0.25	0.0088(2)

[a]U_{eq} is defined as 1/3 of the trace of the orthogonalized U_{ij} tensor.

SEM/EDS experiments were completed using a Hitachi S-3600N Variable Pressure scanning electron microscope equipped with an energy dispersive spectrometer. The accelerating voltage was 15 kV with a beam to sample distance of 15 mm. These results are provided in Table 4.4. Four crystals each scanned 3 times resulting in 12 total compiled data points were used to determine composition for $CeCu_2(Al,Si)_5$. For the $LaCu_2(Al,Si)_5$ sample, a small aggregate of single crystals was selected and a total to 10 data points collected on separate single crystals in the aggregate were used to determine composition. The results of the elemental analysis showed Cu was present in stoichiometric ratios closer to 2 and additionally that Si was present at significant quantities close to one. In light of these findings the starting model was inspected for mixed occupancy of Cu and Al in a similar fashion to the mixing observed in

$EuAu_2Ga_5$ and $SrAu_2Ga_5$ [9]. It is worth noting that Cu/Al and Cu/Si mixing has been previously observed.[16,20] Modeling the 2*h* Wyckoff position as having mixed occupancy of Cu and Al resulted in more well behaved atomic displacement parameters, a disorder observed in both $LnNi_{1+x}Al_{6-x}$ and $LnPd_{1+x}Al_{6-x}$.[17,18] Additionally, the 4*i* Wyckoff position was disordered to represent occupancy of both Al and Si, resulting in a structural model that converged with small final difference residual peaks and well behaved atomic displacement parameters. Additionally, ground single crystal samples were characterized by powder X-ray diffraction with a Bruker AXS D8 Advance Diffractometer.

Table 4.4 Composition as Obtained from Energy Dispersive X-ray Spectroscopy

	$LaCu_2(Al,Si)_5$	$CeCu_2(Al,Si)_5$
Ln[a]	1.00(2)	1.00(2)
Cu	1.95(6)	1.96(4)
Al	4.14(7)	4.08(4)
Si	0.97(3)	0.95(3)
Ln:X[b]	1:7.07(9)	1:6.99(6)

[a] Composition is normalized to lanthanide.
[b] X = Cu, Al, and Si

4.2.3. Physical Properties

In light of small amounts of impurities on the single crystals after mechanical separation, polycrystalline samples of $CeCu_2(Al,Si)_5$ were used for magnetic measurements. Magnetic data were collected using a Quantum Design Magnetic Property Measurement System (MPMS). The temperature-dependent susceptibility data were measured under field-cooled (FC) conditions between 2.25 K to 400 K for $CeCu_2(Al,Si)_5$ under an applied field of 0.1 T. Field-dependent magnetization data were measured at 5, 7, 9, 11, 15, and 20 K with applied fields up to 5 T. The electrical resistivity measurements were measured on single crystals by the standard four-probe AC technique.

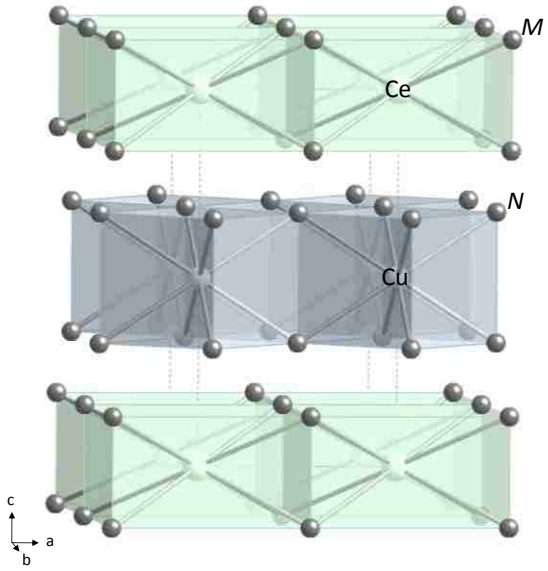

Figure 4.1 The crystal structure of $CeCu_2(Al,Si)_5$ is shown. (a) Ce (1*a*) atoms are represented with large light green spheres, Cu (1*b*) atoms are denoted as medium light blue spheres, Al/Cu (2*h*) atoms are denoted as *M* in small grey spheres, and Al/Si (4*i*) atoms are denoted as *N* in small grey spheres. Dashed lines show the unit cell. The local 8 coordinate Ce environment is shown as a light green translucent rectangular prism with the 8 coordinate Cu local environment shown as a translucent light blue rectangular prism.

4.3. Results and Discussion

4.3.1 Structure

The $SrAu_2Ga_5$ structure type has been shown to crystallize with a range compositions that more closely resemble the general formula $LnM_{2-x}Y_{5+x}$ where the x can have values up to 1 when M = Pd and Y = Ga. [8,9,17,18] Herein, $CeCu_2(Al,Si)_5$ will be discussed as the general structural model for both analogues, $LaCu_2(Al,Si)_5$ and $CeCu_2(Al,Si)_5$, as only unit cell parameters and interatomic distance change due to the lanthanide contraction. The pseudo-ternary $CeCu_2(Al,Si)_5$ crystallizes in the *P*4/*mmm* space group (No. 123) with lattice parameters of *a* = 4.2040(15) and c = 7.925(4), and the Ce, Cu, M, and N (M = Al/Cu and N = Al/Si) atoms occupying the 1*a*, 1*b*, 2*h*, and 4*i* Wyckoff position, respectively.

The structure of $CeCu_2(Al,Si)_5$ is shown in Figure 4.1, and can be best described as a stacking of rectangular prisms in alternating face/edge sharing arrangements rotated by 45 ° with

respect to the other in the crystallographic *c* direction. The local environments, as can been seen in Figure 4.1, of Ce (1*a*) can be described as a face-sharing 8-coordinate rectangular prismatic environment ($CeM_{8/4}$, M = Cu and Al) where the local environment of Cu (1*b*) can be described similarly as an edge-sharing rectangular prismatic environment ($CuN_{8/2}$, N = Al and Si). In $SrAu_2Ga_5$ the 2*h* position is equally occupied by Ga and Au.[9] In a similar fashion we observe an equal distribution of Cu and Al atoms on this position in $CeCu_2(Al,Si)_5$. Additional disorder was observed with Al and Si jointly occupying the 4*i* Wyckoff position. It is worthwhile to note that several synthetic attempts were made to grow Si free single crystals, all of which resulted in the isolation of undesired phases. Both the 2*h* and 4*i* positions were checked for Si occupancy, but only mixing the occupancy of the 4*i* position with Si lead to a stable structural model. It is difficult to refine structural models, obtained from X-ray diffraction, and isolate quantitative data relating to the chemical composition when constituents differ by only one atomic number (Si and Al). Therefore, the model was adjusted to reflect the composition of Si that resulted from SEM/EDS measurements; Cu was refined separately from the EDS results and independently reflected the values obtained from SEM/EDS. The final model resulted in a composition that reflected well the elemental composition found by SEM/EDS. Ce to M (M = Cu/Al) distances agree well with other compounds that share a similar disorder of Cu and Al mixing. Ce – Cu/Al distances in $CeCu_2(Al,Si)_5$ of 3.2086(16) agree well with previously reported distances observed in $Ce(Cu,Al)_{12}$ and $CeCuAl_3$ of 3.2427(10) and 3.245(12) respectively.[16,24] Cu – Al/Si distances in the title phase of 2.5126(18) agree well with distance found in related CuSi and CuAl containing phases [$Ce(Cu,Al)_{12}$ – 2.6972(7), $CeCu_2Al_3$ – 2.5893(1), $CeCu_2Si_2$ – 2.415, and CeCuSi – 2.4479(8)].[16,25-27]

4.3.2 Physical Properties

Figures 4.2 and 4.3 show the temperature dependence of the magnetic susceptibility of single crystal of $CeCu_2(Al,Si)_5$ measured with an applied field of 0.1 Tesla and the field dependence of magnetization at 3 K. The magnetic susceptibility was fit to a modified Curie-Weiss equation of the following form: $\chi(T) = \chi_0 + C/(T - \theta)$, where C represents the Curie constant and θ is the Weiss temperature in the paramagnetic state, and where χ_0 is representative of a constant background. The effective moments obtained from C were compared to the calculated values using $\mu_{eff} = g_J(J(J+1))^{1/2}$, they are both summarized in Table 4.5.

The temperature-dependent magnetic susceptibility of $CeCu_2(Al,Si)_5$ in an applied field of 0.1 T is shown in Figure 4.2. $CeCu_2(Al,Si)_5$ is paramagnetic down to 3 K and displays Curie-Weiss behavior above 200 K as can be seen in Figure 4.2. The recovered magnetic moment of 2.19 μ_B/mol Ce, fit over the range 200 – 400 K, which is somewhat lower than the calculated moment of 2.54 μ_B/mol for a free Ce^{3+} ion, $\chi_0 = 6.0x10^{-4}$. A negative Weiss constant, θ = -41.0 K, indicates strong antiferromagnetic correlations yet no clear transition is observed down to 3 K. The field-dependent magnetization up to 5 T at 5, 7, 9, 11, 15, and 20 K are presented in Figure 4.3 for $CeCu_2(Al,Si)_5$. The magnetization data above 10 K is linear and shows no sign of saturation where the data at 5, 7, and 9 K show a continually changing slope as would be expected for a paramagnet.

The observation of a somewhat smaller effective moment in $CeCu_2(Al,Si)_5$ is in good agreement with the $\mu_{eff(poly)}$ of 2.32 μ_B/mol Ce for $CePd_{1.5}Al_{5.5}$ ($\mu_{eff(poly)} = 2/3\ \chi_a + 1/3\ \chi_c$; T_c = 3 K).[18] Single crystals of $CePd_{1.5}Al_{5.5}$ displayed highly anisotropic magnetic behavior with μ_{eff} = 2.18 and 2.59 μ_B/mol Ce for H $\|$ *ab* and H $\|$ *c* respectively. Magnetic susceptibility on the single

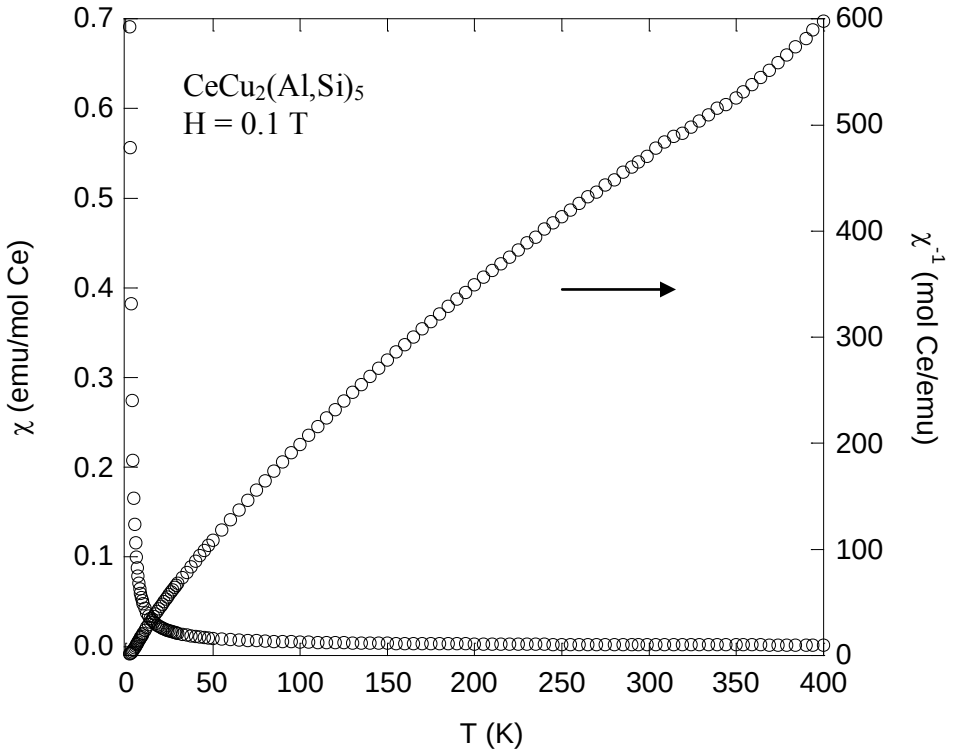

Figure 4.2 Molar magnetic susceptibility, χ_m = M/H (emu/mol), of $CeCu_2(Al,Si)_5$ as a function of temperature measured under an applied field of 0.1 T on the left axis, and inverse molar magnetic susceptibility, χ_m = H/M (mol/emu) as a function of temperature on the right axis.

crystals reveal a ferromagnetic transition at 3 K and θ_W values indicate that ferromagnetic correlations predominate in the *ab* plane (easy axis of magnetization) where antiferromagnetic correlations exist along the *c* axis (hard axis of magnetization). This is in markedly different then the magnetization observed in $CePdGa_6$, which orders antiferromagnetically in both crystallographically unique directions at 5 K.[7] The increase in disorder and change in lattice constants associated with $CeCu_2(Al,Si)_5$ could explain the suppression any magnetic transition below 2.25 K.

The electrical resistivity as a function of temperature for $CeCu_2(Al,Si)_5$ is shown in Figure 4.4. Metallic behavior is observed down to 10 K for $CeCu_2(Al,Si)_5$. Resistivity from 5 < T < 10 K increases with decreasing temperature reaching a maximum value at 5 K. A broad features above the minimum in the resistivity data and the upturn below the minimum is

consistent with Kondo behavior or increased scattering due to site disorder. A linear fit from the minimum to the magnetic transition in the resistivity (10 K < T < 5 K) scales linearly with the lnT, reinforcing Kondo behavior. This observation is not that surprising as most related analogues show heavy fermion behavior.[7,17,18] The peak in resistivity data at 5 K and a sudden drop in resistivity is possible due to reduced spin disorder scattering. The resistivity may reflect contamination from the $BaAl_4$ impurity as is was performed on single crystal samples. We currently await resistance data on the polycrystalline sample. Additionally, resistivity, 1 < T < 5 K, scales as T^2 indicative of electron-electron scattering, again consistent with the enhanced Sommerfeld coefficient. Magnetoresistance is shown in the inset of Figure 4.4 and is small and negative. This rules out the possibility of the sharp drop in resistivity at 5 K being due to a superconducting impurity phase.

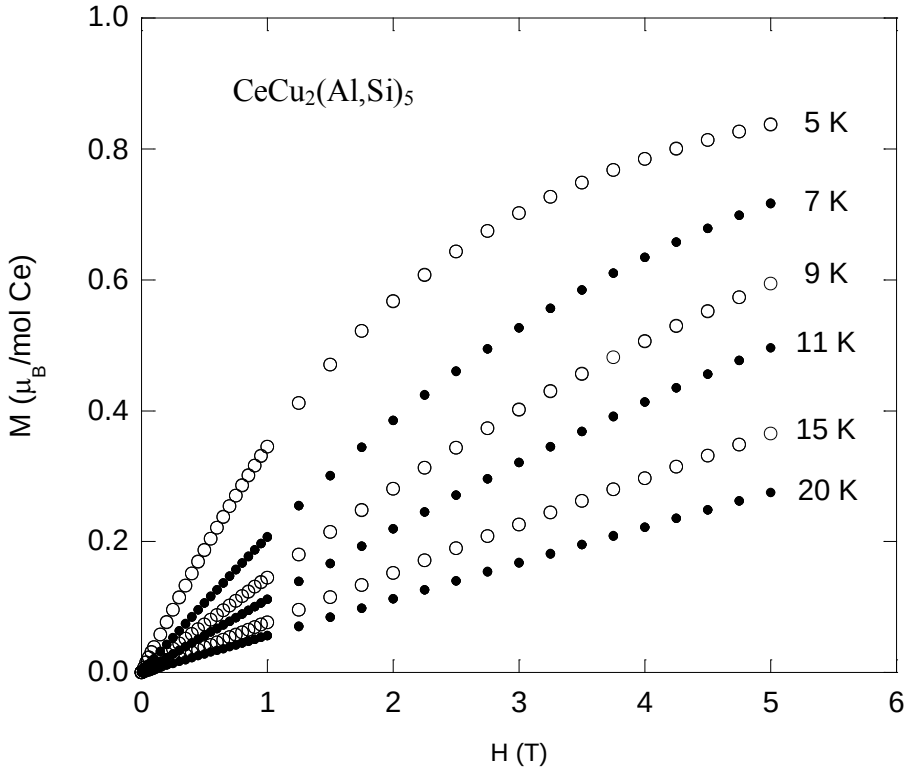

Figure 4.3 Magnetization of $CeCu_2(Al,Si)_5$ as a function of applied field at 5, 7, 9, 11, 15, and 20 K.

Table 4.5. Magnetic Properties of $CeCu_2(Al,Si)_5$.

	Applied field (T)	C	θ	μ_{calc} (μ_B)	μ_{eff} (μ_B)	Fit range (K)	Ordering, T_N (K)
$CeCu_2(Al,Si)_5$*	0.1	0.60(3)	-41.0	2.19	2.58	200-400	PM[a]

[a] paramagnetic

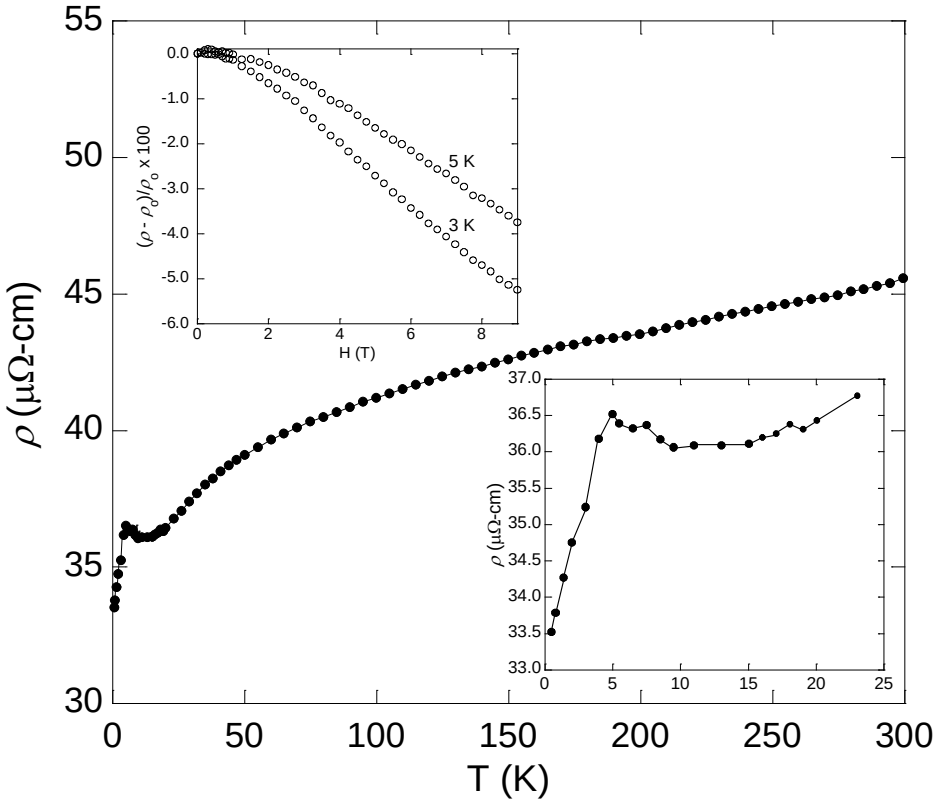

Figure 4.4 Electrical resistivity of $CeCu_2(Al,Si)_5$ as a function of temperature. The upper left inset shows the magnetoresistance, (%) [$((\rho - \rho_0)/\rho_0)$ x 100], as a function of applied field. The lower right inset is an enlarged view of the low temperature resistivity.

Single crystals of $LaCu_2(Al,Si)_5$ and $CeCu_2(Al,Si)_5$ were grown by the flux growth technique, and subsequent phase-pure polycrystalline samples were prepared by arc melting constituent elements in stoichiometric ratios and annealing. Single crystals of both $LaCu_2(Al,Si)_5$ and $CeCu_2(Al,Si)_5$ were characterized by single crystal X-ray diffraction and composition determined by SEM/EDXS. Polycrystalline samples were characterized by both powder X-ray diffraction, both in house and at Argonne's Advanced Photon Source. Polycrystalline samples were sent for physical property measurements. We have shown that

$CeCu_2(Al,Si)_5$ does not order and remains paramagnetic down to 2.25 K. In addition, the transport behavior of $CeCu_2(Al,Si)_5$ is consistent with Kondo interactions but may have contributions from a $BaAl_4$ type impurity.

4.4 References

(1) Hegger, H., Petrovic, C., Moshopoulou, E.G., Hundley, M.F., Sarrao, J.L., Fisk, Z., and Thompson, J.D., Pressure-induced superconductivity in quasi-2D $CeRhIn_5$. *Phys. Rev. Let.* **2000,** *84*, 4986.

(2) Macaluso, R.T., Sarrao, J.L., Moreno, N.O., Pagliuso, P.G., Thompson, J.D., Fronczek, F.R., Hundley, M.F., Malinowski, A., and Chan, J.Y., Single-crystal growth of Ln_2MIn_8 (Ln = La, Ce; M = Rh, Ir): implications for the heavy-fermion ground state. *Chem. Mater.* **2003,** *15*, 1394-1398.

(3) Moshopoulou, E.G., Fisk, Z., Sarrao, J.L., and Thompson, J.D., Crystal growth and intergrowth structure of the new heavy fermion materials $CeIrIn_5$ and $CeRhIn_5$. *J. Solid State Chem.* **2001,** *158*, 25-33.

(4) Moshopoulou, E.G., Sarrao, J.L., Pagliuso, P.G., Moreno, N.O., Thompson, J.D., Fisk, Z., and Ibberson, R.M., Comparison of the crystal structure of the heavy-fermion materials $CeCoIn_5$, $CeRhIn_5$ and $CeIrIn_5$. *Appl. Phys. A-Mater.* **2002,** *74*, s895-s897.

(5) Petrovic, C., Movshovich, R., Jaime, M., Pagliuso, P.G., Hundley, M.F., Sarrao, J.L., Fisk, Z., and Thompson, J.D., A new heavy-fermion superconductor $CeIrIn_5$: A relative of the cuprates? *Europhys. Lett.* **2001,** *53*, 354.

(6) Petrovic, C., Pagliuso, P.G., Hundley, M.F., Movshovich, R., Sarrao, J.L., Thompson, J.D., Fisk, Z., and Monthoux, P., Heavy-fermion superconductivity in $CeCoIn_5$ at 2.3 K. *J. Phys. Condens. Mat.* **2001,** *13*, L337.

(7) Macaluso, R.T., Millican, J.N., Nakatsuji, S., Lee, H.-O., Carter, B., Moreno, N.O., Fisk, Z., and Chan, J.Y., A comparison of the structure and localized magnetism in Ce_2PdGa_{12} with the heavy fermion $CePdGa_6$. *J. Solid State Chem.* **2005,** *178*, 3547-3553.

(8) Macaluso, R.T., Nakatsuji, S., Lee, H., Fisk, Z., Moldovan, M., Young, D.P., and Chan, J.Y., Synthesis, structure, and magnetism of a new heavy-fermion antiferromagnet, $CePdGa_6$. *J. Solid State Chem.* **2003,** *174*, 296-301.

(9) Cordier, G., Dietrich, C., and Friedrich, T., Crystal structures of europium digold pentagallide, $EuAu_2Ga_5$ and strontium digold pentagallide, $SrAu_2Ga_5$. *Z. Kristallogr.* **1996,** *211*, 627-628.

(10) Chen, X.Z., Small, P., Sportouch, S., Zhuravleva, M., Brazis, P., Kannewurf, C.R., and Kanatzidis, M.G., Molten Ga as a solvent for exploratory synthesis: The new ternary polygallide Sm_2NiGa_{12}. *Chem. Mater.* **2000,** *12*, 2520.

(11) Cho, J.Y., Millican, J.N., Capan, C., Sokolov, D.A., Moldovan, M., Karki, A.B., Young, D.P., Aronson, M.C., and Chan, J.Y., Crystal growth, structure, and physical properties of Ln_2MGa_{12} (Ln = La, Ce; M = Ni, Cu). *Chem. Mater.* **2008,** *20*, 6116-6123.

(12) Thomas, K.R., Cho, J.Y., Millican, J.N., Hembree, R.D., Moldovan, M., Karki, A., Young, D.P., and Chan, J.Y., Crystal growth and physical properties of Ln_2MGa_{12} (*Ln* = Pr, Nd, and Sm; *M* = Ni, Cu). *J. Cryst. Growth* **2010,** *312*, 1098-1103.

(13) Romaka, V.A., Grin, Y.N., and Yarmolyuk, Y.P., Magnetic and crystallographic characteristics of rare earth metal-nickel-gallium ($RENiGa_4$) compounds. *Ukr. Fiz. Zh.* **1983,** *28*, 1095-1097.

(14) Menard, M.C., Drake, B.L., McCandless, G.T., Thomas, K.R., Hembree, R.D., Haldolaarachchige, N., DiTusa, J., Young, D.P., and Chan, J.Y., A Tale of Two Polymorphs: Growth and Characterization of α-$LnNiGa_4$ (Ln = Y, Gd-Yb) and β–$LnNi_{1-x}Ga_4$ (Ln = Tb-Er). *Eur. J. Inorg. Chem.* **2011,** *In Press*, .

(15) Cho, J.Y., Capan, C., Young, D.P., and Chan, J.Y., Crystal growth, structure, and physical properties of $SmCu_4Ga_8$. *Inorg. Chem.* **2008,** *47*, 2472-2476.

(16) Drake, B.L., Capan, C., Cho, J.Y., Nambu, Y., Kuga, K., Xiong, Y.M., Karki, A.B., Nakatsuji, S., Adams, P.W., Young, D.P., and Chan, J.Y., Crystal growth, structure, and physical properties of $Ln(Cu,Al)_{12}$ (Ln = Y, Ce, Pr, Sm, and Yb) and $Ln(Cu,Ga)_{12}$ (Ln = Y, Gd-Er, and Yb). *J. Phys. Condens. Mat.* **2010,** *22*, 066001.

(17) Gout, D., Benbow, E., Gourdon, O., and Miller, G.J., Composition-structure relationships in polar intermetallics: experimental and theoretical studies of $LaNi_{1+x}Al_{6-x}$ (x = 0.44). *Inorg. Chem.* **2004,** *43*, 4604-4609.

(18) Tobash, P.H., Ronning, F., Thompson, J.D., Bobev, S., and Bauer, E.D., Magnetic order and heavy fermion behavior in $CePd_{1-x}Al_{6-x}$: Synthesis, structure, and physical properties. *J. Solid State Chem.* **2010,** *183*, 707-711.

(19) Cho, J.Y., Thomas, E.L., Nambu, Y., Capan, C., Karki, A.B., Young, D.P., Kuga, K., Nakatsuji, S., and Chan, J.Y., Crystal growth, structure, and physical properties of $Ln(Cu,Ga)_{13-x}$ (Ln = La-Nd, Eu; x ~ 0.2). *Chem. Mater.* **2009,** *21*, 3072-3078.

(20) Drake, B.L., Kangas, M.J., Capan, C., Haldolaarachchige, N., Xiong, Y.M., Adams, P.W., Young, D.P., and Chan, J.Y., Crystal growth, structure, and physical properties of $Ln(Ag,Al,Si)_2$ (Ln = Ce and Gd). *J Phys. Condens. Mat.* **2010,** *22*, 426002.

(21) Canfield, P.C. and Fisk, Z., Growth of single crystals from metallic fluxes. *Philos. Mag. B* **1992,** *65*, 1117-1123.

(22) Altomare, A., Burla, M.C., Camalli, M., Luca, G.L., Gaicovazzo, C., Guagliardi, A., Moliterni, A.G.G., Polidori, G., and Spagna, R., SIR97: a new tool for crystal structure determination and refinement. *J. Appl. Cryst.* **1999,** *32*, 115.

(23) Sheldrick, G.M., A short history of SHELX. *Acta Crystallogr. A* **2008,** *64*, 112-122.

(24) Zarechnyuk, O.S., Kripyakevich, P.I., and Gladyshevskii, E.I., Ternary intermetallic compounds with a $BaAl_4$-type superlattice. *Kristallografiya* **1964,** *9*, 835-838.

(25) Kim, S.M., Buyers, W.J.L., Lin, H., and Bauer, E., Structure of the heavy electron compounds cerium-copper-aluminum ($Ce(Cu_xAl_{1-x})_5$) and cerium-copper-gallium ($Ce(CuxGa_{1-x})_5$), [$0.6 \leq x \leq 0.8$] *Z. Phys. B. Con. Mat.* **1991,** *84*, 201-203.

(26) Bodak, O.I., Gladyshevskii, E., and Kripyakevich, P.I., Crystal structure of the compound $CeNi_2S_2$ and isostructural compounds in related systems. *Izv. An. SSSR.* **1966,** *2*, 1861-1864.

(27) Landelli, A., A low temperature crystal modification of the rare earth ternary compounds RCuSi. *J. Less-Common Met.* **1983,** *90*, 121-126.

CHAPTER 5. OTHER COLLABORATIVE PROJECTS AND CONCLUSIONS

5.1 Introduction

As a materials science group, our focus is on the growth and structural characterization of new materials with a concomitant interest in their physical properties. Simply growing a material is not enough. Materials science, by its nature, is intrinsically interdisciplinary. When we design or discover new materials, we want to know what are the properties of the material and how are they derived through the interaction of the charge, spin, and lattice degrees of freedom. This is not a question of one strict discipline, but rather a question that easily spills into chemistry, crystallography, physics, and in some labs, biology. We rely heavily upon our collaborators for the physical property measurements as they often rely on or groups expertise for structural elucidation. Understanding our and our collaborators areas of strength, allows for a more complete end product while minimizing the overhead.

The works in the preceding chapters would not have been possible if it were not for the collaborations with outside groups. The remaining work presented in this chapter is more eclectic, as the projects described herein are more collaborative in nature and represent my contribution to the future final product. They include projects that contain contributions from both internal and external group collaborations. I feel it to be best to begin with a discussion of my contributions to a series of gallium containing materials (Ln(Cu,Al,Ga)$_{13-x}$, Ln_4FeGa$_{12}$, and two polymorphs α and β LnNiGa$_4$) that involve both internal and external collaborative efforts.

5.2 Lanthanide and Transition Metal Containing Gallides (Ln(Cu,Al,Ga)$_{13-x}$, α and β LnNiGa$_4$, and Ln_4FeGa$_{12}$)

5.2.1 Ln(Cu,Al,Ga)$_{13-x}$ (Ln = La, Ce, Pr, and Eu)

5.2.1.1 Introduction

Intermetallic compounds adopting the NaZn$_{13}$ structure-type display highly correlated electron behavior and are of great interest to the solid state physicists and chemists.[1,2] Examples

of such behavior are found in the compounds UBe_{13} and $CeBe_{13}$. UBe_{13} was reported to be a heavy-fermion compound defined by the anomalously large electronic specific-heat coefficient $\gamma \sim 1100$ mJ mol^{-1} K^{-2} at low temperatures and shows an unconventional superconducting state mediated by *f*-electrons below 0.85 K.[3-7] Enhanced mass ($\gamma \sim 58$ mJ mol^{-1} K^{-2}) has also been reported for $CeBe_{13}$ which is a mixed-valence system.[6,8]

Heavy-fermion behavior is commonly associated with the valence instability of the 4*f* electrons in Ce-, U-, or Yb-based compounds.[1,9-11] However, more recently several Pr-based heavy-fermion compounds have been reported. Heavy-fermion behavior in Pr-based intermetallic compounds is exotic as it is well-known that the localized $4f^2$-electrons of Pr^{3+} ions are stable. The Heusler-type $PrInAg_2$ ($\gamma \approx 6500$ mJ mol^{-1} K^{-2}) has been reported as the first Pr-based heavy-fermion compound and its resistivity is not quadratic in T.[12-15] Previously we have reported that $Pr(Cu,Ga)_{13}$ shows heavy fermion behavior with $\gamma \sim 100$ mJ mol^{-1} K^{-2} and it follows what is expected for the Kadowaki-Woods relation (0.727×10^{-5}).[16-18]

In light of the discovery of an enhanced mass state in $Pr(Cu,Ga)_{13}$, it was of interest how a systematic shift to Al would impact the low temperature physics. Early attempts to grow $Pr(Cu,Al)_{13}$ were unsuccessful. The addition of Ga metal as a second flux to suppress the melting temperature of Al led to crystallization of large (> 5 x 5 x 5 mm^3) cubes of $Ln(Cu,Ag,Ga)_{13}$ (Ln = La, Ce, Pr, and Eu). A survey of the literature reveals that $CeCu_{6.5}Al_{6.5}$ was successfully grown and single crystal data collection reveals mixed occupancy on both the 96*i* and 8*b* Wyckoff positions.[19] It is also worth noting that $Ln(Cu,Al)_{13}$ (*Ln* = Nd and Eu) shows the onset of ferromagnetism at 6 and 16 K respectively, however $Ln(Cu,Ga)_{13}$ (*Ln* = La, Ce, Pr, Nd, and Eu) remain paramagnetic down to 3 K for all analogues. The unit cell volumes for the Eu analogues reported were as follow: $Eu(Cu,Al)_{13}$ (V ~ 1697) and $Eu(Cu,Ga)_{13}$ (V ~ 1683 $Å^3$).

An increase in the *Ln* - *Ln* nearest-neighbor distance resulted in a switch from paramagnetic coupling to ferromagnetic coupling. Interestingly, the unit cell volume found for $Eu(Cu,Al,Ga)_{13}$ is V ~ 1701 $Å^3$, a slight increase from $Eu(Cu,Al)_{13}$ and not expected from Al/Ga disorder. Understanding how Cu, Ga, and Al are disordered could shed light, not only on the enhancement or disappearance of an enhanced mass state in $Ln(Cu,Al,Ga)_{13}$ for *Ln* = Pr and Eu, but how the magnetic coupling is impacted for the Eu analogue with further lattice expansion.

As mentioned above, the previously reported pseudo-binary analogues of $Ln(Cu,Ga)_{13}$ (*Ln* = La, Ce, Pr, Nd, and Eu), Cu and Ga preferentially disorder on the 96*i* Wyckoff position. SEM/EDS measurements support the off stoichiometric ratios of $Ln(Cu,Al,Ga)_{13}$ (Ln = La, Ce, Pr, and Eu). These cubic crystals were cleaved so we could ensure the appearance of Ga was not just at the surface. Cleaved crystals of each analogue were oriented such that EDS studies could be performed on the surface and interior of each crystal. This confirmed the presence of Ga both at the surface and throughout the single crystal. In addition to mixed occupancy in $Ln(Cu,Ga)_{13}$ on the 96*i* position, the 8*b* Wyckoff position is partially occupied. We have collected single crystal X-ray diffraction data for $Ln(Cu,Al,Ga)_{13}$ (*Ln* = La, Ce, and Pr) analogues. Multiple attempts to model the disorder in single crystal X-ray diffraction data have failed. The degree of disorder and similarities of Cu and Ga X-ray structure factors result in models that do not converge if the disorder is probed.

5.2.1.2 Synthesis

Single crystals of $Ln(Cu,Al,Ga)_{13-x}$ (*Ln* = La – Pr and Eu) were grown in the presence of excess Al and Ga mixed metal flux.[20] *Ln* (3N, chunks, Alfa Aesar), Cu (5N, powder, Alfa Aesar), Al (5N, pellets, Alfa Aesar) and Ga (7N, pellets, Alfa Aesar) were used as received and loaded into an alumina crucible with a reaction ratio of 1:9:10:10 for *Ln*:Cu:Al:Ga respectively.

Rare earth elements are stored in vacuum desiccators to prevent oxidation (0.1 mmHg). The crucibles were placed into a fused silica tube and the contents were evacuated (0.05 – 0.07 mmHg) and sealed. The charged vessel capped with silica wool was loaded into a furnace and heated to a dwell temperature of 1100 °C for 10 h at 200 °C/h. Samples were slowly cooled to a final dwell temperature of 480 °C at a rate of 2 °C/h upon which the samples were centrifuged to separate crystals from the Al and Ga flux. In all growths, silver metallic crystals were retrieved via etching in NaOH (1-3 M) or 6 M I_2 in DMF until excess aluminum or Ga was removed. The crystals were subsequently cleaned with 10% HNO_3, retrieving flux-free single crystals which were observed to be air stable. Crystal morphology is best described as large (1 – 5 mm) faceted cubes for all analogues as can be seen in the collage in chapter 1, Figure 1.1.

The central theme of our research group has been, and continues to be, the discovery of novel, highly correlated electron systems in large, single crystal form. These systems are known to exhibit exotic properties such as heavy fermion behavior as mentioned above. Moreover, we employ the flux-growth method to discover and grow large single crystalline materials so that we may accurately determine structure/physical property relationships. The ability to derive correlations between the crystal structure and physical property measurements such as: directional magnetic anisotropic, transport measurements, and the electronic structure necessitates the need for high quality single crystals. This project currently awaits neutron beam line time at Oak Ridge National Lab (ORNL) using the TOPAZ single crystal beam line such that the nature of the Cu/Al/Ga disorder may be probed.

5.2.2 α-*Ln*$NiGa_4$ (*Ln* = Y, Gd-Yb) and β-*Ln*$Ni_{1-x}Ga_4$ (*Ln* = Tb-Er)

5.2.2.1 Synthesis

Synthesis was achieved by melting *Ln*-Ni-Ga constituents with a reaction ratio of 1.5:1:15 for both the *α*-*Ln*$NiGa_4$ (*Ln* = Y, Gd-Yb)[21] and *β*-*Ln*$Ni_{1-x}Ga_4$ (*Ln* = Tb-Er). Careful

selection of the cooling regime allowed for phase segregation and isolation of single crystals. More synthetic details are given in Figure 5.1.

5.2.2.2 Physical Properties

Figure 5.2 shows the temperature dependent magnetic susceptibility, χ_m, of β-*Ln*$Ni_{1-x}Ga_4$ (*Ln* = Tb-Er) measured under zero-field-cooled conditions from 2 K to 300 K with an applied field of 0.1 T perpendicular to the direction of the plate, and the inset of Figure 5.2 shows the inverse susceptibility, χ_m^{-1}, for the same series. All analogues, Tb-Er, were fit with a modified Curie-Weiss equation of the form: $\chi(T) = \chi_0 + C/(T - \theta_W)$, where C is the Curie constant, θ_W is the Weiss temperature (K), and χ_0 is a constant, representative of any Larmor diamagnetic, Pauli paramagnetic, and background contributions to the magnetic susceptibility. In all cases, the modified Curie-Weiss equation was fit over the linear region of χ_m^{-1}. Table 5.1 gives a summary of the magnetic properties of β-*Ln*$Ni_{1-x}Ga_4$ (*Ln* = Tb-Er), including the T_N, μ_{eff} (calculated and experimental), θ_W, and fit range. When making reference to the applied field and its direction relative to the *c*-axis, crystals grew as plate-like aggregates, and directions were assigned as the *c*-axis being perpendicular to the plates for β-*Ln*$Ni_{1-x}Ga_4$ (*Ln* = Tb-Er).

β-*Ln*$Ni_{1-x}Ga_4$ (*Ln* = Tb, Dy, and Er) undergoes an antiferromagnetic transition (T_N) at ~7, 3.5, and 7 K, respectively, with the Ho analogue remaining paramagnetic down to 2 K with H = 0.1 T. The inset of Figure 5.2 shows the inverse magnetic susceptibility, $\chi_m^{-1}(T)$. Above 20 K for $H \| c$, the series exhibits paramagnetic Curie type behavior. The magnetic properties of β-$TbNi_{0.9(1)}Ga_4$ are similar to that of $TbNiGa_3Ge$ (T_N ~ 5 K and observed μ_{sat} ~ 3 μ_B).[22] Fitting the data above 25 K for Tb and Dy and above 20 K for Ho and Er, respectively, resulted in θ_W = –43.6(5), –22.7(2), –14.1(5), and –6.1(1) K for Tb, Dy, Ho, and Er, respectively. The negative θ_W values indicate that antiferromagnetic coupling predominates and are consistent with the

ordering observed for both $TbNi_{0.9(1)}Ga_4$, $DyNi_{0.9(1)}Ga_4$, and $ErNi_{0.9(1)}Ga_4$. Frustration values, $|\theta_W|/T_N$, of 2-5 are considered typical for an antiferromagnetic system.[23] A quick assessment of Tb and Dy reveal values close to 7, an intermediate value for frustration, as values of 10 and larger are typically considered frustrated.[23] The frustration parameters, 6.2, 6.5, >10, and 0.9 for Tb, Dy, Ho, and Er analogues respectively, indicate increasing frustration across the series β-$Ln Ni_{0.9(1)}Ga_4$ (*Ln* = Tb-Ho), followed by a decrease in magnetic frustration in β-$ErNi_{0.8(1)}Ga_4$.[23] The decrease in magnetic frustration on moving across the series β-$LnNi_{1-x}Ga_4$ (*Ln* = Tb, Dy, and Er) is consistent with decreasing structural frustration as seen in the increasing *Ln*-Ga4/Ga5 interatomic distances, when comparing β-$HoNi_{0.9(1)}Ga_4$ and β-$ErNi_{0.8(1)}Ga_4$. The disorder in the local environment of the *Ln* in β-$LnNi_{1-x}Ga_4$ (*Ln* = Tb-Er) can be attributed to the varying local electronic environment of the *Ln* which manifests as magnetic frustration; the spin-glass behavior observed in $Ce_2Ag_{1-x}Ga_{10-y}$,[24] Ce_2CuSi_3,[25] and Ce_2CuGe_3[26] has been attributed to such structural disorder in the local Ln^{3+} environments. Frustration due to structural disorder in β-$LnNi_{1-x}Ga_4$ (*Ln* = Tb-Er) is consistent with the large discrepancy between T_N and θ_W in β-$LnNi_{1-x}Ga_4$ (*Ln* = Tb-Er), as shown in Table 5.1.

Table 5.1 Magnetic Properties of β-$LnNi_{1-x}Ga_4$ (*Ln* = Tb-Er)

	T_N (K)	μ_{eff} (μ_B) calculated	μ_{eff} (μ_B) experimental	θ_W (K)	T (K)
β-$TbNi_{0.9(1)}Ga_4$	7	9.72	9.8(1)	-43.6(5)	25-300
β-$DyNi_{0.9(1)}Ga_4$	3.5	10.65	10.5(1)	-22.7(2)	25-300
β-$HoNi_{0.9(1)}Ga_4$	-----	10.61	10.5(2)	-14.1(5)	20-300
β-$ErNi_{0.8(1)}Ga_4$	7	9.58	8.9(2)	-6.1(1)	20-300

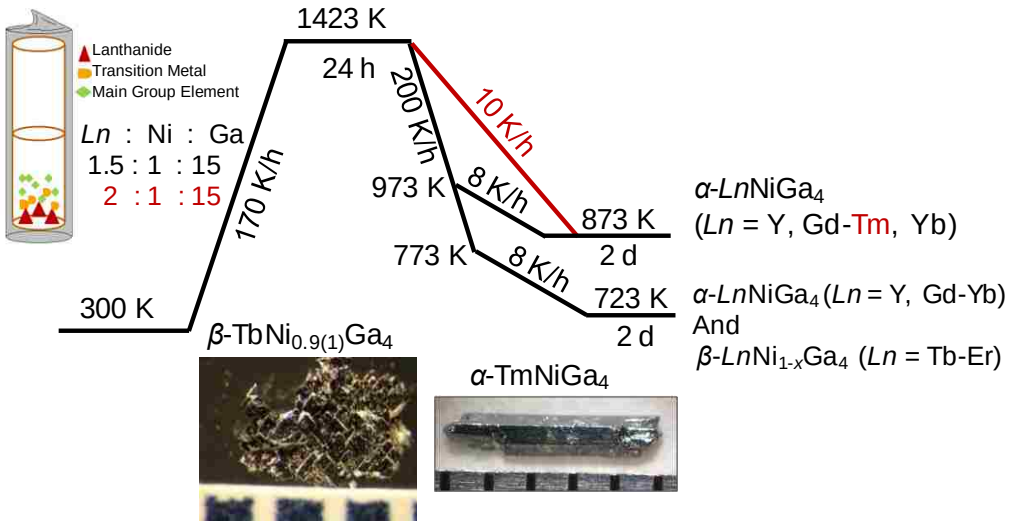

Figure 5.1 Depiction of the temperature profile used to grow both the α- and β- *Ln*NiGa$_4$. Below the temperature profile are optical images of the β- TbNiGa$_4$ α- TmNiGa$_4$ analogues.

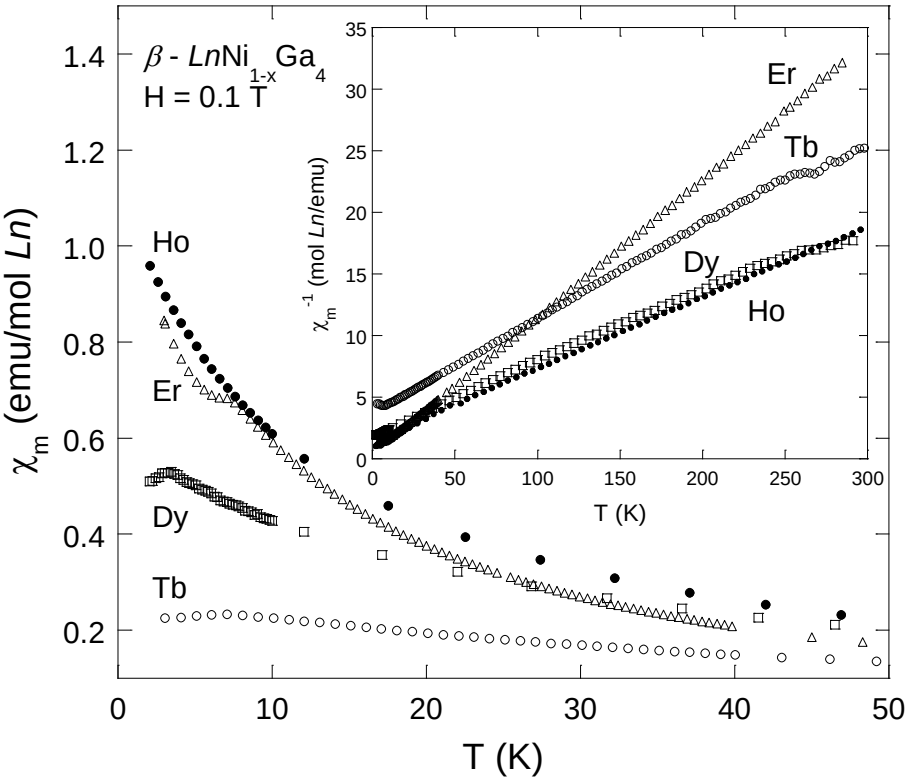

Figure 5.2 Magnetic susceptibility, χ_m = M/H (emu/mol *Ln*), as a function of temperature, T (K), with an applied field of H = 0.1 T for *β*-TbNi$_{0.9(1)}$Ga$_4$ (open circles), *β*-DyNi$_{0.9(1)}$Ga$_4$ (open squares), *β*-HoNi$_{0.9(1)}$Ga$_4$ (closed circles), and *β*-ErNi$_{0.8(1)}$Ga$_4$ (open triangles). The inset shows the inverse magnetic susceptibility, χ_m^{-1} = H/M (mol *Ln*/emu).

The magnetic moments recovered, 9.8(1), 10.5(1), 10.5(2), and 8.9(2) μ_B for Tb, Dy, Ho, and Er analogues of β-*Ln*$Ni_{1-x}Ga_4$ are in good agreement with the calculated spin-only effective moments of 9.72, 10.65, 10.61, and 9.5 μ_B for trivalent Tb, Dy, Ho, and Er, respectively. In all cases, the recovered moment is reflective of the respective Ln^{3+} (*Ln* = Tb-Er) moment, which indicates that Ni atoms show no localized magnetic moment, and their contribution to the magnetism is diamagnetic. Additionally, the relationship between θ_W (K) and nearest *Ln-Ln* distance (Å) for the α-*Ln*$NiGa_4$ (*Ln* = Gd – Yb) series, as obtained from Romaka *et. al.*,[27] and for the β-*Ln*$Ni_{1-x}Ga_4$ (*Ln* = Tb-Er) series, as obtained from this work, is shown in Figure 5.3. The trend for the β-*Ln*$Ni_{1-x}Ga_4$ (*Ln* = Tb–Er) series is similar to that of the α-*Ln*$NiGa_4$ (*Ln* = Gd – Yb) series indicating the mechanism for the magnetism of both the α-*Ln*$NiGa_4$ and β-*Ln*$Ni_{1-x}Ga_4$ phases are similar.[27] The similarity in scaling between the two polymorphs would be expected as the nearest *Ln* – *Ln* distances are similar.

The field dependence of the magnetization at 3 K for each β-*Ln*$Ni_{1-x}Ga_4$ analogue is shown in Figure 5.4. The expected saturated moment for a free Tb^{3+} ion is 9.0 μ_B. β-$TbNi_{0.9(1)}Ga_4$ does not saturate in an applied field up to 9 T and reaches a maximum value of ~ 3.3 μ_B. The absence of saturation is common for an antiferromagnetic compound. Similarly, the magnetization of β-$DyNi_{0.9(1)}Ga_4$ increases linearly up to 5 T, at which point a decrease in slope is observed. For applied fields of $5 < H < 9$ T for β-$DyNi_{0.9(1)}Ga_4$, a linear increase is observed with maximum saturated moment of 5.6 μ_B at 9 T (μ_{sat} = 10.0 μ_B for Dy^{3+}). β-$HoNi_{0.9(1)}Ga_4$ does not order magnetically down to 2 K, as noted from the magnetic susceptibility. This is reinforced by the magnetization data collected at 3 K. The magnetization of β-$HoNi_{0.9(1)}Ga_4$ is linear at low applied fields ($H < 3$ T) with fields larger than 3 T, and a change in slope is observed, indicative of the onset of spin saturation in a paramagnet. A maximum value of 6.5 μ_B at 9 T is recovered

(μ_{sat} = 10.0 μ_B for Ho^{3+}). Under low applied field, the magnetization of β-$ErNi_{0.8(1)}Ga_4$ is very similar to β-$HoNi_{0.9(1)}Ga_4$ with linear magnetization. Instead, a change of slope is observed when larger than 2 T external fields are applied with a maximum of ~ 4.9 μ_B at 9 T.

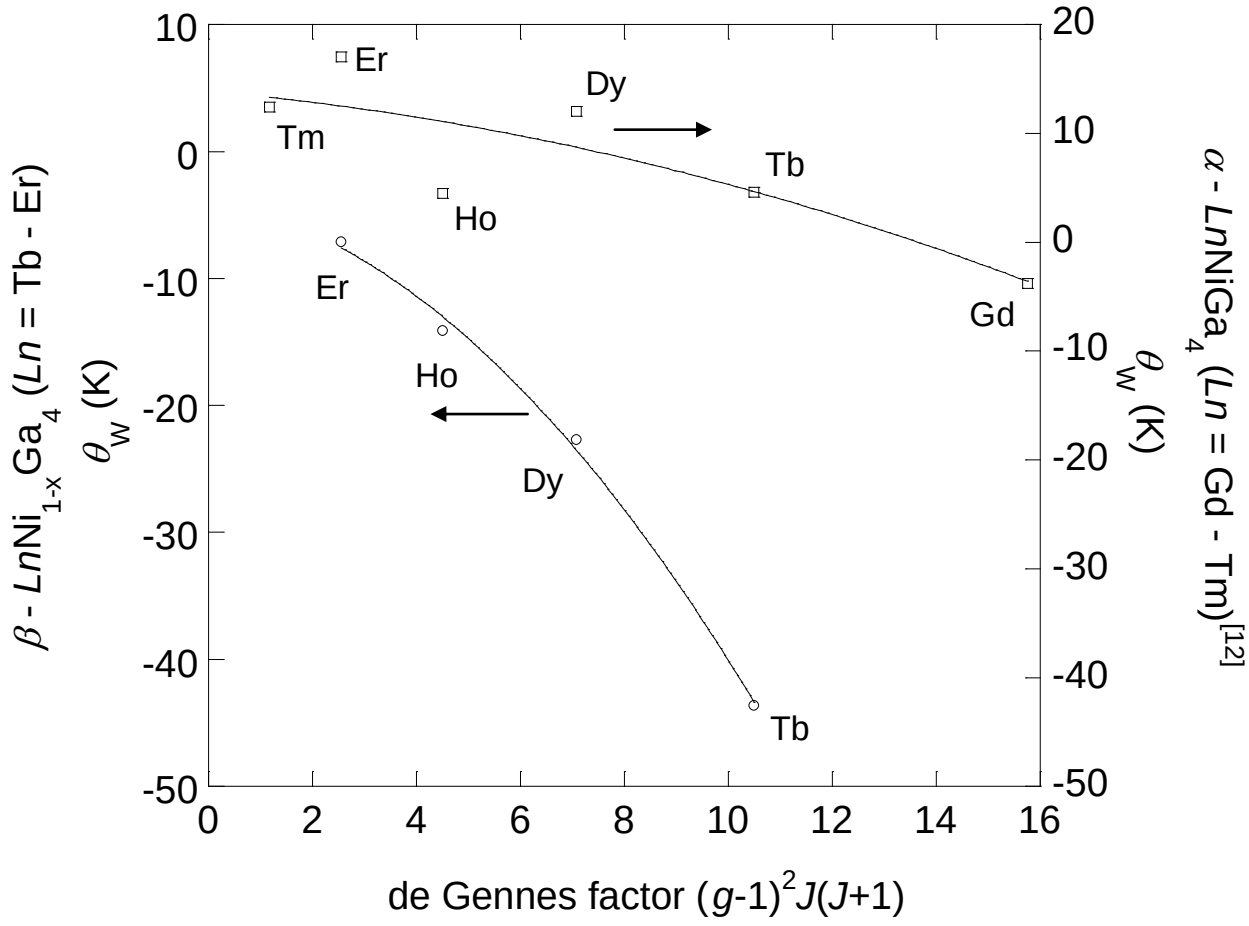

Figure 5.3 The variation of θ_W (K) as a function of de Gennes factor for the α-$Ln$$NiGa_4$ (Ln = Gd – Tm, open squares) series, as obtained from Romaka *et al.*,[27] and the β-$Ln$$Ni_{1-x}Ga_4$ (Ln = Tb – Er, open circles) series, as obtained from this work. α-$Ln$$NiGa_4$ (Ln = Gd – Tm) corresponds to the right (y) axis where β-$Ln$$NiGa_4$ (Ln = Tb – Er) corresponds to the left (y) axis.

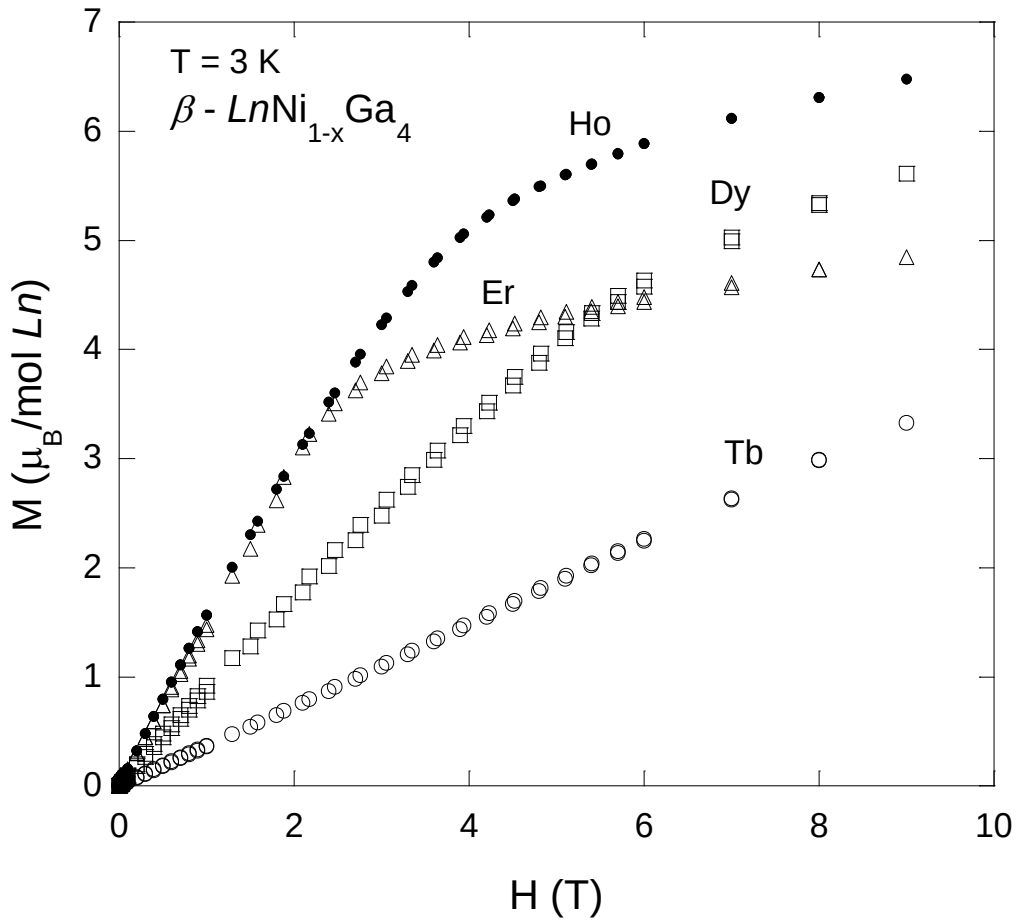

Figure 5.4 Isothermal magnetization of β-$TbNi_{0.9(1)}Ga_4$ (open circles), β-$DyNi_{0.9(1)}Ga_4$(open squares), β-$HoNi_{0.9(1)}Ga_4$ (closed circles), and β-$ErNi_{0.8(1)}Ga_4$ (open triangles) as a function of applied field at T = 3 K. Data were recorded while sweeping between 0 to 9 T.

The resistance data for β-$LnNi_{1-x}Ga_4$ (*Ln* = Tb-Er) are shown in Figure 5.5 (with β-$ErNi_{0.8(1)}Ga_4$ shown in the inset) with all analogues displaying metallic behavior down to 3 K. RRR values [ρ(290 K)/ρ(3 K)] of 3.8, 2.0, 1.4, and 6.0 for the Tb, Dy, Ho, and Er analogues, respectively, are fairly small and attest to the structural disorder. Additionally, a positive magnetoresistance [MR = ($\rho(H) - \rho(H = 0)$)/ $\rho(H = 0)$] was measured to be 26, 17, 12, and 67% for Tb, Dy, Ho, and Er β-$LnNi_{1-x}Ga_4$ analogues at 9 T, respectively, are indicative of a classical mechanism for Tb, Dy, and Ho, while the Er sample shows enhanced scattering upon application of an external field (the Er sample also showed the largest RRR value).

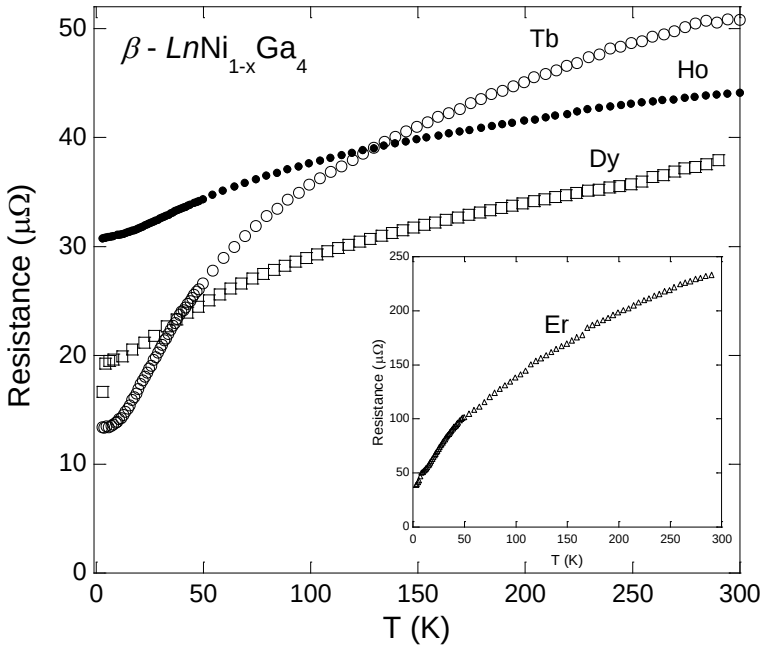

Figure 5.5 The electrical resistance of β-$TbNi_{0.9(1)}Ga_4$ (open circles), β-$DyNi_{0.9(1)}Ga_4$(open squares), β-$HoNi_{0.9(1)}Ga_4$ (closed circles), and β-$ErNi_{0.8(1)}Ga_4$ (open triangles, inset) as a function of temperature is shown.

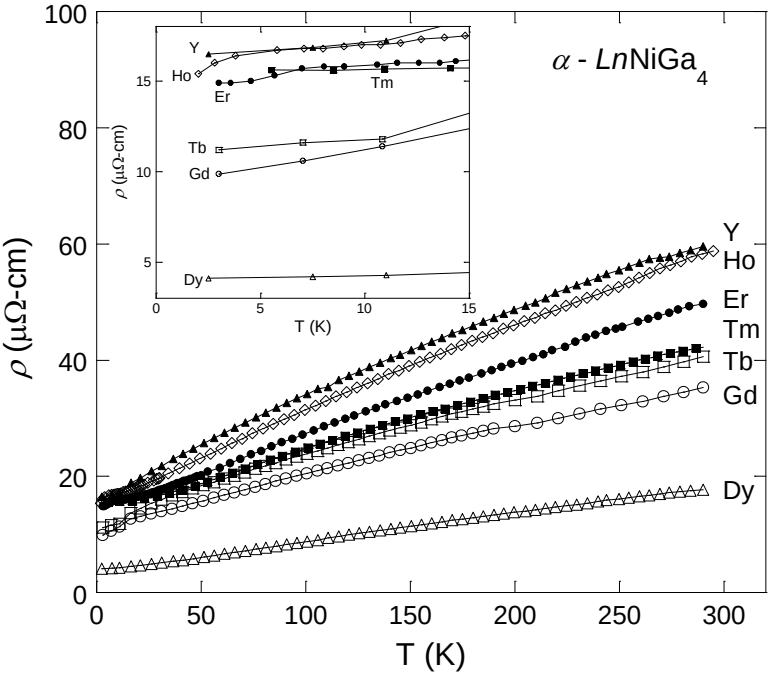

Figure 5.6 The electrical resistivity of α-$GdNiGa_4$ (open circles), α-$TbNiGa_4$ (open squares), α-$DyNiGa_4$ (open triangles), α-$HoNiGa_4$ (open diamonds), α-$ErNiGa_4$ (closed circles), α-$TmNiGa_4$ (closed squares), and α-$YNiGa_4$ (closed triangles) as a function of temperature is shown. The inset shows the low temperature resistivity for clarity.

The resistivity data for α-*Ln*$Ni_{0.9(1)}Ga_4$ (*Ln* = Y, Gd – Tm) are shown in Figure 5.6. All analogues show metallic behavior down low temperature, with the Tm analogue showing metallic behavior down to 5 K. However the Er analogue does not follow the Ho analogue's linear trend up to 3 T. RRR values of 3.6, 3.6, 3.6, 4.3, 3.9, 3.3, and 2.7 were found for Y and Gd-Tm, respectively, with α-*Dy*$Ni_{0.9(1)}Ga_4$ having the largest positive MR value of 32% at 9 T. Similar to β-*Ln*$Ni_{1-x}Ga_4$, α-*Ln*$NiGa_4$ analogues show small values of MR, again indicative of a classical scattering mechanism upon application of an external field.

Crystals of two polymorphs of *Ln*$NiGa_4$ (α and β) were successfully grown. β-*Ln*$Ni_{1-x}Ga_4$ (*Ln* = Tb-Er), a defect variant of the Ce_2NiGa_{10}-structure type,[28] is isotypic to *Ln*$NiGa_3Ge$ (*Ln* = Y, Sm, Gd, Tb, Er, Tm)[22] with an additional split Ga site. The structural distortion found in β-*Ln*$Ni_{1-x}Ga_4$ (*Ln* = Tb-Er) can be attributed to the Ni occupation at the 4*e* site which induces a distortion in the surrounding Ga environment. We have reported, for the first time, the magnetic properties of β-*Ln*$Ni_{1-x}Ga_4$ (*Ln* = Tb-Er) and the transport properties of β-*Ln*$Ni_{1-x}Ga_4$ (*Ln* = Tb-Er) and α-*Ln*$NiGa_4$ (*Ln* = Gd – Tm). The magnetic moments as obtained for β-*Ln*$Ni_{1-x}Ga_4$ (*Ln* = Tb-Er) from Curie-Weiss fits are consistent with the trivalent lanthanide moment and interestingly, both θ_W for α-*Ln*$NiGa_4$ (*Ln* = Gd – Tm)[27] and β-*Ln*$Ni_{1-x}Ga_4$ (*Ln* = Tb-Er) scale as a function of de Gennes factor, indicating the mechanism of magnetism is similar between the analogues and the magnetic behavior is dominated by an RKKY-type interaction.

5.2.3 Ln_4FeGa_{12} (*Ln* = Tb – Er)

5.2.3.1 Synthesis

Synthesis was achieved by melting *Ln*-Fe-Ga constituents with a reaction ratio of 1:1:20 for Ln_4NiGa_{12} (*Ln* = Tb-Er). Further synthetic detail can be found in Drake, B. L. *et. al.*, *Inorganic Chemistry*, 2010. [29]

5.2.3.2 Single Crystal X-ray Diffraction of Ln_4FeGa_{12}

Crystal fragments with dimensions of ca. $0.05 \times 0.05 \times 0.05$ mm^3 were manually selected with an optical microscope for structural analysis. The crystals were glued onto a glass fiber and mounted on a Nonius Kappa CCD diffractometer that used 0.71073 Å Mo K_α radiation. Structural and refinement parameters are given in Table 5.2. The structure of Ln_4FeGa_{12} where *Ln* is Y, Tb, Dy, Ho, and Er, was solved by direct methods using SHELXS97 and refined using SHELXL97;[30,31] the model of the refined structures were compared with that of the parent compound Y_4PdGa_{12}.[32] After refinement, the data were corrected for extinction effects and spherical absorption and the displacement parameters were refined anisotropically. Table 5.3 gives the atomic positions and thermal displacement parameters for the above compounds. Additional information in CIF format is provided as supporting information.

The Ln_4FeGa_{12} compounds, where *Ln* is Y, Tb, Dy, Ho, and Er, all crystallize in the cubic Y_4PdGa_{12} structure, with the $Im\bar{3}m$, number 229, space group.[22,32] The crystal structure of Tb_4FeGa_{12}, as is shown in Figure 5.7a, consists of face sharing $TbGa_3$ cuboctahedra with corner sharing $FeGa_6$ octahedra. Selected bond distances are given in Table 5.4. The Fe–Ga2 interatomic distances are ca. 2.4 Å for all compounds, a distance that is only slightly smaller than the sum of the respective iron and gallium atomic radii of 1.24 and 1.22 to 1.25 Å, respectively.[33,34] The *Ln*–Ga_6 cuboctahedra in Ln_4FeGa_{12} have six *Ln*–Ga1 and six *Ln*–Ga2 interatomic distances of ca. 3.0 Å, see Table 5.4. These values are only slightly shorter than the sum of the atomic radii of the respective rare earth and gallium.

The structure of iron deficient $Er_4Fe_{0.67}Ga_{12}$ is directly related to Dy_4FeGa_{12} as can be seen in Figure 5.7b. Energy dispersive spectroscopy measurements yielded an Er : Fe : Ga ratio of 4.2 (2) : 0.53 (5) : 11.8 (3), ratios that are in good agreement with the refined single crystal

composition of $Er_4Fe_{0.67}Ga_{12}$. In $Er_4Fe_{0.67}Ga_{12}$ the unique Ga2 12*e* site, found in the other compounds, is divided into two crystallographically distinct sites, a Ga2 12*e* site and a second Ga3 12*e* site, each of which is half occupied. This splitting results because of a partial 0.38(3) occupancy of the Fe1 site. As is shown in Figure 5.7b, when Fe1 is present, Ga2 is occupied and yields the expected octahedral coordination environment. If the Fe1 site is unoccupied the Ga2 atoms move toward the octahedral hole giving rise to occupancy of the Ga3 position and distorting the cuboctahedra such that it resembles the binary $ErGa_3$ (*Pm*–3*m*) subunit that is shown in Figure 5.7d. Inspection of the differences between the structures of $ErGa_3$ and $Er_4Fe_xGa_{12}$ indicates that $Er_4Fe_xGa_{12}$ is a body centered variant of $ErGa_3$. Examination of the Fe1 local environment, as is shown in Figure 5.7e, indicates that the presence of Fe1 yields the isostructural environment of Dy_4FeGa_{12}. If Fe1 is unoccupied, the structure collapses to that of $ErGa_3$. The $Er_4Fe_{0.67}Ga_{12}$ compound is the end member of the Ln_4FeGa_{12} series, and its single crystal structure indicates that the $Tm_4Fe_xGa_{12}$ and $Yb_4Fe_xGa_{12}$ do not form because the iron is unable to occupy the body centered position. This inability is observed in $Er_4Fe_{0.67}Ga_{12}$ as the partial occupancy of the Fe1 position. With $Tm_4Fe_xGa_{12}$ and $Yb_4Fe_xGa_{12}$ the body centered Fe1 position is not favored and, thus, the 1:3 primitive binary compound is formed. As may also be seen in Figures 5.7b and 5.7c, an Fe2 site with a 0.096(16) occupancy is observed and occupies the octahedral holes unoccupied by Fe1. A close inspection of the Fe2 environment, once again reveals a remarkable resemblance to the 1:3 binary structure. The best description of the structure of $Er_4Fe_xGa_{12}$ is that of an intergrowth of the $ErGa_3$ and Er_4FeGa_{12} structures. Thus the structure of $Er_4Fe_xGa_{12}$ can be viewed as a primitive cubic packing of $ErGa_3$ with half of the cubes occupied by Fe1 and Fe2. In this view, Fe1 and Fe2 are crystallographically equivalent because they both occupy the ½, ½, ½ position of the primitive unit cell of $ErGa_3$. This

description effectively reproduces the $Er_4Fe_xGa_{12}$ structure when x is sufficiently high, such that the full symmetry of the body centered cubic structure is observed by single crystal diffraction.

Table 5.2. Unit Cell and Structural Refinement Parameters

Compound	Y_4FeGa_{12}	Tb_4FeGa_{12}	Dy_4FeGa_{12}	Ho_4FeGa_{12}	$Er_4Fe_{0.67}Ga_{12}$
Space group	$Im\bar{3}m$	$Im\bar{3}m$	$Im\bar{3}m$	$Im\bar{3}m$	$Im\bar{3}m$
a (Å)	8.5650(4)	8.5610(4)	8.5350(3)	8.5080(3)	8.4760(3)
V (Å^3)	628.32(5)	627.44(5)	621.74(4)	615.86(4)	608.94(4)
Z	2	2	2	2	2
Crystal dimensions (mm^3)	0.05x0.05x0.5	0.05x0.05x0.05	0.05x0.05x0.05	0.05x0.05x0.05	0.03x0.03x0.04
Temperature (K)	298(2)	298(2)	298(2)	298(2)	298(2)
ρ (g/cm^3)	6.597	8.089	8.239	8.370	8.417
θ-range	3.36-29.86	3.37-29.88	3.38-29.98	3.39-29.85	2.55-34.97
μ (mm^{-1})	44.528	48.543	50.275	52.184	53.981
Collected reflections	294	304	295	278	2130
Unique reflections	103	108	105	107	159
h	$-11 \leq h \leq 12$	$-11 \leq h \leq 12$	$-11 \leq h \leq 12$	$-11 \leq h \leq 11$	$-13 \leq h \leq 13$
k	$-8 \leq k \leq 8$	$-8 \leq k \leq 8$	$-8 \leq k \leq 8$	$-8 \leq k \leq 8$	$-13 \leq k \leq 13$
l	$-7 \leq l \leq 7$	$-7 \leq l \leq 7$	$-7 \leq l \leq 7$	$-7 \leq l \leq 7$	$-13 \leq l \leq 12$
$\Delta\rho_{max}$ (eÅ^{-3})	2.605	2.641	3.748	1.513	2.998
$\Delta\rho_{min}$ (eÅ^{-3})	–1.631	–3.330	–2.342	–3.902	–4.102
R_1 (F)[a]	0.0382	0.0383	0.0305	0.0256	0.0304
R_w[b]	0.0655	0.0936	0.0871	0.0730	0.0500
GOF	1.165	1.298	1.238	1.230	1.161

[a] $R_1 = \Sigma||F_o| - |F_c||/\Sigma|F_o|$

[b] $R_w = [\Sigma\,[w(F_o^2 - F_c^2)^2]/\Sigma\,[w(F_o^2)^2]]^{1/2}$; $w = 1/[\sigma^2(F_o^2) + (0.00000P)^2 + 4.7941P]$, $w = 1/[\sigma^2(F_o^2) + (0.0390P)^2 + 7.8321P]$, $w = 1/[\sigma^2(F_o^2) + (0.0311P)^2 + 17.4653P]$, $w = 1/[\sigma^2(F_o^2) + (0.0138P)^2 + 20.5004P]$, and $w = 1/[\sigma^2(F_o^2) + (0.0000P)^2 + 39.2741P]$ for the Y, Tb, Dy, Ho, and Er compounds, respectively.

Table 5.3. Atomic Positions and Atomic Displacement Parameters

Atom	Wyckoff site	*x*	*y*	*z*	U_{eq}(Å^2)[a]	Occ.
			Y_4FeGa_{12}			
Y1	8*c*	1/4	1/4	1/4	0.0070(4)	1.0
Fe1	2*a*	0	0	0	0.0128(10)	1.0
Ga1	12*d*	1/4	0	1/2	0.0128(7)	1.0
Ga2	12*e*	0.2848(3)	0	0	0.0154(9)	1.0
			Tb_4FeGa_{12}			
Tb1	8*c*	1/4	1/4	1/4	0.0074(6)	1.0
Fe1	2*a*	0	0	0	0.0124(12)	1.0
Ga1	12*d*	1/4	0	1/2	0.0127(10)	1.0
Ga2	12*e*	0.2850(4)	0	0	0.0158(13)	1.0
			Dy_4FeGa_{12}			
Dy1	8*c*	1/4	1/4	1/4	0.0051(5)	1.0
Fe1	2*a*	0	0	0	0.0148(15)	1.0
Ga1	12*d*	1/4	0	1/2	0.0109(10)	1.0
Ga2	12*e*	0.2828(4)	0	0	0.0184(13)	1.0
			Ho_4FeGa_{12}			
Ho1	8*c*	1/4	1/4	1/4	0.0082(5)	1.0
Fe1	2*a*	0	0	0	0.0208(14)	1.0
Ga1	12*d*	1/4	0	1/2	0.0128(9)	1.0
Ga2	12*e*	0.2814(4)	0	0	0.0237(12)	1.0
			$Er_4Fe_{0.67}Ga_{12}$			
Er1	8*c*	1/4	1/4	1/4	0.0080(2)	1.0
Fe1	2*a*	0	0	0	0.007(4)	0.38(3)
Fe2	6*b*	1/2	0	0	0.010(9)	0.096(16)
Ga1	12*d*	1/4	0	1/2	0.0144(4)	1.0
Ga2	12*e*	0.280(4)	0	0	0.017(4)	0.5
Ga3	12*e*	0.249(4)	0	0	0.017(4)	0.5

[a] U_{eq} is defined as one-third of the trace of the orthogonalized U_{ij} tensor.

Table 5.4. Selected Intermetallic Distances

	Y_4FeGa_{12}	Tb_4FeGa_{12}	Dy_4FeGa_{12}	Ho_4FeGa_{12}	$Er_4Fe_{0.67}Ga_{12}$
Ln cuboctahedra					
*Ln*1–Ga1(x6)	3.02818(14)	3.02677(14)	3.01758(11)	3.00803(11)	2.99672(11)
*Ln*1–Ga2(x6)	3.0428(3)	3.0416(4)	3.0305(4)	3.0199(4)	3.008(3)
*Ln*1–Ga3(x6)[1]	-	-	-	-	2.99673(14)
Ga1–Ga2(x4)	2.8255	2.823(2)	2.827(2)	2.825(2)	2.82(2)
Fe octahedra					
Fe1–Ga2(x6)	2.439(2)	2.440(4)	2.413(4)	2.394 (4)	2.37(4)

[1] Ga3 is only present when Fe1 does not occupy the center of the octahedral hole.

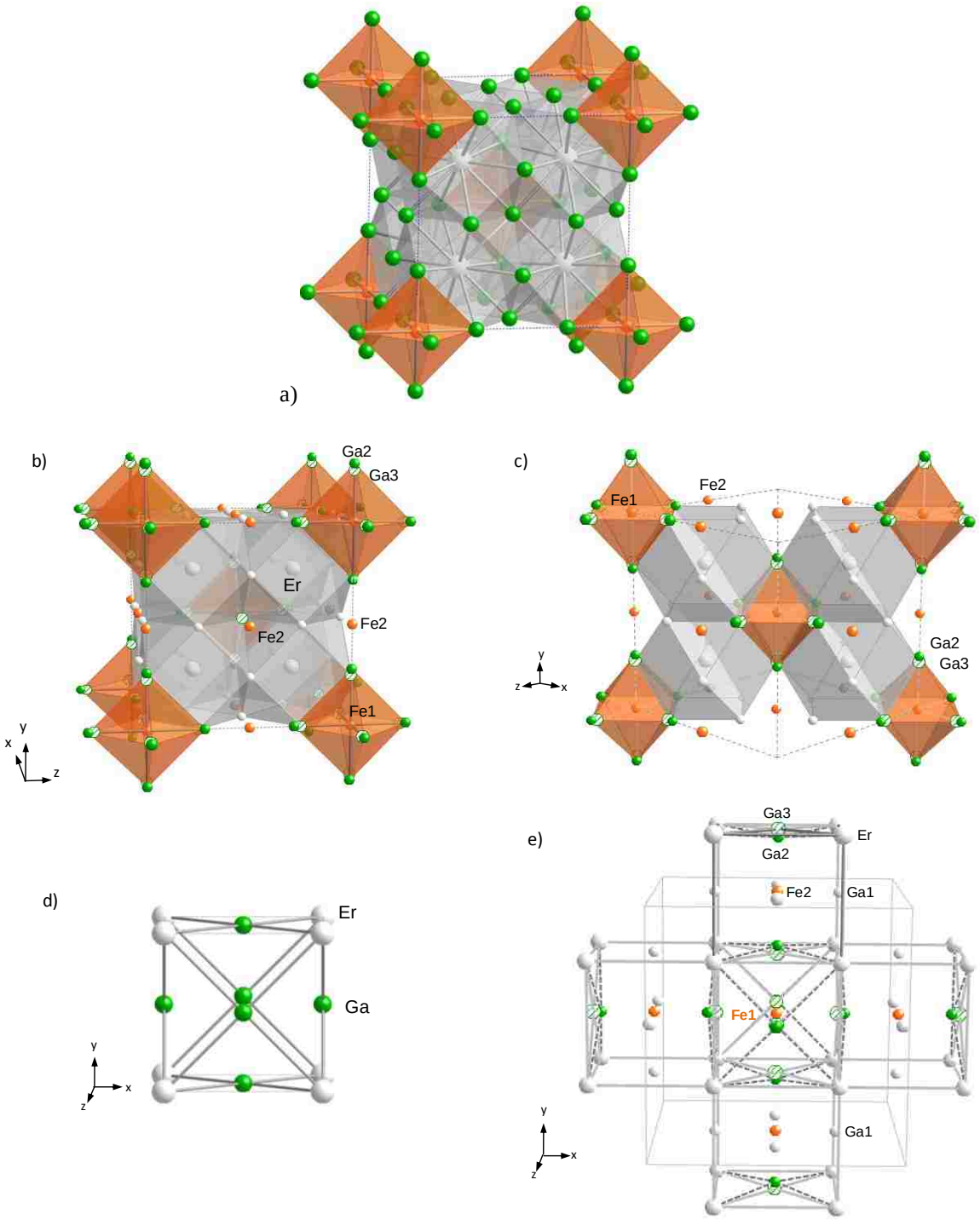

Figure 5.7a – e (a)The crystal structure of Dy_4FeGa_{12}. The Dy, Fe, and Ga atoms are shown in grey, orange, and green, respectively. (b) The crystal structure of $Er_4Fe_{0.67}Ga_{12}$. Er and Ga1 are shown in grey, Fe1 and Fe2 are shown in orange, and Ga2 and Ga3 are shown in solid green and green striped spheres, respectively. (c) The local erbium and iron environments along the [101] plane. (d) Primitive unit cell of $ErGa_3$ ($Pm\bar{3}m$). (e) Simple cubic packing $ErGa_3$ subunits with iron partially occupying the interstitial sites to form $Er_4Fe_{0.67}Ga_{12}$.

5.3 Conclusions

Throughout this work, a central them has been the growth of new, interesting or novel phases and understanding the structure as it relates to disorder/complexity and concomitantly the physical properties in hopes of providing sufficient justification that the search for highly correlated material can be rationalized by searching for relations between the crystal chemistry and physical nature. The understanding derived from analysis of local environments and structural subunits shed light directly on the electronic environment of the lanthanide atoms. The isolation/growth of large (> 1 mm), high quality single crystals is paramount in the elucidation of these relationships, as it acts as a window giving a clear view of the structure, and therefore local environments, allowing anisotropic physical properties measurements. These coupled with an understanding of the structure allows for rational analysis and a more probative understanding of the observed properties of a material.

An understanding of why specific structure-types stabilize over others, and therefore why structure-types have terminal members in the midst of the lanthanide series, could provide a more encompassing perspective on the topic of crystal growth. This has been termed in intermetallic systems "the coloring problem".[35] With the theoretical treatment of a system (density functional theory, local density approximations, and linear tin-muffin orbital to mention a few) it is possible to garner an understanding of a materials range of stability in a structure type as it relates to the materials valence electron count (VEC). This shifts the focus from the growth of new materials to their theoretical modeling, an endeavor our group is not equipped to undertake. Yet, in select systems, we can contribute and understand why specific analogues are the terminal member of a series via careful analysis of the crystal chemistry of that specific analogue or the isostructural series.

The $ThMn_{12}$ structure type has a rather substantial formation range across all lanthanides and with a host of transition metals with both Al, In, and Ga main group elements.[19,36-49] When searching for new materials this is an attractive caveat that many systems do not boast. This allows one to isolate all variables, barring crystallographic disorder, and study the materials as a function of lanthanide (a function of electronic configuration). One then can better understand the driving force behind the observed magnetism. Yet other ternary systems form for only a limited number of rare earths. $Ln(Cu,Al,Ga)_{13-x}$ and $Ln(Cu,Ga)_{13-x}$ crystallizing in the $NaZn_{13}$ structure type only form for *Ln* = La – Eu. A burgeoning question is why. This is a question best answered by theory as no clear order exists in the disordered Cu/Al and Cu/Ga positions. The structure can be described as a face centered cubic unit cell with a 3 dimensional network of connected, filled icosahedra, where the center is occupied by Cu and the surface is statistically disordered with 4 Cu and 8 Al atoms. The inability to resolve this disorder, crystallographically, hinders the experimentalist from firmly grasping a reason the Eu analogues are the terminal member of the series. Electronic structure calculations reveal the lowest energy configuration arises from maximization of the Cu – Cu distances in the icosahedra and a narrow range of stability exists for VEC close to 40.5 e-/f.u.[35,50] Progression to latter rare earths, past Eu, continues to further compress the Cu – Cu distances in the icosahedra, as a result of the disorder increase as a result of the desire to optimize the Cu – Cu distances.. Simply, the lanthanide contraction. This decreases the valence electron count as vacancies from dynamically resulting in a structure that arises from Gd substitution and contains short, energetically unfavorable Cu – Cu distances and a VEC outside optimal bonding.

Here after we hope to provide insight on a collection of systems and their disorder and/or valence electron count in hopes to provide a clear understanding as it relates to the stabilization or termination of a structure-type from the perspective of an experimentalist.

$Er_4Fe_{0.67}Ga_{12}$ is one example where an experimentalist can clearly explain the termination of a structure. Inspection of the atomic displacement parameters (ADP) across the series Ln_4FeGa_{12} (*Ln* = Tb – Er) reveal that the Fe1 (2*a*) and Ga2 (12*e*) positions show significantly increased atomic displacement parameters with respect to other positions, a red flag. Commonly this can arise from the incorrect assignment of atom type or crystallographic disorder (statistical or dynamic) on said position. Additionally, the Fe1 – Ga2 distance was abnormally short for the Er analogue when compared to the isostructural series. Probative examination of the remnant electron density also revealed a small (~5 e-/$Å^3$) peak in the center of a previously unoccupied octahedral hole, the same environment Fe1 resides. This position is weakly populated by an Fe2 atom (present 10% of the time) and governed by the occupancy of the Fe1 and Ga2 positions. Analysis of the large atomic displacement parameters associated with Fe1 and Ga2 reveal two types of disorder, statistical and dynamic respectively. The Fe1 position is populated ~ 40% with the Ga2 position being split into 2 positions adjacent to the original Ga2 Wyckoff position. The disorder found for Fe1 and Ga2 plus the occupation of octahedral hole with an Fe2 atom, is reminiscent of a "stuffing" of the binary $ErGa_3$. This disorder can be initially observed in the Ho derivative, as the ADPs associated with Fe1 and Ga2 are slightly large but one cannot clearly observe the Fe2 position from X-ray diffraction data. The corrected model, which accounted for the considerable disorder mentioned above, resulted in well behaved ADPs and Fe1 – Ga2 distances that scale well with the lanthanide series. These modifications can be best described as an intergrowth of the $ErGa_3$ and Er_4FeGa_{12} structures. $Tm_4Fe_{1-x}Ga_{12}$ single crystals could not be

grown, but large single crystal of $TmGa_3$ were synthesized. From an experimentalists/crystallographers view, the decreasing radii of the lanthanides effectively "squeezed" the Fe1 and Fe2 positions to the point that Fe could no longer populate the octahedral holes, resulting in the isolation of the $TmGa_3$ binary.

The β polymorph of $Ln Ni_{1-x}Ga_4$ (*Ln* = Tb - Er) shows similar disorder to $Er_4Fe_{0.67}Ga_{12}$. Both statistical and dynamic crystallographic disorder is observed in all analogues. Though, the observed disorder is increased in the β-$ErNi_{1-x}Ga_4$ derivative. Additionally, the population of the Ni position is reduced as a function of rare earth, and the Ga atoms dynamic disorder becomes more complex in an attempt to correct for decreasing Ni concentrations. The differences in occupancies of the disordered sites not only illustrate the effects of the lanthanide contraction, but also mark the end of the series β-$Ln Ni_{1-x}Ga_4$ (*Ln* = Tb-Er) due to increasing structural instability with decreasing lanthanide size. β-$TbNi_{0.9}Ga_4$ and β-$DyNi_{0.9}Ga_4$ show antiferromagnetic transitions at 7 and 3.5 K, where β-$HoNi_{0.9}Ga_4$ is paramagnetic down to 3 K. β-$ErNi_{1-x}Ga_4$ undergoes an antiferromagnetic transition at 7 K. This reinforces that something structural may be amiss, as one would not predict that β-$ErNi_{1-x}Ga_4$ would be antiferromagnetic at 7 K in light of the observed trend in magnetism for the β-$TbNi_{0.9}Ga_4$, β-$DyNi_{0.}9Ga_4$, and β-$HoNi_{0.9}Ga_4$ analogues. The decreasing size of the lanthanide increasingly renders the population of the Ni position more difficult, resulting in the termination of the β polymorphs stability at the Er analogue.

More recently, with an appreciation for serendipity, we have returned to a phase that launched our groups initial research into rare earth intermetallics, $CePdGa_6$. Systematic progression to Ni, Cu, and Ag has not yielded, until recently, an isostructural analogue to $CePdGa_6$ using Ga as a flux, but has been fruitful, as many interesting materials have been

found: Ln_2TGa_{12} (*Ln* = early *f* elements and *T* = Pd, Ni, and Cu), Ln_2TGa_{10} (*Ln* = early *f* elements and *T* = Pd and Ag), $Ln(Cu,Ga)_{12}$ (*Ln* = latter *f* elements), α and β $LnNiGa_4$ (*Ln* = early - mid *f* elements and mid *f* elements, respectively), $Ln(Cu,Ga)_{13-x}$ (*Ln* = early *f* elements)… Exploration of the *Ln*-Cu-Al phase space was a logical progression for comparative analysis with the phases found while exploring the *Ln*-Cu-Ga system in an attempt to understand the main group elements impact on crystal growth, phase stabilization, and physical properties. During this exploration, contamination from silica wool, the filtering medium, was observed and permitted the stabilization of $LnCu_2Al_4Si$, isostructural to $CePdGa_6$. After finding reproducible synthetic conditions, $LnCu_2Al_4Si$ (*Ln* = La and Ce) could be grown. Through judicious experimentation, Si seems critical for the stabilization of the Cu derivative. As may be indicated by the chemical formula, when compared to $CePdGa_6$, $LnCu_2Al_4Si$ elicits considerable statistical disorder in the form of Cu/Al and Al/Si mixing. The similarities of the elements that comprise the disorder render X-ray diffraction incapable of understanding or observing any order other than the 2*h* and 4*i* are randomly populated with Cu/Al and Al/Si respectively. This does not explain why Si was critical to stabilize this phase; it's when we return to VEC that we find an answer. $CePdGa_6$ has a VEC of 21 e-/Å^3 (3 + 0 + 3 x 6) and $CeCu_2Al_4Si$ has a VEC of 21 (3 + 1 x 2 + 3 x 4 + 4). Synthetic attempts to change the amount of Si have all resulted in ~ 1 equivalent of Si being present in the structure, indicating a rather narrow width of formation, which is justified by the VEC. Replacing Si with Al in this structure reduces the overall VEC to 20, a value that may lay outside the range of stability, supported by the requirement of Si in the reaction melt.

This work tells a story of crystal growth, an understanding of structure and disorder, and a search for highly correlated materials. It has served as a reminder of a common yet frequently forgotten force, the lanthanide contraction, which is often induces or enhances disorder within a

system. Probing disorder can result in understanding something about the formation or termination of a structure type and the material's respective physical properties. Yet none of this is possible without crystal growth. The growth of large, high quality single crystals is paramount in furthering our understanding and building a working knowledge comparable to synthetic organic chemists.

A full circle, from beginning to end, is often realized upon reflection. One joins a group with an insatiable thirst and desire to learn. I am leaving this group with the same desire, just different questions. Where those lead me are yet to be written.

In closing, I hope to leave the readers of this work with a statement I hold true:

"To know the road ahead, ask those coming back."

-Chinese Proverb

5.4 References

(1) Fisk, Z., Sarrao, J.L., Smith, J.L., and Thompson, J.D., The physics and chemistry of heavy fermions. *Proc. Natl. Acad. Sci. U.S.A.* **1995,** *92*, 6663.

(2) Fisk, Z., Sarrao, J.L., and Thompson, J.D., Heavy fermions. *Curr. Opin. Solid State Mater. Sci.* **1996,** *1*, 42-46.

(3) Ott, H.R., Rudigier, H., Fisk, Z., and Smith, J.L., UBe_{13}: An unconventional actinide superconductor. *Phys. Rev. Lett.* **1983,** *50*, 1595.

(4) Smith, J.L., Fisk, Z., Willis, J.O., Batlogg, B., and Ott, H.R., Impurities in the heavy-fermion superconductor uranium-beryllium (UBe_{13}). *J. Appl. Phys.* **1984,** *55*, 1996.

(5) Maple, M.B., Chen, J.W., Lambert, S.E., Fisk, Z., Smith, J.L., Ott, H.R., Brooks, J.S., and Naughton, M.J., Upper critical magnetic field of the heavy-fermion superconductor UBe_{13}. *Phys. Rev. Lett.* **1985,** *54*, 477-480.

(6) Cox, D.L., Quadrupolar Kondo effect in uranium heavy-electron materials? *Phys. Rev. B* **1987,** *35*, 1240–1243.

(7) Kim, J.S. and Stewart, G.R., Observation of low-lying levels in UBe_{13}. *Phys. Rev. B* **1995,** *51*, 16190.

(8) Besnus, M.J., Kappler, J.P., and Meyer, A., On the valence regime in the (CexLa1-x)Be13 system. *Solid State Commun.* **1983,** *48*, 835-838.

(9) Holmes, A.T., Jaccard, D., and Miyake, K., Valence instability and superconductivity in heavy fermion systems. *J. Phys. Soc. Jpn.* **2007,** *76*, 051002/051001.

(10) Steglich, F., Superconductivity and magnetism in heavy-fermion compounds. *J. Phys. Soc. Jpn.* **2005,** *74*, 167-177.

(11) Miyake, K., Narikiyo, O., and Onishi, Y., Superconductivity of Ce-based heavy fermions under pressure: valence fluctuation mediated pairing associated with valence instability of Ce. *Physica B* **1999,** *259−261*, 676.

(12) Yatskar, A., Beyermann, W.P., Movshovich, R., and Canfield, P.C., Possible correlated-electron behavior from quadrupolar fluctuations in $PrInAg_2$. *Phys. Rev. Lett.* **1996,** *77*, 3637.

(13) Yatskar, A., Beyermann, W.P., Movshovich, R., Canfield, P.C., Panchula, A., and Bud'ko, S.L., Unexpected heavy-electron behavior at low temperatures in $PrInAg_2$. *Physica B* **1997,** *230−232*, 46-48.

(14) Matsuda, T.D., Okada, H., Sugawara, H., Aoki, Y., Sato, H., Andreev, A.V., Shiokawa, Y., Sechovsky, V., Honma, T., Yamamoto, E., and Onuki, Y., Specific-heat anomaly of metamagnetism on $PrFe_4P_{12}$ and UCoAl. *Physica B* **2000,** *281&282*, 220-222.

(15) Mitamura, H., Takeshita, N., Uwatoko, Y., Mori, H., Yamaguchi, A., Tomita, T., Wada, H., Mori, N., Ishimoto, H., and Goto, T., Precise resistivity measurement in $PrInAg_2$ down to 50 mK. *Physica B* **2000,** *281&282*, 150.

(16) Kadowaki, K. and Woods, S.B., Universal relationship of the resistivity and specific heat in heavy-Fermion compounds. *Solid State Commun.* **1986,** *58*, 507-509.

(17) Shimura, Y. and et al., Low-temperature magnetic properties of Pr(Cu,Ga) 12.85. *Journal of Physics: Conference Series* **2011,** *273*, 012054.

(18) Cho, J.Y., Thomas, E.L., Nambu, Y., Capan, C., Karki, A.B., Young, D.P., Kuga, K., Nakatsuji, S., and Chan, J.Y., Crystal growth, structure, and physical properties of $Ln(Cu,Ga)_{13-x}$ (Ln = La-Nd, Eu; x ~ 0.2). *Chem. Mater.* **2009,** *21*, 3072-3078.

(19) Felner, I., Crystal structures of ternary rare earth-3d transition metal compounds of the RT6Al6 type. *J. Less-Common Met.* **1980,** *72*, 241-249.

(20) Canfield, P.C. and Fisk, Z., Growth of single crystals from metallic fluxes. *Philos. Mag. B* **1992,** *65*, 1117-1123.

(21) Romaka, V.A., Grin, Y.N., and Yarmolyuk, Y.P., Magnetic and crystallographic characteristics of rare earth metal-nickel-gallium ($RENiGa_4$) compounds. *Ukr. Fiz. Zh.* **1983,** *28*, 1095-1097.

(22) Zhuravleva, M.A., Pcionek, R.J., Wang, X., Schultz, A.J., and Kanatzidis, M.G., *ReM*Ga_3Ge and $Re_3Ni_3Ga_8Ge_3$ (*M* = Ni, Co; *Re* = rare-earth element): new intermetallics synthesized in liquid gallium. x-ray, electron, and neutron strucutre determination and magnetism. *Inorg. Chem.* **2003,** *42*, 6412-6424.

(23) Greedan, J.E., Geometrically frustrated magnetic materials. *J. Mater. Chem.* **2001,** *11*, 37-53.

(24) Menard, M.C., Xiong, Y., Karki, A.B., Drake, B.L., Adams, P.W., Fronczek, F.R., Young, D.P., and Chan, J.Y., Synthesis, structure, and characterization of $Ln_2Ag_{1-x}Ga_{10-y}$ (*Ln* = La, Ce). *J. Solid State Chem.* **2010,** *183*, 1935-1942.

(25) Hwang, J.S., Lin, K.J., and Tien, C., Antiferromagnetism and mass-enhanced behavior in Ce_2CuSi_3. *Solid State Commun.* **1996,** *100*, 169-172.

(26) Tien, C., Feng, C.H., Wur, C.S., and Lu, J.J., Ce_2CuGe_3: a nonmagnetic atom-disorder spin glass. *Phys. Rev. B* **2000,** *61*, 12151.

(27) Romaka, V.A., Grin, Y.N., and Yarmolyuk, Y.P., Magnetic and crystallographic characteristics of rare earth metal-nickel-gallium ($RENiGa_4$) compounds. *Ukr. Fiz. Zh.* **1983,** *28*, 1095-1097.

(28) Yarmolyuk, Y.P., Grin, Y.N., Rozhdestvenskaya, I.V., Usov, O.A., Kuzmin, A.M., Bruskov, V.A., and Gladyshevskij, E.I., Crystal chemistry of series of inhomogeneous linear structures. III. the crystal structures of $Ce_2Ga_{10}Ni$ and $La_2Ga_{10}Ni$. *Kristallografiya* **1982,** *27*, 599-600.

(29) Drake, B.L., Grandjean, F., Kangas, M.J., Okudzeto, E.K., Karki, A.B., Sougrati, M.T., Young, D.P., Long, G.J., and Chan, J.Y., Crystal growth, transport, and the structural and magnetic properties of Ln_4FeGa_{12} with Ln = Y, Tb, Dy, Ho, and Er. *Inorg. Chem.* **2009,** *49*, 445-456.

(30) Sheldrick, G.M., "SHELXL-97, Program for Refinement of Crystal Structures", Göttingen, Germany, **1997**..

(31) Sheldrick, G.M., A short history of SHELX. *Acta Crystallogr. A* **2008,** *64*, 112-122.

(32) Vasilenko, L.O., Noga, A.S., Grin, Y.N., Koterlin, M.D., and Yarmolyuk, Y.P., Crystal-structure and some properties of R_4MGa_{12} compounds. *Russ. Metall.* **1988,** 216-220.

(33) Emsley, J., "The Elements." Oxford University Press, 1999.

(34) Sutton, L., "Tables of Interatomic Distances and Configurations in Molecules and Ions, Vol. Spec. Publ. No. 18." The Chemical Society, London, 1965.

(35) Miller, G.J., The "Coloring Problem" in Solids: How It Affects Structure, Composition and Properties. *European Journal of Inorganic Chemistry* **1998,** *1998*, 523-536.

(36) Baio, G., Moze, O., Amoretti, G., Sonntag, R., Stusser, N., and Buschow, K.H.J., Neutron diffraction study of $R$$Mn_4Al_8$ (R = Nd, Dy, Ho, Er), $ErCr_4Al_8$, and $ErCu_4Al_8$. *Z. Phys. B - Con. Mat.* **1997,** *102*, 449-453.

(37) Christides, C., Kostikas, A., Zouganelis, G., Psyharis, V., Kou, X.C., and Grossinger, R., Spin-glass-like magnetic properties for rare earth (R)-iron-molybdenum ($R$$Fe_{10}Mo_2$) compounds ($R$ = yttrium or lutetium) with the $ThMn_{12}$-type structure. *Phys. Rev. B* **1993,** *47*, 11220-11229.

(38) Coldea, M., Neumann, M., Lutkehoff, S., Mahl, S., and Coldea, R., Spin and valence fluctuations in $CeMn_4Al_8$ and $CeMn_6Al_6$. *J. Alloys Compd.* **1998,** *278*, 72-79.

(39) Dmitriev, V.M., Stepien-Damm, J., Suski, W., Talik, E., and Prentslau, N.N., Possible coexistence of antiferromagnetism, spin-glass, and superconductivity in $ScFe_4Al_8$ and YFe_4Al_8 single crystals. *Phys. Status Solidi C* **2004,** *1*, 1824-1827.

(40) Dmitriev, V.M., Terekhov, A.V., Suski, W., Ishchenko, L.A., Cwik, J., Palewski, T., Kotur, B.Y., and Talik, E., Negative magnetoresistivity of the $R$$M_4Al_8$ (R = Sc, Y, Ce, Yb, Lu; M=Cr, Mn, Fe) ternaries with the $ThMn_{12}$-type crystal structure. *J. Alloys Compd.* **2008,** *452*, 217-224.

(41) Florio, J.V., Rundle, R.E., and Snow, A.I., Compounds of thorium with transition metals. The thorium-manganese system. *Acta Crystallogr.* **1952,** *5*, 449-457.

(42) Gladishevskii, E.I., Kripyakevich, P.I., Teslvuk, M.Y., Zarechnyuk, O.S., and Kuz'ma, Y.B., Crystal structure of some intermetallic compounds. *Kristallografiya* **1961,** *6*, 267-268.

(43) Gladyshevskii, E.I., Kripyakevich, P.I., Cherkashin, E.E., Zarechnyuk, O.S., Zalutskii, I.I., and Evdokimenko, V.I., Crystal structure of the intermetallic compounds of the rare-earth elements. *Redkozem. Elementy* **1963,** 67.

(44) Gottwick, U., Held, R., Sparn, G., Steglich, F., Vey, K., Assmus, W., Rietschel, H., Stewart, G.R., and Giorgi, A.L., Seebeck coefficient of heavy fermion compounds. *J. Magn. Magn. Mater.* **1987,** *63-64*, 341-343.

(45) Hagmusa, I.H., Klaasse, J.C.P., Bruck, E., de Boer, F.R., and Buschow, K.H.J., A specific-heat study of $R$$Cr_4Al_8$ compounds (R = La, Ce, Pr, Gd, Er). *J. Alloys Compd.* **2001,** *314*, 37-41.

(46) Kontani, M., Hamada, M., Mizukoshi, T., and Mukai, H., NMR/NQR and specific heat studies on the $ThMn_{12}$-type $CeCu_{4+x}Al_{8-x}$ system. *Physica B* **2000,** *284-288*, 1267-1268.

(47) Paci, B., Caciuffo, R., Amoretti, G., Moze, O., Buschow, K.H.J., and Murani, A.P., Neutron scattering determination of the crystal field parameters in $ErCu_4Al_8$ and $ErFe_4Al_8$ intermetallics. *Solid State Commun.* **1995,** *94*, 489-493.

(48) Suski, W., Karl A. Gschneidner, Jr., and LeRoy, E., "Chapter 149 The ThMn12-Type compounds of rare earths and actinides: Structure, magnetic and related properties." Elsevier, Amsterdam, 1996.

(49) Yamasaki, T., Matsui, K., Nakamura, H., and Shiga, M., Nearly antiferromagnetic metal with linear spin chains: $LaMn_4Al_8$. *Solid State Commun.* **2001,** *119*, 415-418.

(50) Nordell, K.J. and Miller, G.J., Linking intermetallics and zintl compounds: An investigation of ternary trielides (Al, Ga, In) forming the $NaZn_{13}$ structure type. *Inorg. Chem.* **1999,** *38*, 579.

APPENDIX 1. SINGLE CRYSTAL X-RAY DIFFRACTION OF MnGe

A1.1 Introduction

As a solid state chemistry group, our expertise lies with crystal growth and structural characterization. Considerable time is spent attempting to find, understand, and describe possible structure property relationships. To do this, we spend copious amounts of time thinking about local environments, connectivity networks, dimensionality, and disorder (dynamic and statistical). As a group, we are often approached to phase or structurally identify a compound for our collaborators. Often we can assist in building a more thorough understanding of the phase.

A sample of MnGe, grown from high pressure synthesis, was sent to our lab for phase identification. Upon inspection of the of the sample, single crystals large enough for single crystal X-ray diffraction were observed and subsequently cleaved for single crystal X-ray diffraction. The remaining sample was ground for phase identification.

A1.2 Single Crystal X-ray Diffraction

Single crystals of MnGe we prepared by collaborators and used as received. Crystals were cut to suitable size (0.05 x 0.05 x 0.05 mm^3) for data collection and mounted onto a glass fiber using epoxy. They were then positioned onto the goniometer of a Nonius Kappa CCD diffractometer equipped with Mo K_α radiation (λ = 0.71073 Å). Further crystallographic parameters for MnGe are provided in Table A1.1. Direct methods were used to solve the structured. SIR97 was employed to give a starting model and SHELXL97 used to refine the structural model and data were corrected with extinction coefficients and refined with anisotropic displacement parameters.[1,2] Based on the lattice parameters and initial refinements, our intial structural model was found to isostructural to FeSi. However, the structural solution was the inversion twin of the absolute structure and the MOVE command was utilized to give the correct

absolute structure. Selected interatomic distances are presented in Table A1.2, and atomic positions and displacement are provided in Table A1.3.

Table A1.1 Crystallographic parameters for MnGe

Formula	MnGe
a (Å)	4.797(4)
V (Å^3)	110.41(14)
Z	4
Crystal system	Cubic
Space group	$P2_13$
θ range (°)	6.01-29.80
μ (mm^{-1})	37.679
Data collection	
Measured reflections	107
Independent reflections	107
Reflections with $I>2\sigma(I)$	102
R_{int}	0.039
h	-4 – 4
k	-6 – 6
l	-4 – 4
Refinement	
[a]$R_1[F^2>2\sigma(F^2)]$	0.0219
[b]$wR_2(F^2)$	0.0435
Reflections	107
Parameters	8
GOOF	0.972
Extinction	0.016(3)
$\Delta\rho_{max}$ (eÅ^{-3})	0.721
$\Delta\rho_{min}$ (eÅ^{-3})	-0.734

[a]$R_1=\sum \| F_o \| - | F_c \| / \sum | F_o |$, [b]$wR_2 = [\sum[w(F_o^2 - F_c^2)]/\sum[w(F_o^2)^2]]^{1/2}$
$w = 1/[\sigma^2(F_o^2)+(0.0000P)^2 + 0.0000P]$

Table A1.2 Select Interatomic Distances in MnGe

		MnGe
Mn – Ge (Å)	(x1)	2.440(2)
	(x3)	2.5128(19)
	(x3)	2.681(2)
Mn - Mn (Å)	(x4)	2.942(2)

Table A1.3 Atomic Positions and Displacement Parameters for MnGe

Atom	Wyckoff position	x	y	z	U_{eq}(Å^2)[a]
Ge	4*a*	0.15628(9)	0.15628(9)	0.15628(9)	0.0085(3)
Mn	4*a*	0.86268(12)	0.86268(12)	0.86268(12)	0.0076(3)

[a]U_{eq} is defined as 1/3 of the trace of the orthogonalized U_{ij} tensor.

MnGe crystallizes in the cubic non-centrosymmetric space group $P2_13$ with lattice parameters of a = 4.797(4). MnGe is isostructural to FeSi. MnGe can best be viewed as a series of 7 coordinate Mn polyhedra, with 3 unique Mn - Ge distances. The local environment and asymmetric unit are shown in Figure A1.1. Temperature dependent studies were completed to understand if any distortions occurred upon cooling. These results show that now obvious distortion is detected and the structure does not undergo any first order transitions.

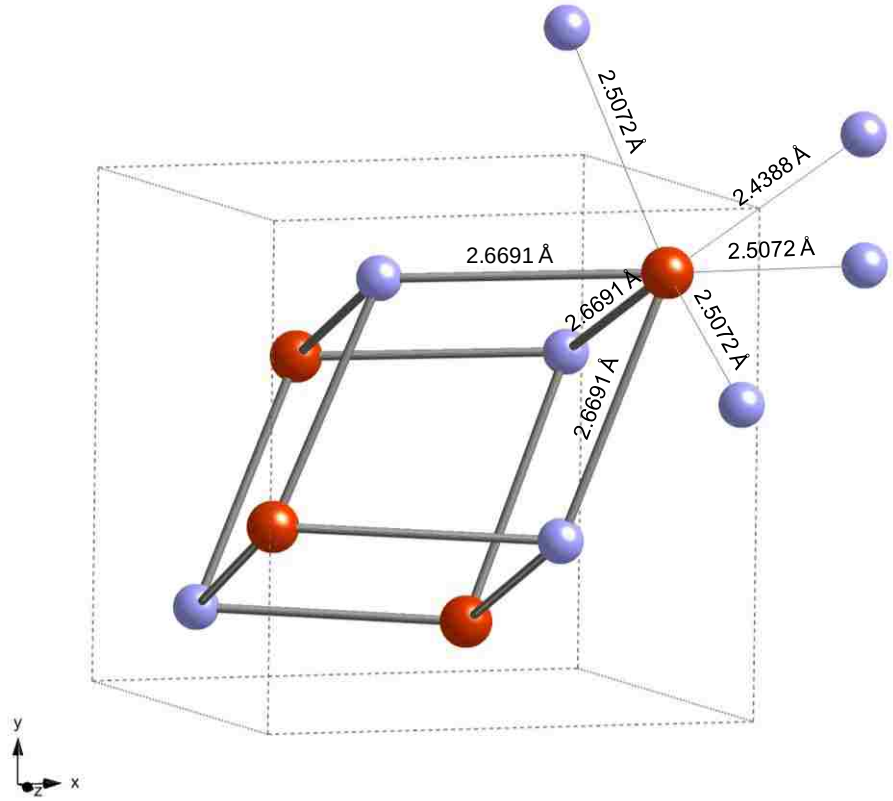

Figure A1.1 The unit cell of MnGe is shown with the asymmetric unit highlighted with thick grey lines. Mn-Ge interatomic distances are also given. Mn atoms are shown as red spheres and Ge atoms are shown as light blue spheres.

A1.3 References

(1) Altomare, A., Burla, M.C., Camalli, M., Luca, G.L., Gaicovazzo, C., Guagliardi, A., Moliterni, A.G.G., Polidori, G., and Spagna, R., SIR97: a new tool for crystal structure determination and refinement. *J. Appl. Cryst.* **1999,** *32*, 115.

(2) Sheldrick, G.M., A short history of SHELX. *Acta Crystallogr. A* **2008,** *64*, 112-122.

APPENDIX 2. UNPUBLISHED CRYSTALLOGRAPHIC INFORMATION FILES

A2.1 $LaCu_2(Al,Si)_5$

```
data_bld74

_audit_creation_method
SHELXL-97
_chemical_name_systematic
;
 ?
;
_chemical_name_common            ?
_chemical_melting_point          ?
_chemical_formula_moiety         'Al4
Cu2 La Si'
_chemical_formula_sum
 'Al4 Cu2 La Si'
_chemical_formula_weight         402.00

loop_
 _atom_type_symbol
 _atom_type_description
 _atom_type_scat_dispersion_real
 _atom_type_scat_dispersion_imag
 _atom_type_scat_source
 'La'  'La'  -0.2871   2.4523
 'International Tables Vol C Tables
4.2.6.8 and 6.1.1.4'
 'Cu'  'Cu'   0.3201   1.2651
 'International Tables Vol C Tables
4.2.6.8 and 6.1.1.4'
 'Al'  'Al'   0.0645   0.0514
 'International Tables Vol C Tables
4.2.6.8 and 6.1.1.4'
 'Si'  'Si'   0.0817   0.0704
 'International Tables Vol C Tables
4.2.6.8 and 6.1.1.4'

_symmetry_cell_setting
'Tetragonal'
_symmetry_space_group_name_H-M
'P 4/m m m'
_symmetry_space_group_name_Hall   '-
P 4 2'

loop_
 _symmetry_equiv_pos_as_xyz
 'x, y, z'
 '-x, -y, z'
 'x, -y, -z'
 '-x, y, -z'
 '-y, -x, -z'
 'y, x, -z'
 'y, -x, z'
 '-y, x, z'
 '-x, -y, -z'
 'x, y, -z'
 '-x, y, z'
 'x, -y, z'
 'y, x, z'
 '-y, -x, z'
 '-y, x, -z'
 'y, -x, -z'

_cell_length_a                   4.221(2)
_cell_length_b                   4.221(2)
_cell_length_c                   7.916(3)
_cell_angle_alpha                90.000
_cell_angle_beta                 90.000
_cell_angle_gamma                90.000
_cell_volume                     141.04(11)
_cell_formula_units_Z            1
_cell_measurement_temperature
298(2)
_cell_measurement_reflns_used    256
_cell_measurement_theta_min
2.546
_cell_measurement_theta_max
31.507

_exptl_crystal_description       'plate'
_exptl_crystal_colour            'silver'
_exptl_crystal_size_max          0.05
_exptl_crystal_size_mid          0.05
_exptl_crystal_size_min          0.05
_exptl_crystal_density_meas      ?
_exptl_crystal_density_diffrn    4.733
_exptl_crystal_density_method    'not
measured'
_exptl_crystal_F_000             181
_exptl_absorpt_coefficient_mu    15.589
_exptl_absorpt_correction_type   'multi-
scan'
_exptl_absorpt_correction_T_min
0.5095
_exptl_absorpt_correction_T_max
0.5095
_exptl_absorpt_process_details   'denzo
scale pack'

_exptl_special_details
;
 ?
;

_diffrn_ambient_temperature      298(2)
_diffrn_radiation_wavelength
0.71073
_diffrn_radiation_type           MoK\a
_diffrn_radiation_source         'fine-
focus sealed tube'
_diffrn_radiation_monochromator
graphite
_diffrn_measurement_device_type
'KappaCCD'
_diffrn_measurement_method
'CCD'
_diffrn_detector_area_resol_mean  9
_diffrn_standards_number         ?
_diffrn_standards_interval_count  ?
_diffrn_standards_interval_time   ?
_diffrn_standards_decay_%        ?
_diffrn_reflns_number            475
_diffrn_reflns_av_R_equivalents
0.0159
_diffrn_reflns_av_sigmaI/netI    0.0157
_diffrn_reflns_limit_h_min       -6
_diffrn_reflns_limit_h_max       6
_diffrn_reflns_limit_k_min       -4
_diffrn_reflns_limit_k_max       4
_diffrn_reflns_limit_l_min       -11
_diffrn_reflns_limit_l_max       11
_diffrn_reflns_theta_min         4.83
_diffrn_reflns_theta_max         31.46
_reflns_number_total             178
_reflns_number_gt                178
_reflns_threshold_expression     >2\s(I)

_computing_data_collection
'KappaCCD'
_computing_cell_refinement       'HKL
Scalepack (Otwinowski & Minor 1997)'
_computing_data_reduction        'Denzo
and Scalepak (Otwinowski & Minor,
1997)'
_computing_structure_solution
'SHELXS-97 (Sheldrick, 1990)'
_computing_structure_refinement
'SHELXL-97 (Sheldrick, 2008)'
_computing_molecular_graphics    ?
_computing_publication_material  ?

_refine_special_details
;
 Refinement of F^2^ against ALL
reflections.  The weighted R-factor wR
and
 goodness of fit S are based on F^2^,
conventional R-factors R are based
 on F, with F set to zero for negative
F^2^. The threshold expression of
 F^2^ > 2\s(F^2^) is used only for
calculating R-factors(gt) etc. and is
 not relevant to the choice of reflections
for refinement.  R-factors based
 on F^2^ are statistically about twice as
large as those based on F, and R-
 factors based on ALL data will be even
larger.
;

_refine_ls_structure_factor_coef  Fsqd
_refine_ls_matrix_type           full
_refine_ls_weighting_scheme      calc
_refine_ls_weighting_details
 'calc
w=1/[\s^2^(Fo^2^)+(0.0344P)^2^+0.130
7P] where P=(Fo^2^+2Fc^2^)/3'
_atom_sites_solution_primary     direct
_atom_sites_solution_secondary
difmap
_atom_sites_solution_hydrogens   ?
_refine_ls_hydrogen_treatment    ?
_refine_ls_extinction_method
SHELXL
_refine_ls_extinction_coef
0.254(19)
_refine_ls_extinction_expression

'Fc^*^=kFc[1+0.001xFc^2^\l^3^/sin(2\q
)]^-1/4^'
_refine_ls_number_reflns         178
_refine_ls_number_parameters     13
_refine_ls_number_restraints     0
_refine_ls_R_factor_all          0.0232
```

```
_refine_ls_R_factor_gt          0.0232
_refine_ls_wR_factor_ref        0.0619
_refine_ls_wR_factor_gt         0.0619
_refine_ls_goodness_of_fit_ref  1.456
_refine_ls_restrained_S_all     1.456
_refine_ls_shift/su_max         0.000
_refine_ls_shift/su_mean        0.000

loop_
 _atom_site_label
 _atom_site_type_symbol
 _atom_site_fract_x
 _atom_site_fract_y
 _atom_site_fract_z
 _atom_site_U_iso_or_equiv
 _atom_site_adp_type
 _atom_site_occupancy
 _atom_site_symmetry_multiplicity
 _atom_site_calc_flag
 _atom_site_refinement_flags
 _atom_site_disorder_assembly
 _atom_site_disorder_group
La1 La 0.0000 0.0000 0.0000 0.0050(3)
Uani 1 16 d S . .
Cu2 Cu 0.0000 0.0000 0.5000 0.0068(3)
Uani 1 16 d S . .
Al3 Al 0.5000 0.5000 0.14862(14)
0.0056(3) Uani 0.50 8 d SP . .
Cu3 Cu 0.5000 0.5000 0.14862(14)
0.0056(3) Uani 0.50 8 d SP . .
Al4 Al 0.0000 0.5000 0.32749(17)
0.0086(4) Uani 0.75 4 d SP . .
Si4 Si 0.0000 0.5000 0.32749(17)
0.0086(4) Uani 0.25 4 d SP . .

loop_
 _atom_site_aniso_label
 _atom_site_aniso_U_11
 _atom_site_aniso_U_22
 _atom_site_aniso_U_33
 _atom_site_aniso_U_23
 _atom_site_aniso_U_13
 _atom_site_aniso_U_12
La1 0.0044(3) 0.0044(3) 0.0061(4)
0.000 0.000 0.000
Cu2 0.0064(4) 0.0064(4) 0.0074(5)
0.000 0.000 0.000
Al3 0.0061(4) 0.0061(4) 0.0047(5) 0.000
0.000 0.000
Cu3 0.0061(4) 0.0061(4) 0.0047(5)
0.000 0.000 0.000
Al4 0.0111(7) 0.0076(7) 0.0071(5) 0.000
0.000 0.000
Si4 0.0111(7) 0.0076(7) 0.0071(5) 0.000
0.000 0.000

_geom_special_details
;
 All s.u.'s (except the s.u. in the dihedral
angle between two l.s. planes)
 are estimated using the full covariance
matrix.  The cell s.u.'s are taken
 into account individually in the
estimation of s.u.'s in distances, angles
 and torsion angles; correlations between
s.u.'s in cell parameters are only
 used when they are defined by crystal
symmetry.  An approximate (isotropic)
 treatment of cell s.u.'s is used for
estimating s.u.'s involving l.s. planes.
;

loop_
 _geom_bond_atom_site_label_1
 _geom_bond_atom_site_label_2
 _geom_bond_distance
 _geom_bond_site_symmetry_2
 _geom_bond_publ_flag
La1 Cu3 3.2082(14) 9 ?
La1 Al3 3.2082(14) . ?
La1 Al3 3.2082(14) 9 ?
La1 Cu3 3.2082(14) 9_665 ?
La1 Cu3 3.2082(14) 1_445 ?
La1 Al3 3.2082(14) 9_665 ?
La1 Al3 3.2082(14) 1_445 ?
La1 Cu3 3.2082(14) 9_565 ?
La1 Cu3 3.2082(14) 9_655 ?
La1 Al3 3.2082(14) 1_545 ?
La1 Al3 3.2082(14) 1_455 ?
Cu2 Si4 2.5137(12) 13_455 ?
Cu2 Si4 2.5137(12) 5_656 ?
Cu2 Si4 2.5137(12) 9_566 ?
Cu2 Al4 2.5137(12) 1_545 ?
Cu2 Si4 2.5137(12) 1_545 ?
Cu2 Al4 2.5137(12) 9_566 ?
Cu2 Al4 2.5137(12) 13_455 ?
Cu2 Al4 2.5137(12) 5_656 ?
Cu2 Si4 2.5137(12) 13 ?
Cu2 Al4 2.5137(12) 13 ?
Cu2 Al4 2.5137(12) 5_556 ?
Cu2 Si4 2.5137(12) 9_556 ?
Al3 Cu3 2.353(2) 9_665 ?
Al3 Al3 2.353(2) 9_665 ?
Al3 Si4 2.5415(14) 13_565 ?
Al3 Si4 2.5415(14) 1_655 ?
Al3 Al4 2.5415(14) 13_565 ?
Al3 Al4 2.5415(14) 1_655 ?
Al3 Al4 2.5415(14) . ?
Al3 Si4 2.5415(14) 13 ?
Al3 Al4 2.5415(14) 13 ?
Al3 La1 3.2082(14) 1_665 ?
Al4 Cu2 2.5137(12) 1_565 ?
Al4 Cu3 2.5415(14) 1_455 ?
Al4 Al3 2.5415(14) 1_455 ?
Al4 Si4 2.731(3) 9_566 ?
Al4 Al4 2.731(3) 9_566 ?
Al4 Al4 2.9847(14) 13_565 ?
Al4 Al4 2.9847(14) 13_455 ?
Al4 Al4 2.9847(14) 13_465 ?
Al4 Al4 2.9847(14) 13 ?

loop_
 _geom_angle_atom_site_label_1
 _geom_angle_atom_site_label_2
 _geom_angle_atom_site_label_3
 _geom_angle
 _geom_angle_site_symmetry_1
 _geom_angle_site_symmetry_3
 _geom_angle_publ_flag
Cu3 La1 Al3 180.00(4) 9 . ?
Cu3 La1 Al3 0.00(4) 9 9 ?
Al3 La1 Al3 180.00(4) . 9 ?
Cu3 La1 Cu3 136.97(4) 9 9_665 ?
Al3 La1 Cu3 43.03(4) . 9_665 ?
Al3 La1 Cu3 136.97(4) 9 9_665 ?
Cu3 La1 Cu3 43.03(4) 9 1_445 ?
Al3 La1 Cu3 136.97(4) . 1_445 ?
Al3 La1 Cu3 43.03(4) 9 1_445 ?
Cu3 La1 Cu3 180.00(4) 9_665 1_445 ?
Cu3 La1 Al3 136.97(4) 9 9_665 ?
Al3 La1 Al3 43.03(4) . 9_665 ?
Al3 La1 Al3 136.97(4) 9 9_665 ?
Cu3 La1 Al3 0.00(4) 9_665 9_665 ?
Cu3 La1 Al3 180.00(4) 1_445 9_665 ?
Cu3 La1 Al3 43.03(4) 9 1_445 ?
Al3 La1 Al3 136.97(4) . 1_445 ?
Al3 La1 Al3 43.03(4) 9 1_445 ?
Cu3 La1 Al3 180.00(4) 9_665 1_445 ?
Cu3 La1 Al3 0.00(4) 1_445 1_445 ?
Al3 La1 Al3 180.00(4) 9_665 1_445 ?
Cu3 La1 Cu3 82.271(15) 9 9_565 ?
Al3 La1 Cu3 97.729(15) . 9_565 ?
Al3 La1 Cu3 82.271(15) 9 9_565 ?
Cu3 La1 Cu3 82.271(15) 9_665 9_565 ?
Cu3 La1 Cu3 97.729(15) 1_445 9_565 ?
Al3 La1 Cu3 82.271(15) 9_665 9_565 ?
Al3 La1 Cu3 97.729(15) 1_445 9_565 ?
Cu3 La1 Cu3 82.271(15) 9 9_655 ?
Al3 La1 Cu3 97.729(15) . 9_655 ?
Al3 La1 Cu3 82.271(15) 9 9_655 ?
Cu3 La1 Cu3 82.271(15) 9_665 9_655 ?
Cu3 La1 Cu3 97.729(15) 1_445 9_655 ?
Al3 La1 Cu3 82.271(15) 9_665 9_655 ?
Al3 La1 Cu3 97.729(15) 1_445 9_655 ?
Cu3 La1 Cu3 136.97(4) 9_565 9_655 ?
Cu3 La1 Al3 97.729(15) 9 1_545 ?
Al3 La1 Al3 82.271(15) . 1_545 ?
Al3 La1 Al3 97.729(15) 9 1_545 ?
Cu3 La1 Al3 97.729(15) 9_665 1_545 ?
Cu3 La1 Al3 82.271(15) 1_445 1_545 ?
Al3 La1 Al3 97.729(15) 9_665 1_545 ?
Al3 La1 Al3 82.271(15) 1_445 1_545 ?
Cu3 La1 Al3 180.00(4) 9_565 1_545 ?
Cu3 La1 Al3 43.03(4) 9_655 1_545 ?
Cu3 La1 Al3 97.729(15) 9 1_455 ?
Al3 La1 Al3 82.271(15) . 1_455 ?
Al3 La1 Al3 97.729(15) 9 1_455 ?
Cu3 La1 Al3 97.729(15) 9_665 1_455 ?
Cu3 La1 Al3 82.271(15) 1_445 1_455 ?
Al3 La1 Al3 97.729(15) 9_665 1_455 ?
Al3 La1 Al3 82.271(15) 1_445 1_455 ?
Cu3 La1 Al3 43.03(4) 9_565 1_455 ?
Cu3 La1 Al3 180.00(4) 9_655 1_455 ?
Al3 La1 Al3 136.97(4) 1_545 1_455 ?
Si4 Cu2 Si4 180.0 13_455 5_656 ?
Si4 Cu2 Si4 107.16(3) 13_455 9_566 ?
Si4 Cu2 Si4 72.84(3) 5_656 9_566 ?
Si4 Cu2 Al4 72.84(3) 13_455 1_545 ?
Si4 Cu2 Al4 107.16(3) 5_656 1_545 ?
Si4 Cu2 Al4 180.0 9_566 1_545 ?
Si4 Cu2 Si4 72.84(3) 13_455 1_545 ?
Si4 Cu2 Si4 107.16(3) 5_656 1_545 ?
Si4 Cu2 Si4 180.0 9_566 1_545 ?
Al4 Cu2 Si4 0.0 1_545 1_545 ?
Si4 Cu2 Al4 107.16(3) 13_455 9_566 ?
Si4 Cu2 Al4 72.84(3) 5_656 9_566 ?
Si4 Cu2 Al4 0.00(5) 9_566 9_566 ?
Al4 Cu2 Al4 180.0 1_545 9_566 ?
Si4 Cu2 Al4 180.0 1_545 9_566 ?
Si4 Cu2 Al4 0.0 13_455 13_455 ?
Si4 Cu2 Al4 180.0 5_656 13_455 ?
Si4 Cu2 Al4 107.16(3) 9_566 13_455 ?
Al4 Cu2 Al4 72.84(3) 1_545 13_455 ?
Si4 Cu2 Al4 72.84(3) 1_545 13_455 ?
Al4 Cu2 Al4 107.16(3) 9_566 13_455 ?
Si4 Cu2 Al4 180.0 13_455 5_656 ?
Si4 Cu2 Al4 0.00(5) 5_656 5_656 ?
Si4 Cu2 Al4 72.84(3) 9_566 5_656 ?
Al4 Cu2 Al4 107.16(3) 1_545 5_656 ?
Si4 Cu2 Al4 107.16(3) 1_545 5_656 ?
```

Al4 Cu2 Al4 72.84(3) 9_566 5_656 ?
Al4 Cu2 Al4 180.0 13_455 5_656 ?
Si4 Cu2 Si4 114.19(6) 13_455 13 ?
Si4 Cu2 Si4 65.81(6) 5_656 13 ?
Si4 Cu2 Si4 107.16(3) 9_566 13 ?
Al4 Cu2 Si4 72.84(3) 1_545 13 ?
Si4 Cu2 Si4 72.84(3) 1_545 13 ?
Al4 Cu2 Si4 107.16(3) 9_566 13 ?
Al4 Cu2 Si4 114.19(6) 13_455 13 ?
Al4 Cu2 Si4 65.81(6) 5_656 13 ?
Si4 Cu2 Al4 114.19(6) 13_455 13 ?
Si4 Cu2 Al4 65.81(6) 5_656 13 ?
Si4 Cu2 Al4 107.16(3) 9_566 13 ?
Al4 Cu2 Al4 72.84(3) 1_545 13 ?
Si4 Cu2 Al4 72.84(3) 1_545 13 ?
Al4 Cu2 Al4 107.16(3) 9_566 13 ?
Al4 Cu2 Al4 114.19(6) 13_455 13 ?
Al4 Cu2 Al4 65.81(6) 5_656 13 ?
Si4 Cu2 Al4 0.00(5) 13 13 ?
Si4 Cu2 Al4 65.81(6) 13_455 5_556 ?
Si4 Cu2 Al4 114.19(6) 5_656 5_556 ?
Si4 Cu2 Al4 72.84(3) 9_566 5_556 ?
Al4 Cu2 Al4 107.16(3) 1_545 5_556 ?
Si4 Cu2 Al4 107.16(3) 1_545 5_556 ?
Al4 Cu2 Al4 72.84(3) 9_566 5_556 ?
Al4 Cu2 Al4 65.81(6) 13_455 5_556 ?
Al4 Cu2 Al4 114.19(6) 5_656 5_556 ?
Si4 Cu2 Al4 180.0 13 5_556 ?
Al4 Cu2 Al4 180.0 13 5_556 ?
Si4 Cu2 Si4 107.16(3) 13_455 9_556 ?
Si4 Cu2 Si4 72.84(3) 5_656 9_556 ?
Si4 Cu2 Si4 114.19(6) 9_566 9_556 ?
Al4 Cu2 Si4 65.81(6) 1_545 9_556 ?
Si4 Cu2 Si4 65.81(6) 1_545 9_556 ?
Al4 Cu2 Si4 114.19(6) 9_566 9_556 ?
Al4 Cu2 Si4 107.16(3) 13_455 9_556 ?
Al4 Cu2 Si4 72.84(3) 5_656 9_556 ?
Si4 Cu2 Si4 107.16(3) 13 9_556 ?
Al4 Cu2 Si4 107.16(3) 13 9_556 ?
Al4 Cu2 Si4 72.84(3) 5_556 9_556 ?
Cu3 Al3 Al3 0.0 9_665 9_665 ?
Cu3 Al3 Si4 123.86(4) 9_665 13_565 ?
Al3 Al3 Si4 123.86(4) 9_665 13_565 ?
Cu3 Al3 Si4 123.86(4) 9_665 1_655 ?
Al3 Al3 Si4 123.86(4) 9_665 1_655 ?
Si4 Al3 Si4 71.92(4) 13_565 1_655 ?
Cu3 Al3 Al4 123.86(4) 9_665 13_565 ?
Al3 Al3 Al4 123.86(4) 9_665 13_565 ?
Si4 Al3 Al4 0.00(5) 13_565 13_565 ?
Si4 Al3 Al4 71.92(4) 1_655 13_565 ?
Cu3 Al3 Al4 123.86(4) 9_665 1_655 ?
Al3 Al3 Al4 123.86(4) 9_665 1_655 ?
Si4 Al3 Al4 71.92(4) 13_565 1_655 ?
Si4 Al3 Al4 0.00(5) 1_655 1_655 ?
Al4 Al3 Al4 71.92(4) 13_565 1_655 ?
Cu3 Al3 Al4 123.86(4) 9_665 . ?
Al3 Al3 Al4 123.86(4) 9_665 . ?
Si4 Al3 Al4 71.92(4) 13_565 . ?
Si4 Al3 Al4 112.28(8) 1_655 . ?
Al4 Al3 Al4 71.92(4) 13_565 . ?
Al4 Al3 Al4 112.28(8) 1_655 . ?
Cu3 Al3 Si4 123.86(4) 9_665 13 ?
Al3 Al3 Si4 123.86(4) 9_665 13 ?
Si4 Al3 Si4 112.28(8) 13_565 13 ?
Si4 Al3 Si4 71.92(4) 1_655 13 ?
Al4 Al3 Si4 112.28(8) 13_565 13 ?
Al4 Al3 Si4 71.92(4) 1_655 13 ?
Al4 Al3 Si4 71.92(4) . 13 ?
Cu3 Al3 Al4 123.86(4) 9_665 13 ?
Al3 Al3 Al4 123.86(4) 9_665 13 ?
Si4 Al3 Al4 112.28(8) 13_565 13 ?
Si4 Al3 Al4 71.92(4) 1_655 13 ?
Al4 Al3 Al4 112.28(8) 13_565 13 ?
Al4 Al3 Al4 71.92(4) 1_655 13 ?
Al4 Al3 Al4 71.92(4) . 13 ?
Si4 Al3 Al4 0.0 13 13 ?
Cu3 Al3 La1 68.49(2) 9_665 . ?
Al3 Al3 La1 68.49(2) 9_665 . ?
Si4 Al3 La1 138.642(12) 13_565 . ?
Si4 Al3 La1 138.642(12) 1_655 . ?
Al4 Al3 La1 138.642(12) 13_565 . ?
Al4 Al3 La1 138.642(12) 1_655 . ?
Al4 Al3 La1 70.00(3) . . ?
Si4 Al3 La1 70.00(3) 13 . ?
Al4 Al3 La1 70.00(3) 13 . ?
Cu3 Al3 La1 68.49(2) 9_665 1_665 ?
Al3 Al3 La1 68.49(2) 9_665 1_665 ?
Si4 Al3 La1 70.00(3) 13_565 1_665 ?
Si4 Al3 La1 70.00(3) 1_655 1_665 ?
Al4 Al3 La1 70.00(3) 13_565 1_665 ?
Al4 Al3 La1 70.00(3) 1_655 1_665 ?
Al4 Al3 La1 138.642(12) . 1_665 ?
Si4 Al3 La1 138.642(12) 13 1_665 ?
Al4 Al3 La1 138.642(12) 13 1_665 ?
La1 Al3 La1 136.97(4) . 1_665 ?
Cu2 Al4 Cu2 114.19(6) 1_565 . ?
Cu2 Al4 Cu3 107.617(18) 1_565 1_455 ?
Cu2 Al4 Cu3 107.617(18) . 1_455 ?
Cu2 Al4 Al3 107.617(18) 1_565 1_455 ?
Cu2 Al4 Al3 107.617(18) . 1_455 ?
Cu3 Al4 Al3 0.0 1_455 1_455 ?
Cu2 Al4 Al3 107.617(18) 1_565 . ?
Cu2 Al4 Al3 107.617(18) . . ?
Cu3 Al4 Al3 112.28(8) 1_455 . ?
Al3 Al4 Al3 112.28(8) 1_455 . ?
Cu2 Al4 Si4 57.10(3) 1_565 9_566 ?
Cu2 Al4 Si4 57.10(3) . 9_566 ?
Cu3 Al4 Si4 123.86(4) 1_455 9_566 ?
Al3 Al4 Si4 123.86(4) 1_455 9_566 ?
Al3 Al4 Si4 123.86(4) . 9_566 ?
Si4 Al4 Si4 0.0 9_566 9_566 ?
Cu2 Al4 Al4 53.582(15) 1_565 13_565 ?
Cu2 Al4 Al4 126.418(15) . 13_565 ?
Cu3 Al4 Al4 125.958(19) 1_455 13_565 ?
Al3 Al4 Al4 125.958(19) 1_455 13_565 ?
Al3 Al4 Al4 54.042(19) . 13_565 ?
Si4 Al4 Al4 90.0 9_566 13_565 ?
Al4 Al4 Al4 90.0 9_566 13_565 ?
Cu2 Al4 Al4 126.418(15) 1_565 13_455 ?
Cu2 Al4 Al4 53.582(15) . 13_455 ?
Cu3 Al4 Al4 54.042(19) 1_455 13_455 ?
Al3 Al4 Al4 54.042(19) 1_455 13_455 ?
Al3 Al4 Al4 125.958(19) . 13_455 ?
Si4 Al4 Al4 90.0 9_566 13_455 ?
Al4 Al4 Al4 90.0 9_566 13_455 ?
Al4 Al4 Al4 180.0 13_565 13_455 ?
Cu2 Al4 Al4 53.582(15) 1_565 13_465 ?
Cu2 Al4 Al4 126.418(15) . 13_465 ?
Cu3 Al4 Al4 54.042(19) 1_455 13_465 ?
Al3 Al4 Al4 54.042(19) 1_455 13_465 ?
Al3 Al4 Al4 125.958(19) . 13_465 ?
Si4 Al4 Al4 90.0 9_566 13_465 ?
Al4 Al4 Al4 90.0 9_566 13_465 ?
Al4 Al4 Al4 90.0 13_565 13_465 ?
Al4 Al4 Al4 90.0 13_455 13_465 ?
Cu2 Al4 Al4 126.418(15) 1_565 13 ?
Cu2 Al4 Al4 53.582(15) . 13 ?
Cu3 Al4 Al4 125.958(19) 1_455 13 ?
Al3 Al4 Al4 125.958(19) 1_455 13 ?
Al3 Al4 Al4 54.042(19) . 13 ?
Si4 Al4 Al4 90.0 9_566 13 ?
Al4 Al4 Al4 90.0 9_566 13 ?
Al4 Al4 Al4 90.0 13_565 13 ?
Al4 Al4 Al4 90.0 13_455 13 ?
Al4 Al4 Al4 180.0 13_465 13 ?

_diffrn_measured_fraction_theta_max 0.994
_diffrn_reflns_theta_full 31.46
_diffrn_measured_fraction_theta_full 0.994
_refine_diff_density_max 1.156
_refine_diff_density_min -2.607
_refine_diff_density_rms 0.539

A2.2 $CeCu_2(Al,Si)_5$

```
data_bld73
_audit_creation_method
SHELXL-97
_chemical_name_systematic
;
 ?
;
_chemical_name_common            ?
_chemical_melting_point          ?
_chemical_formula_moiety         'Al4
Ce Cu2 Si'
_chemical_formula_sum
 'Al4 Ce Cu2 Si'
_chemical_formula_weight         403.21

loop_
 _atom_type_symbol
 _atom_type_description
 _atom_type_scat_dispersion_real
 _atom_type_scat_dispersion_imag
 _atom_type_scat_source
 'Ce'  'Ce'  -0.2486   2.6331
 'International Tables Vol C Tables
4.2.6.8 and 6.1.1.4'
 'Cu'  'Cu'   0.3201   1.2651
 'International Tables Vol C Tables
4.2.6.8 and 6.1.1.4'
 'Al'  'Al'   0.0645   0.0514
 'International Tables Vol C Tables
4.2.6.8 and 6.1.1.4'
 'Si'  'Si'   0.0817   0.0704
 'International Tables Vol C Tables
4.2.6.8 and 6.1.1.4'

_symmetry_cell_setting
'tetragonal'
_symmetry_space_group_name_H-M
'P 4/m m m     '
_symmetry_space_group_name_Hall
               '-P 4 2 '

loop_
 _symmetry_equiv_pos_as_xyz
 'x, y, z'
 '-x, -y, z'
 'x, -y, -z'
 '-x, y, -z'
 '-y, -x, -z'
 'y, x, -z'
 'y, -x, z'
 '-y, x, z'
 '-x, -y, -z'
 'x, y, -z'
 '-x, y, z'
 'x, -y, z'
 'y, x, z'
 '-y, -x, z'
 '-y, x, -z'
 'y, -x, -z'

_cell_length_a                 4.2040(15)
_cell_length_b                 4.2040(15)
_cell_length_c                 7.925(4)
_cell_angle_alpha               90.00
_cell_angle_beta                90.00
_cell_angle_gamma                 90.00
_cell_volume                   140.06(10)
_cell_formula_units_Z            1
_cell_measurement_temperature
298(2)
_cell_measurement_reflns_used     294
_cell_measurement_theta_min       2.55
_cell_measurement_theta_max       34.97

_exptl_crystal_description       'plate'
_exptl_crystal_colour            'silver'
_exptl_crystal_size_max           0.05
_exptl_crystal_size_mid           0.05
_exptl_crystal_size_min           0.05
_exptl_crystal_density_meas       ?
_exptl_crystal_density_diffrn     4.780
_exptl_crystal_density_method     'not
measured'
_exptl_crystal_F_000              182
_exptl_absorpt_coefficient_mu     16.197
_exptl_absorpt_correction_type    'multi-
scan'
_exptl_absorpt_correction_T_min
0.4981
_exptl_absorpt_correction_T_max
0.4981
_exptl_absorpt_process_details    'denzo
scale pack'


_exptl_special_details
;
 ?
;

_diffrn_ambient_temperature       298(2)
_diffrn_radiation_wavelength
0.71073
_diffrn_radiation_type            MoK\a
_diffrn_radiation_source          'fine-
focus sealed tube'
_diffrn_radiation_monochromator
graphite
_diffrn_measurement_device_type
'KappaCCD'
_diffrn_measurement_method
'CCD'
_diffrn_detector_area_resol_mean  9
_diffrn_standards_number          ?
_diffrn_standards_interval_count  ?
_diffrn_standards_interval_time   ?
_diffrn_standards_decay_%         ?
_diffrn_reflns_number             303
_diffrn_reflns_av_R_equivalents
0.0136
_diffrn_reflns_av_sigmaI/netI     0.0141
_diffrn_reflns_limit_h_min        0
_diffrn_reflns_limit_h_max        6
_diffrn_reflns_limit_k_min        -4
_diffrn_reflns_limit_k_max        4
_diffrn_reflns_limit_l_min        0
_diffrn_reflns_limit_l_max        12
_diffrn_reflns_theta_min          4.85
_diffrn_reflns_theta_max          34.16
_reflns_number_total              211
_reflns_number_gt                 205
_reflns_threshold_expression      >2\s(I)

_computing_data_collection
'KappaCCD'
_computing_cell_refinement        'HKL
Scalepack (Otwinowski & Minor 1997)'
_computing_data_reduction         'Denzo
and Scalepak (Otwinowski & Minor,
1997)'
_computing_structure_solution
'SHELXS-97 (Sheldrick, 1990)'
_computing_structure_refinement
'SHELXL-97 (Sheldrick, 2008)'
_computing_molecular_graphics     ?
_computing_publication_material   ?

_refine_special_details
;
 Refinement of F^2^ against ALL
reflections.  The weighted R-factor wR
and
 goodness of fit S are based on F^2^,
conventional R-factors R are based
 on F, with F set to zero for negative
F^2^. The threshold expression of
 F^2^ > 2\s(F^2^) is used only for
calculating R-factors(gt) etc. and is
 not relevant to the choice of reflections
for refinement.  R-factors based
 on F^2^ are statistically about twice as
large as those based on F, and R-
 factors based on ALL data will be even
larger.
;

_refine_ls_structure_factor_coef  Fsqd
_refine_ls_matrix_type            full
_refine_ls_weighting_scheme       calc
_refine_ls_weighting_details
 'calc
w=1/[\s^2^(Fo^2^)+(0.0181P)^2^+0.208
0P] where P=(Fo^2^+2Fc^2^)/3'
_atom_sites_solution_primary      direct
_atom_sites_solution_secondary
difmap
_atom_sites_solution_hydrogens    ?
_refine_ls_hydrogen_treatment     ?
_refine_ls_extinction_method
SHELXL
_refine_ls_extinction_coef        0.085(5)
_refine_ls_extinction_expression

'Fc^*^=kFc[1+0.001xFc^2^\l^3^/sin(2\q
)]^-1/4^'
_refine_ls_number_reflns          211
_refine_ls_number_parameters      13
_refine_ls_number_restraints      0
_refine_ls_R_factor_all           0.0164
_refine_ls_R_factor_gt            0.0153
_refine_ls_wR_factor_ref          0.0387
_refine_ls_wR_factor_gt           0.0378
_refine_ls_goodness_of_fit_ref    1.266
_refine_ls_restrained_S_all       1.266
_refine_ls_shift/su_max           0.000
_refine_ls_shift/su_mean          0.000

loop_
 _atom_site_label
 _atom_site_type_symbol
 _atom_site_fract_x
 _atom_site_fract_y
```

```
 _atom_site_fract_z
 _atom_site_U_iso_or_equiv
 _atom_site_adp_type
 _atom_site_occupancy
 _atom_site_symmetry_multiplicity
 _atom_site_calc_flag
 _atom_site_refinement_flags
 _atom_site_disorder_assembly
 _atom_site_disorder_group
Ce1 Ce 0.0000 0.0000 0.0000
0.00526(14) Uani 1 16 d S . .
Cu2 Cu 0.0000 0.0000 0.5000
0.00639(18) Uani 1 16 d S . .
Al3 Al 0.5000 0.5000 0.14747(10)
0.00616(18) Uani 0.50 8 d SP . .
Cu3 Cu 0.5000 0.5000 0.14747(10)
0.00616(18) Uani 0.50 8 d SP . .
Al4 Al 0.0000 0.5000 0.32658(12)
0.0088(2) Uani 0.75 4 d SP . .
Si4 Si 0.0000 0.5000 0.32658(12)
0.0088(2) Uani 0.25 4 d SP . .

loop_
 _atom_site_aniso_label
 _atom_site_aniso_U_11
 _atom_site_aniso_U_22
 _atom_site_aniso_U_33
 _atom_site_aniso_U_23
 _atom_site_aniso_U_13
 _atom_site_aniso_U_12
Ce1 0.00445(15) 0.00445(15)
0.00689(19) 0.000 0.000 0.000
Cu2 0.0058(2) 0.0058(2) 0.0076(3)
0.000 0.000 0.000
Al3 0.0062(2) 0.0062(2) 0.0061(3) 0.000
0.000 0.000
Cu3 0.0062(2) 0.0062(2) 0.0061(3)
0.000 0.000 0.000
Al4 0.0111(4) 0.0074(4) 0.0080(4) 0.000
0.000 0.000
Si4 0.0111(4) 0.0074(4) 0.0080(4) 0.000
0.000 0.000

_geom_special_details
;
 All s.u.'s (except the s.u. in the dihedral
angle between two l.s. planes)
 are estimated using the full covariance
matrix.  The cell s.u.'s are taken
 into account individually in the
estimation of s.u.'s in distances, angles
 and torsion angles; correlations between
s.u.'s in cell parameters are only
 used when they are defined by crystal
symmetry.  An approximate (isotropic)
 treatment of cell s.u.'s is used for
estimating s.u.'s involving l.s. planes.
;

loop_
 _geom_bond_atom_site_label_1
 _geom_bond_atom_site_label_2
 _geom_bond_distance
 _geom_bond_site_symmetry_2
 _geom_bond_publ_flag
Ce1 Cu3 3.1942(11) 9 ?
Ce1 Al3 3.1942(11) . ?
Ce1 Al3 3.1942(11) 9 ?
Ce1 Cu3 3.1942(11) 9_665 ?
Ce1 Al3 3.1942(11) 1_445 ?
Ce1 Cu3 3.1942(11) 1_445 ?
Ce1 Al3 3.1942(11) 9_665 ?
Ce1 Al3 3.1942(11) 1_545 ?
Ce1 Al3 3.1942(11) 9_655 ?
Ce1 Al3 3.1942(11) 9_565 ?
Ce1 Cu3 3.1942(11) 9_565 ?
Cu2 Si4 2.5114(9) 13_455 ?
Cu2 Si4 2.5114(9) 5_656 ?
Cu2 Si4 2.5114(9) 9_566 ?
Cu2 Al4 2.5114(9) 1_545 ?
Cu2 Si4 2.5114(9) 1_545 ?
Cu2 Al4 2.5114(9) 9_566 ?
Cu2 Al4 2.5114(9) 13_455 ?
Cu2 Al4 2.5114(9) 5_656 ?
Cu2 Si4 2.5114(9) 13 ?
Cu2 Al4 2.5114(9) 13 ?
Cu2 Al4 2.5114(9) 5_556 ?
Cu2 Si4 2.5114(9) 9_556 ?
Al3 Cu3 2.337(2) 9_665 ?
Al3 Al3 2.337(2) 9_665 ?
Al3 Si4 2.5364(10) 13_565 ?
Al3 Si4 2.5364(10) 1_655 ?
Al3 Al4 2.5364(10) 13_565 ?
Al3 Al4 2.5364(10) 1_655 ?
Al3 Al4 2.5364(10) . ?
Al3 Si4 2.5364(10) 13 ?
Al3 Al4 2.5364(10) 13 ?
Al3 Ce1 3.1942(11) 1_665 ?
Al4 Cu2 2.5114(9) 1_565 ?
Al4 Cu3 2.5364(10) 1_455 ?
Al4 Al3 2.5364(10) 1_455 ?
Al4 Si4 2.749(2) 9_566 ?
Al4 Al4 2.749(2) 9_566 ?
Al4 Al4 2.9727(11) 13_565 ?
Al4 Al4 2.9727(11) 13_455 ?
Al4 Al4 2.9727(11) 13_465 ?
Al4 Al4 2.9727(11) 13 ?

loop_
 _geom_angle_atom_site_label_1
 _geom_angle_atom_site_label_2
 _geom_angle_atom_site_label_3
 _geom_angle
 _geom_angle_site_symmetry_1
 _geom_angle_site_symmetry_3
 _geom_angle_publ_flag
Cu3 Ce1 Al3 180.00(3) 9 . ?
Cu3 Ce1 Al3 0.00(3) 9 9 ?
Al3 Ce1 Al3 180.00(3) . 9 ?
Cu3 Ce1 Cu3 137.08(4) 9 9_665 ?
Al3 Ce1 Cu3 42.92(4) . 9_665 ?
Al3 Ce1 Cu3 137.08(4) 9 9_665 ?
Cu3 Ce1 Al3 42.92(4) 9 1_445 ?
Al3 Ce1 Al3 137.08(4) . 1_445 ?
Al3 Ce1 Al3 42.92(4) 9 1_445 ?
Cu3 Ce1 Al3 180.00(3) 9_665 1_445 ?
Cu3 Ce1 Cu3 42.92(4) 9 1_445 ?
Al3 Ce1 Cu3 137.08(4) . 1_445 ?
Al3 Ce1 Cu3 42.92(4) 9 1_445 ?
Cu3 Ce1 Cu3 180.00(3) 9_665 1_445 ?
Al3 Ce1 Cu3 0.00(3) 1_445 1_445 ?
Cu3 Ce1 Al3 137.08(4) 9 9_665 ?
Al3 Ce1 Al3 42.92(4) . 9_665 ?
Al3 Ce1 Al3 137.08(4) 9 9_665 ?
Cu3 Ce1 Al3 0.00(3) 9_665 9_665 ?
Al3 Ce1 Al3 180.00(3) 1_445 9_665 ?
Cu3 Ce1 Al3 180.00(3) 1_445 9_665 ?
Cu3 Ce1 Al3 97.693(13) 9 1_545 ?
Al3 Ce1 Al3 82.307(13) . 1_545 ?
Al3 Ce1 Al3 97.693(13) 9 1_545 ?
Cu3 Ce1 Al3 97.693(12) 9_665 1_545 ?
Al3 Ce1 Al3 82.307(12) 1_445 1_545 ?
Cu3 Ce1 Al3 82.307(12) 1_445 1_545 ?
Al3 Ce1 Al3 97.693(12) 9_665 1_545 ?
Cu3 Ce1 Al3 82.307(12) 9 9_655 ?
Al3 Ce1 Al3 97.693(13) . 9_655 ?
Al3 Ce1 Al3 82.307(12) 9 9_655 ?
Cu3 Ce1 Al3 82.307(12) 9_665 9_655 ?
Al3 Ce1 Al3 97.693(12) 1_445 9_655 ?
Cu3 Ce1 Al3 97.693(12) 1_445 9_655 ?
Al3 Ce1 Al3 82.307(12) 9_665 9_655 ?
Al3 Ce1 Al3 42.92(4) 1_545 9_655 ?
Cu3 Ce1 Al3 82.307(12) 9 9_565 ?
Al3 Ce1 Al3 97.693(13) . 9_565 ?
Al3 Ce1 Al3 82.307(12) 9 9_565 ?
Cu3 Ce1 Al3 82.307(12) 9_665 9_565 ?
Al3 Ce1 Al3 97.693(12) 1_445 9_565 ?
Cu3 Ce1 Al3 97.693(12) 1_445 9_565 ?
Al3 Ce1 Al3 82.307(12) 9_665 9_565 ?
Al3 Ce1 Al3 180.0 1_545 9_565 ?
Al3 Ce1 Al3 137.08(4) 9_655 9_565 ?
Cu3 Ce1 Cu3 82.307(12) 9 9_565 ?
Al3 Ce1 Cu3 97.693(13) . 9_565 ?
Al3 Ce1 Cu3 82.307(12) 9 9_565 ?
Cu3 Ce1 Cu3 82.307(12) 9_665 9_565 ?
Al3 Ce1 Cu3 97.693(12) 1_445 9_565 ?
Cu3 Ce1 Cu3 97.693(12) 1_445 9_565 ?
Al3 Ce1 Cu3 82.307(12) 9_665 9_565 ?
Al3 Ce1 Cu3 180.0 1_545 9_565 ?
Al3 Ce1 Cu3 137.08(4) 9_655 9_565 ?
Al3 Ce1 Cu3 0.0 9_565 9_565 ?
Si4 Cu2 Si4 180.0 13_455 5_656 ?
Si4 Cu2 Si4 107.43(2) 13_455 9_566 ?
Si4 Cu2 Si4 72.57(2) 5_656 9_566 ?
Si4 Cu2 Al4 72.57(2) 13_455 1_545 ?
Si4 Cu2 Al4 107.43(2) 5_656 1_545 ?
Si4 Cu2 Al4 180.0 9_566 1_545 ?
Si4 Cu2 Si4 72.57(2) 13_455 1_545 ?
Si4 Cu2 Si4 107.43(2) 5_656 1_545 ?
Si4 Cu2 Si4 180.0 9_566 1_545 ?
Al4 Cu2 Si4 0.0 1_545 1_545 ?
Si4 Cu2 Al4 107.43(2) 13_455 9_566 ?
Si4 Cu2 Al4 72.57(2) 5_656 9_566 ?
Si4 Cu2 Al4 0.00(4) 9_566 9_566 ?
Al4 Cu2 Al4 180.0 1_545 9_566 ?
Si4 Cu2 Al4 180.0 1_545 9_566 ?
Si4 Cu2 Al4 0.0 13_455 13_455 ?
Si4 Cu2 Al4 180.0 5_656 13_455 ?
Si4 Cu2 Al4 107.43(2) 9_566 13_455 ?
Al4 Cu2 Al4 72.57(2) 1_545 13_455 ?
Si4 Cu2 Al4 72.57(2) 1_545 13_455 ?
Al4 Cu2 Al4 107.43(2) 9_566 13_455 ?
Si4 Cu2 Al4 180.0 13_455 5_656 ?
Si4 Cu2 Al4 0.00(4) 5_656 5_656 ?
Si4 Cu2 Al4 72.57(2) 9_566 5_656 ?
Al4 Cu2 Al4 107.43(2) 1_545 5_656 ?
Si4 Cu2 Al4 107.43(2) 1_545 5_656 ?
Al4 Cu2 Al4 72.57(2) 9_566 5_656 ?
Al4 Cu2 Al4 180.0 13_455 5_656 ?
Si4 Cu2 Si4 113.64(5) 13_455 13 ?
Si4 Cu2 Si4 66.36(5) 5_656 13 ?
Si4 Cu2 Si4 107.43(2) 9_566 13 ?
Al4 Cu2 Si4 72.57(2) 1_545 13 ?
Si4 Cu2 Si4 72.57(2) 1_545 13 ?
Al4 Cu2 Si4 107.43(2) 9_566 13 ?
Al4 Cu2 Si4 113.64(5) 13_455 13 ?
Al4 Cu2 Si4 66.36(5) 5_656 13 ?
Si4 Cu2 Al4 113.64(5) 13_455 13 ?
Si4 Cu2 Al4 66.36(5) 5_656 13 ?
Si4 Cu2 Al4 107.43(2) 9_566 13 ?
```

Al4 Cu2 Al4 72.57(2) 1_545 13 ?
Si4 Cu2 Al4 72.57(2) 1_545 13 ?
Al4 Cu2 Al4 107.43(2) 9_566 13 ?
Al4 Cu2 Al4 113.64(5) 13_455 13 ?
Al4 Cu2 Al4 66.36(5) 5_656 13 ?
Si4 Cu2 Al4 0.00(4) 13 13 ?
Si4 Cu2 Al4 66.36(5) 13_455 5_556 ?
Si4 Cu2 Al4 113.64(5) 5_656 5_556 ?
Si4 Cu2 Al4 72.57(2) 9_566 5_556 ?
Al4 Cu2 Al4 107.43(2) 1_545 5_556 ?
Si4 Cu2 Al4 107.43(2) 1_545 5_556 ?
Al4 Cu2 Al4 72.57(2) 9_566 5_556 ?
Al4 Cu2 Al4 66.36(5) 13_455 5_556 ?
Al4 Cu2 Al4 113.64(5) 5_656 5_556 ?
Si4 Cu2 Al4 180.0 13 5_556 ?
Al4 Cu2 Al4 180.0 13 5_556 ?
Si4 Cu2 Si4 107.43(2) 13_455 9_556 ?
Si4 Cu2 Si4 72.57(2) 5_656 9_556 ?
Si4 Cu2 Si4 113.64(5) 9_566 9_556 ?
Al4 Cu2 Si4 66.36(5) 1_545 9_556 ?
Si4 Cu2 Si4 66.36(5) 1_545 9_556 ?
Al4 Cu2 Si4 113.64(5) 9_566 9_556 ?
Al4 Cu2 Si4 107.43(2) 13_455 9_556 ?
Al4 Cu2 Si4 72.57(2) 5_656 9_556 ?
Si4 Cu2 Si4 107.43(2) 13 9_556 ?
Al4 Cu2 Si4 107.43(2) 13 9_556 ?
Al4 Cu2 Si4 72.57(2) 5_556 9_556 ?
Cu3 Al3 Al3 0.0 9_665 9_665 ?
Cu3 Al3 Si4 124.03(3) 9_665 13_565 ?
Al3 Al3 Si4 124.03(3) 9_665 13_565 ?
Cu3 Al3 Si4 124.03(3) 9_665 1_655 ?
Al3 Al3 Si4 124.03(3) 9_665 1_655 ?
Si4 Al3 Si4 71.75(3) 13_565 1_655 ?
Cu3 Al3 Al4 124.03(3) 9_665 13_565 ?
Al3 Al3 Al4 124.03(3) 9_665 13_565 ?
Si4 Al3 Al4 0.00(4) 13_565 13_565 ?
Si4 Al3 Al4 71.75(3) 1_655 13_565 ?
Cu3 Al3 Al4 124.03(3) 9_665 1_655 ?
Al3 Al3 Al4 124.03(3) 9_665 1_655 ?
Si4 Al3 Al4 71.75(3) 13_565 1_655 ?
Si4 Al3 Al4 0.00(4) 1_655 1_655 ?
Al4 Al3 Al4 71.75(3) 13_565 1_655 ?
Cu3 Al3 Al4 124.03(3) 9_665 . ?
Al3 Al3 Al4 124.03(3) 9_665 . ?
Si4 Al3 Al4 71.75(3) 13_565 . ?
Si4 Al3 Al4 111.94(6) 1_655 . ?
Al4 Al3 Al4 71.75(3) 13_565 . ?
Al4 Al3 Al4 111.94(6) 1_655 . ?
Cu3 Al3 Si4 124.03(3) 9_665 13 ?
Al3 Al3 Si4 124.03(3) 9_665 13 ?
Si4 Al3 Si4 111.94(6) 13_565 13 ?
Si4 Al3 Si4 71.75(3) 1_655 13 ?
Al4 Al3 Si4 111.94(6) 13_565 13 ?
Al4 Al3 Si4 71.75(3) 1_655 13 ?
Al4 Al3 Si4 71.75(3) . 13 ?
Cu3 Al3 Al4 124.03(3) 9_665 13 ?
Al3 Al3 Al4 124.03(3) 9_665 13 ?
Si4 Al3 Al4 111.94(6) 13_565 13 ?
Si4 Al3 Al4 71.75(3) 1_655 13 ?
Al4 Al3 Al4 111.94(6) 13_565 13 ?
Al4 Al3 Al4 71.75(3) 1_655 13 ?
Al4 Al3 Al4 71.75(3) . 13 ?
Si4 Al3 Al4 0.0 13 13 ?
Cu3 Al3 Ce1 68.538(18) 9_665 . ?
Al3 Al3 Ce1 68.538(18) 9_665 . ?
Si4 Al3 Ce1 138.602(9) 13_565 . ?
Si4 Al3 Ce1 138.602(9) 1_655 . ?
Al4 Al3 Ce1 138.602(9) 13_565 . ?
Al4 Al3 Ce1 138.602(9) 1_655 . ?
Al4 Al3 Ce1 70.09(2) . . ?
Si4 Al3 Ce1 70.09(2) 13 . ?
Al4 Al3 Ce1 70.09(2) 13 . ?
Cu3 Al3 Ce1 68.538(18) 9_665 1_665 ?
Al3 Al3 Ce1 68.538(18) 9_665 1_665 ?
Si4 Al3 Ce1 70.09(2) 13_565 1_665 ?
Si4 Al3 Ce1 70.09(2) 1_655 1_665 ?
Al4 Al3 Ce1 70.09(2) 13_565 1_665 ?
Al4 Al3 Ce1 70.09(2) 1_655 1_665 ?
Al4 Al3 Ce1 138.602(9) . 1_665 ?
Si4 Al3 Ce1 138.602(9) 13 1_665 ?
Al4 Al3 Ce1 138.602(9) 13 1_665 ?
Ce1 Al3 Ce1 137.08(4) . 1_665 ?
Cu2 Al4 Cu2 113.64(5) 1_565 . ?
Cu2 Al4 Cu3 107.834(17) 1_565 1_455 ?
Cu2 Al4 Cu3 107.834(17) . 1_455 ?
Cu2 Al4 Al3 107.834(17) 1_565 1_455 ?
Cu2 Al4 Al3 107.834(17) . 1_455 ?
Cu3 Al4 Al3 0.0 1_455 1_455 ?
Cu2 Al4 Al3 107.834(17) 1_565 . ?
Cu2 Al4 Al3 107.834(17) . . ?
Cu3 Al4 Al3 111.94(6) 1_455 . ?
Al3 Al4 Al3 111.94(6) 1_455 . ?
Cu2 Al4 Si4 56.82(2) 1_565 9_566 ?
Cu2 Al4 Si4 56.82(2) . 9_566 ?
Cu3 Al4 Si4 124.03(3) 1_455 9_566 ?
Al3 Al4 Si4 124.03(3) 1_455 9_566 ?
Al3 Al4 Si4 124.03(3) . 9_566 ?
Cu2 Al4 Al4 56.82(2) 1_565 9_566 ?
Cu2 Al4 Al4 56.82(2) . 9_566 ?
Cu3 Al4 Al4 124.03(3) 1_455 9_566 ?
Al3 Al4 Al4 124.03(3) 1_455 9_566 ?
Al3 Al4 Al4 124.03(3) . 9_566 ?
Si4 Al4 Al4 0.0 9_566 9_566 ?
Cu2 Al4 Al4 53.713(12) 1_565 13_565 ?
Cu2 Al4 Al4 126.287(12) . 13_565 ?
Cu3 Al4 Al4 125.874(14) 1_455 13_565 ?
Al3 Al4 Al4 125.874(14) 1_455 13_565 ?
Al3 Al4 Al4 54.126(14) . 13_565 ?
Si4 Al4 Al4 90.0 9_566 13_565 ?
Al4 Al4 Al4 90.0 9_566 13_565 ?
Cu2 Al4 Al4 126.287(12) 1_565 13_455 ?
Cu2 Al4 Al4 53.713(12) . 13_455 ?
Cu3 Al4 Al4 54.126(14) 1_455 13_455 ?
Al3 Al4 Al4 54.126(14) 1_455 13_455 ?
Al3 Al4 Al4 125.874(14) . 13_455 ?
Si4 Al4 Al4 90.0 9_566 13_455 ?
Al4 Al4 Al4 90.0 9_566 13_455 ?
Al4 Al4 Al4 180.0 13_565 13_455 ?
Cu2 Al4 Al4 53.713(12) 1_565 13_465 ?
Cu2 Al4 Al4 126.287(12) . 13_465 ?
Cu3 Al4 Al4 54.126(14) 1_455 13_465 ?
Al3 Al4 Al4 54.126(14) 1_455 13_465 ?
Al3 Al4 Al4 125.874(14) . 13_465 ?
Si4 Al4 Al4 90.0 9_566 13_465 ?
Al4 Al4 Al4 90.0 9_566 13_465 ?
Al4 Al4 Al4 90.0 13_565 13_465 ?
Al4 Al4 Al4 90.0 13_455 13_465 ?
Cu2 Al4 Al4 126.287(12) 1_565 13 ?
Cu2 Al4 Al4 53.713(12) . 13 ?
Cu3 Al4 Al4 125.874(14) 1_455 13 ?
Al3 Al4 Al4 125.874(14) 1_455 13 ?
Al3 Al4 Al4 54.126(14) . 13 ?
Si4 Al4 Al4 90.0 9_566 13 ?
Al4 Al4 Al4 90.0 9_566 13 ?
Al4 Al4 Al4 90.0 13_565 13 ?
Al4 Al4 Al4 90.0 13_455 13 ?
Al4 Al4 Al4 180.0 13_465 13 ?

_diffrn_measured_fraction_theta_max 0.968
_diffrn_reflns_theta_full 25.00
_diffrn_measured_fraction_theta_full 0.990
_refine_diff_density_max 1.069
_refine_diff_density_min -0.768
_refine_diff_density_rms 0.202

A2.3 MnGe 100819 at 300 K

```
data_mnge

_audit_creation_method
SHELXL-97
_chemical_name_systematic
;
 ?
;
_chemical_name_common            ?
_chemical_melting_point          ?
_chemical_formula_moiety         'Mn1
Ge1'
_chemical_formula_sum
 'Ge Mn'
_chemical_formula_weight         127.53

loop_
 _atom_type_symbol
 _atom_type_description
 _atom_type_scat_dispersion_real
 _atom_type_scat_dispersion_imag
 _atom_type_scat_source
 'Mn'  'Mn'   0.3368   0.7283
 'International Tables Vol C Tables
4.2.6.8 and 6.1.1.4'
 'Ge'  'Ge'   0.1547   1.8001
 'International Tables Vol C Tables
4.2.6.8 and 6.1.1.4'

_symmetry_cell_setting           'cubic'
_symmetry_space_group_name_H-M
'P 21 3'
_symmetry_space_group_name_Hall  'P
2ac 2ab 3'



loop_
 _symmetry_equiv_pos_as_xyz
 'x, y, z'
 '-x+1/2, -y, z+1/2'
 'x+1/2, -y+1/2, -z'
 '-x, y+1/2, -z+1/2'
 'z, x, y'
 'y, z, x'
 '-z+1/2, -x, y+1/2'
 '-y, z+1/2, -x+1/2'
 'z+1/2, -x+1/2, -y'
 '-y+1/2, -z, x+1/2'
 '-z, x+1/2, -y+1/2'
 'y+1/2, -z+1/2, -x'

_cell_length_a                   4.797(4)
_cell_length_b                   4.797(4)
_cell_length_c                   4.797(4)
_cell_angle_alpha                90.00
_cell_angle_beta                 90.00
_cell_angle_gamma                90.00
_cell_volume                     110.41(14)
_cell_formula_units_Z            4
_cell_measurement_temperature
293(2)
_cell_measurement_reflns_used    65
_cell_measurement_theta_min      0.998
_cell_measurement_theta_max
30.034

_exptl_crystal_description       'plate'
_exptl_crystal_colour            'silver'
_exptl_crystal_size_max          0.05
_exptl_crystal_size_mid          0.05
_exptl_crystal_size_min          0.05
_exptl_crystal_density_meas      ?
_exptl_crystal_density_diffrn    7.672
_exptl_crystal_density_method    'not
measured'
_exptl_crystal_F_000             228
_exptl_absorpt_coefficient_mu    37.679
_exptl_absorpt_correction_type   'multi-
scan'
_exptl_absorpt_correction_T_min
0.2545
_exptl_absorpt_correction_T_max
0.2545
_exptl_absorpt_process_details   'denzo
scale pack'

_exptl_special_details
;
 ?
;


_diffrn_ambient_temperature      293(2)
_diffrn_radiation_wavelength
0.71073
_diffrn_radiation_type           MoK\a
_diffrn_radiation_source         'fine-
focus sealed tube'
_diffrn_radiation_monochromator
graphite
_diffrn_measurement_device_type
'KappaCCD'
_diffrn_measurement_method
'CCD'
_diffrn_detector_area_resol_mean  9
_diffrn_standards_number         ?
_diffrn_standards_interval_count  ?
_diffrn_standards_interval_time   ?
_diffrn_standards_decay_%        ?
_diffrn_reflns_number            107
_diffrn_reflns_av_R_equivalents
0.0000
_diffrn_reflns_av_sigmaI/netI    0.0481
_diffrn_reflns_limit_h_min       -4
_diffrn_reflns_limit_h_max       4
_diffrn_reflns_limit_k_min       -6
_diffrn_reflns_limit_k_max       6
_diffrn_reflns_limit_l_min       -4
_diffrn_reflns_limit_l_max       4
_diffrn_reflns_theta_min         6.01
_diffrn_reflns_theta_max         29.80
_reflns_number_total             107
_reflns_number_gt                102
_reflns_threshold_expression     >2\s(I)

_computing_data_collection       'Nonius
KappaCCD'
_computing_cell_refinement       'HKL
Scalepack (Otwinowski & Minor 1997)'
_computing_data_reduction        'HKL
Denzo and Scalepack (Otwinowski &
Minor 1997)'
_computing_structure_solution
'SHELXS-97 (Sheldrick, 1990)'
_computing_structure_refinement
'SHELXL-97 (Sheldrick, 2008)'
_computing_molecular_graphics    ?
_computing_publication_material  ?

_refine_special_details
;
 Refinement of F^2^ against ALL
reflections.  The weighted R-factor wR
and
 goodness of fit S are based on F^2^,
conventional R-factors R are based
 on F, with F set to zero for negative
F^2^. The threshold expression of
 F^2^ > 2\s(F^2^) is used only for
calculating R-factors(gt) etc. and is
 not relevant to the choice of reflections
for refinement.  R-factors based
 on F^2^ are statistically about twice as
large as those based on F, and R-
 factors based on ALL data will be even
larger.
;

_refine_ls_structure_factor_coef  Fsqd
_refine_ls_matrix_type           full
_refine_ls_weighting_scheme      calc
_refine_ls_weighting_details
 'calc
w=1/[\s^2^(Fo^2^)+(0.0000P)^2^+0.000
0P] where P=(Fo^2^+2Fc^2^)/3'
_atom_sites_solution_primary     direct
_atom_sites_solution_secondary
difmap
_atom_sites_solution_hydrogens   ?
_refine_ls_hydrogen_treatment    ?
_refine_ls_extinction_method
SHELXL
_refine_ls_extinction_coef       0.016(3)
_refine_ls_extinction_expression

'Fc^*^=kFc[1+0.001xFc^2^\l^3^/sin(2\q
)]^-1/4^'
_refine_ls_abs_structure_details
 'Flack H D (1983), Acta Cryst. A39,
876-881'
_refine_ls_abs_structure_Flack   -
0.02(6)
_refine_ls_number_reflns         107
_refine_ls_number_parameters     8
_refine_ls_number_restraints     0
_refine_ls_R_factor_all          0.0242
_refine_ls_R_factor_gt           0.0219
_refine_ls_wR_factor_ref         0.0458
_refine_ls_wR_factor_gt          0.0435
_refine_ls_goodness_of_fit_ref   0.972
_refine_ls_restrained_S_all      0.972
_refine_ls_shift/su_max          0.015
_refine_ls_shift/su_mean         0.004

loop_
 _atom_site_label
 _atom_site_type_symbol
 _atom_site_fract_x
 _atom_site_fract_y
 _atom_site_fract_z
 _atom_site_U_iso_or_equiv
 _atom_site_adp_type
 _atom_site_occupancy
 _atom_site_symmetry_multiplicity
 _atom_site_calc_flag
```

```
 _atom_site_refinement_flags
 _atom_site_disorder_assembly
 _atom_site_disorder_group
Mn01 Mn 0.86268(12) 0.86268(12)
0.86268(12) 0.0076(3) Uani 1 3 d S . .
Ge02 Ge 0.15628(9) 0.15628(9)
0.15628(9) 0.0085(3) Uani 1 3 d S . .

loop_
 _atom_site_aniso_label
 _atom_site_aniso_U_11
 _atom_site_aniso_U_22
 _atom_site_aniso_U_33
 _atom_site_aniso_U_23
 _atom_site_aniso_U_13
 _atom_site_aniso_U_12
Mn01 0.0076(3) 0.0076(3) 0.0076(3)
0.0000(2) 0.0000(2) 0.0000(2)
Ge02 0.0085(3) 0.0085(3) 0.0085(3) -
0.00068(15) -0.00068(15) -0.00068(15)

_geom_special_details
;
 All s.u.'s (except the s.u. in the dihedral
angle between two l.s. planes)
 are estimated using the full covariance
matrix.  The cell s.u.'s are taken
 into account individually in the
estimation of s.u.'s in distances, angles
 and torsion angles; correlations between
s.u.'s in cell parameters are only
 used when they are defined by crystal
symmetry.  An approximate (isotropic)
 treatment of cell s.u.'s is used for
estimating s.u.'s involving l.s. planes.
;

loop_
 _geom_bond_atom_site_label_1
 _geom_bond_atom_site_label_2
 _geom_bond_distance
 _geom_bond_site_symmetry_2
 _geom_bond_publ_flag
Mn01 Ge02 2.440(2) 1_666 ?
Mn01 Ge02 2.5128(19) 4_656 ?
Mn01 Ge02 2.5128(19) 3_566 ?
Mn01 Ge02 2.5128(19) 2_665 ?
Mn01 Ge02 2.681(2) 4_655 ?
Mn01 Ge02 2.681(2) 3_556 ?
Mn01 Ge02 2.681(2) 2_565 ?
Mn01 Mn01 2.942(2) 2_675 ?
Mn01 Mn01 2.942(2) 4_756 ?
Mn01 Mn01 2.942(2) 3_567 ?
Mn01 Mn01 2.942(2) 2_674 ?
Mn01 Mn01 2.942(2) 3_467 ?
Ge02 Mn01 2.440(2) 1_444 ?
Ge02 Mn01 2.5128(19) 3_466 ?
Ge02 Mn01 2.5128(19) 2_664 ?
Ge02 Mn01 2.5128(19) 4_646 ?
Ge02 Mn01 2.681(2) 3_456 ?
Ge02 Mn01 2.681(2) 2_564 ?
Ge02 Mn01 2.681(2) 4_645 ?

loop_
 _geom_angle_atom_site_label_1
 _geom_angle_atom_site_label_2
 _geom_angle_atom_site_label_3
 _geom_angle
 _geom_angle_site_symmetry_1
 _geom_angle_site_symmetry_3
 _geom_angle_publ_flag
Ge02 Mn01 Ge02 73.63(2) 1_666 4_656
?
Ge02 Mn01 Ge02 73.63(2) 1_666 3_566
?
Ge02 Mn01 Ge02 112.39(2) 4_656
3_566 ?
Ge02 Mn01 Ge02 73.63(2) 1_666 2_665
?
Ge02 Mn01 Ge02 112.39(2) 4_656
2_665 ?
Ge02 Mn01 Ge02 112.39(2) 3_566
2_665 ?
Ge02 Mn01 Ge02 140.264(14) 1_666
4_655 ?
Ge02 Mn01 Ge02 134.92(3) 4_656
4_655 ?
Ge02 Mn01 Ge02 106.99(3) 3_566
4_655 ?
Ge02 Mn01 Ge02 69.625(13) 2_665
4_655 ?
Ge02 Mn01 Ge02 140.264(14) 1_666
3_556 ?
Ge02 Mn01 Ge02 69.625(13) 4_656
3_556 ?
Ge02 Mn01 Ge02 134.92(3) 3_566
3_556 ?
Ge02 Mn01 Ge02 106.99(3) 2_665
3_556 ?
Ge02 Mn01 Ge02 67.23(2) 4_655 3_556
?
Ge02 Mn01 Ge02 140.264(14) 1_666
2_565 ?
Ge02 Mn01 Ge02 106.99(3) 4_656
2_565 ?
Ge02 Mn01 Ge02 69.625(13) 3_566
2_565 ?
Ge02 Mn01 Ge02 134.92(3) 2_665
2_565 ?
Ge02 Mn01 Ge02 67.23(2) 4_655 2_565
?
Ge02 Mn01 Ge02 67.23(2) 3_556 2_565
?
Ge02 Mn01 Mn01 58.87(3) 1_666
2_675 ?
Ge02 Mn01 Mn01 54.162(9) 4_656
2_675 ?
Ge02 Mn01 Mn01 58.23(2) 3_566
2_675 ?
Ge02 Mn01 Mn01 132.44(5) 2_665
2_675 ?
Ge02 Mn01 Mn01 155.50(3) 4_655
2_675 ?
Ge02 Mn01 Mn01 107.92(3) 3_556
2_675 ?
Ge02 Mn01 Mn01 88.572(12) 2_565
2_675 ?
Ge02 Mn01 Mn01 58.87(3) 1_666
4_756 ?
Ge02 Mn01 Mn01 132.44(5) 4_656
4_756 ?
Ge02 Mn01 Mn01 54.162(9) 3_566
4_756 ?
Ge02 Mn01 Mn01 58.23(2) 2_665
4_756 ?
Ge02 Mn01 Mn01 88.572(12) 4_655
4_756 ?
Ge02 Mn01 Mn01 155.50(3) 3_556
4_756 ?
Ge02 Mn01 Mn01 107.92(3) 2_565
4_756 ?
Mn01 Mn01 Mn01 95.68(4) 2_675
4_756 ?
Ge02 Mn01 Mn01 58.87(3) 1_666
3_567 ?
Ge02 Mn01 Mn01 58.23(2) 4_656
3_567 ?
Ge02 Mn01 Mn01 132.44(5) 3_566
3_567 ?
Ge02 Mn01 Mn01 54.162(9) 2_665
3_567 ?
Ge02 Mn01 Mn01 107.92(3) 4_655
3_567 ?
Ge02 Mn01 Mn01 88.572(12) 3_556
3_567 ?
Ge02 Mn01 Mn01 155.50(3) 2_565
3_567 ?
Mn01 Mn01 Mn01 95.68(4) 2_675
3_567 ?
Mn01 Mn01 Mn01 95.68(4) 4_756
3_567 ?
Ge02 Mn01 Mn01 115.10(3) 1_666
2_674 ?
Ge02 Mn01 Mn01 155.75(3) 4_656
2_674 ?
Ge02 Mn01 Mn01 54.162(9) 3_566
2_674 ?
Ge02 Mn01 Mn01 91.857(13) 2_665
2_674 ?
Ge02 Mn01 Mn01 52.835(18) 4_655
2_674 ?
Ge02 Mn01 Mn01 104.62(4) 3_556
2_674 ?
Ge02 Mn01 Mn01 51.16(3) 2_565
2_674 ?
Mn01 Mn01 Mn01 109.210(5) 2_675
2_674 ?
Mn01 Mn01 Mn01 60.0 4_756 2_674 ?
Mn01 Mn01 Mn01 145.999(9) 3_567
2_674 ?
Ge02 Mn01 Mn01 115.10(3) 1_666
3_467 ?
Ge02 Mn01 Mn01 54.162(9) 4_656
3_467 ?
Ge02 Mn01 Mn01 91.857(13) 3_566
3_467 ?
Ge02 Mn01 Mn01 155.75(3) 2_665
3_467 ?
Ge02 Mn01 Mn01 104.62(4) 4_655
3_467 ?
Ge02 Mn01 Mn01 51.16(4) 3_556
3_467 ?
Ge02 Mn01 Mn01 52.835(18) 2_565
3_467 ?
Mn01 Mn01 Mn01 60.0 2_675 3_467 ?
Mn01 Mn01 Mn01 145.999(9) 4_756
3_467 ?
Mn01 Mn01 Mn01 109.210(5) 3_567
3_467 ?
Mn01 Mn01 Mn01 103.30(4) 2_674
3_467 ?
Mn01 Ge02 Mn01 137.463(12) 1_444
3_466 ?
Mn01 Ge02 Mn01 137.463(12) 1_444
2_664 ?
Mn01 Ge02 Mn01 71.676(19) 3_466
2_664 ?
Mn01 Ge02 Mn01 137.463(12) 1_444
4_646 ?
```

Mn01 Ge02 Mn01 71.676(19) 3_466 4_646 ?
Mn01 Ge02 Mn01 71.676(19) 2_664 4_646 ?
Mn01 Ge02 Mn01 69.971(15) 1_444 3_456 ?
Mn01 Ge02 Mn01 134.92(3) 3_466 3_456 ?
Mn01 Ge02 Mn01 68.934(13) 2_664 3_456 ?
Mn01 Ge02 Mn01 114.23(3) 4_646 3_456 ?
Mn01 Ge02 Mn01 69.971(15) 1_444 2_564 ?
Mn01 Ge02 Mn01 114.23(3) 3_466 2_564 ?
Mn01 Ge02 Mn01 134.92(3) 2_664 2_564 ?
Mn01 Ge02 Mn01 68.934(13) 4_646 2_564 ?
Mn01 Ge02 Mn01 108.907(16) 3_456 2_564 ?
Mn01 Ge02 Mn01 69.971(15) 1_444 4_645 ?
Mn01 Ge02 Mn01 68.934(13) 3_466 4_645 ?
Mn01 Ge02 Mn01 114.23(3) 2_664 4_645 ?
Mn01 Ge02 Mn01 134.92(3) 4_646 4_645 ?
Mn01 Ge02 Mn01 108.907(16) 3_456 4_645 ?
Mn01 Ge02 Mn01 108.907(16) 2_564 4_645 ?

_diffrn_measured_fraction_theta_max 1.000
_diffrn_reflns_theta_full 29.80
_diffrn_measured_fraction_theta_full 1.000
_refine_diff_density_max 0.721
_refine_diff_density_min -0.734
_refine_diff_density_rms 0.195

APPENDIX 3. LETTERS OF PERMISSION

A3.1 Ln_4FeGa_{12} (Ln = Tb – Er)

AMERICAN CHEMICAL SOCIETY LICENSE
TERMS AND CONDITIONS

Apr 26, 2011

This is a License Agreement between Brenton L Drake ("You") and American Chemical Society ("American Chemical Society") provided by Copyright Clearance Center ("CCC"). The license consists of your order details, the terms and conditions provided by American Chemical Society, and the payment terms and conditions.

All payments must be made in full to CCC. For payment instructions, please see information listed at the bottom of this form.

License Number	2656590729864
License Date	Apr 26, 2011
Licensed content publisher	American Chemical Society
Licensed content publication	Inorganic Chemistry
Licensed content title	Crystal Growth, Transport, and the Structural and Magnetic Properties of Ln4FeGa12 with Ln = Y, Tb, Dy, Ho, and Er
Licensed content author	Brenton L. Drake et al.
Licensed content date	Jan 1, 2010
Volume number	49
Issue number	2
Type of Use	Thesis/Dissertation
Requestor type	Not specified
Format	Print
Portion	Full article
Author of this ACS article	Yes
Order reference number	
Title of the thesis / dissertation	Crystal Growth of Complex Intermetallics in Search for Heavy Electron Systems
Expected completion date	Dec 2011
Estimated size(pages)	125
Billing Type	
Invoice	
Billing Address	315 Lake Worth Dr Baton Rouge, LA 70810
United States	
Customer reference info	
Total	0.00 USD
Terms and Conditions	

Thesis/Dissertation

ACS / RIGHTSLINK TERMS & CONDITIONS
THESIS/DISSERTATION

INTRODUCTION
The publisher for this copyrighted material is the American Chemical Society. By clicking "accept" in connection with completing this licensing transaction, you agree that the following terms and conditions apply to this transaction (along with the Billing and Payment terms and conditions established by Copyright Clearance Center,

Inc. ("CCC"), at the time that you opened your Rightslink account and that are available at any time at <http://myaccount.copyright.com>).

LIMITED LICENSE
Publisher hereby grants to you a non-exclusive license to use this material. Licenses are for one-time use only with a maximum distribution equal to the number that you identified in the licensing process.

GEOGRAPHIC RIGHTS: SCOPE
Licenses may be exercised anywhere in the world.

RESERVATION OF RIGHTS
Publisher reserves all rights not specifically granted in the combination of (i) the license details provided by you and accepted in the course of this licensing transaction, (ii) these terms and conditions and (iii) CCC's Billing and Payment terms and conditions.

PORTION RIGHTS STATEMENT: DISCLAIMER
If you seek to reuse a portion from an ACS publication, it is your responsibility to examine each portion as published to determine whether a credit to, or copyright notice of, a third party owner was published adjacent to the item. You may only obtain permission via Rightslink to use material owned by ACS. Permission to use any material published in an ACS publication, journal, or article which is reprinted with permission of a third party must be obtained from the third party owner. ACS disclaims any responsibility for any use you make of items owned by third parties without their permission.

REVOCATION
The American Chemical Society reserves the right to revoke a license for any reason, including but not limited to advertising and promotional uses of ACS content, third party usage, and incorrect figure source attribution.

LICENSE CONTINGENT ON PAYMENT
While you may exercise the rights licensed immediately upon issuance of the license at the end of the licensing process for the transaction, provided that you have disclosed complete and accurate details of your proposed use, no license is finally effective unless and until full payment is received from you (by CCC) as provided in CCC's Billing and Payment terms and conditions. If full payment is not received on a timely basis, then any license preliminarily granted shall be deemed automatically revoked and shall be void as if never granted. Further, in the event that you breach any of these terms and conditions or any of CCC's Billing and Payment terms and conditions, the license is automatically revoked and shall be void as if never granted. Use of materials as described in a revoked license, as well as any use of the materials beyond the scope of an unrevoked license, may constitute copyright infringement and publisher reserves the right to take any and all action to protect its copyright in the materials.

COPYRIGHT NOTICE: DISCLAIMER
You must include the following copyright and permission notice in connection with any reproduction of the licensed material: "Reprinted (“Adapted” or “in part”) with permission from REFERENCE CITATION. Copyright YEAR American Chemical Society."

WARRANTIES: NONE
Publisher makes no representations or warranties with respect to the licensed material.

INDEMNITY
You hereby indemnify and agree to hold harmless publisher and CCC, and their respective officers, directors, employees and agents, from and against any and all claims arising out of your use of the licensed material other than as specifically authorized pursuant to this license.

NO TRANSFER OF LICENSE
This license is personal to you or your publisher and may not be sublicensed, assigned, or transferred by you to any other person without publisher's written permission.

NO AMENDMENT EXCEPT IN WRITING
This license may not be amended except in a writing signed by both parties (or, in the case of publisher, by CCC on publisher's behalf).

OBJECTION TO CONTRARY TERMS
Publisher hereby objects to any terms contained in any purchase order, acknowledgment, check endorsement or other writing prepared by you, which terms are inconsistent with these terms and conditions or CCC's Billing and Payment terms and conditions. These terms and conditions, together with CCC's Billing and Payment terms and conditions (which are incorporated herein), comprise the entire agreement between you and publisher (and CCC) concerning this licensing transaction. In the event of any conflict between your obligations established by these terms and conditions and those established by CCC's Billing and Payment terms and conditions, these terms and conditions shall control.

JURISDICTION
This license transaction shall be governed by and construed in accordance with the laws of the District of Columbia. You hereby agree to submit to the jurisdiction of the courts located in the District of Columbia for purposes of resolving any disputes that may arise in connection with this licensing transaction.

THESES/DISSERTATION TERMS
Regarding your request for permission to include **your** paper(s) or portions of text from **your** paper(s) in your thesis/dissertation, permission is now automatically granted; please pay special attention to the **implications** paragraph below. The Copyright Subcommittee of the Joint Board/Council Committees on Publications approved the following:

Copyright permission for published and submitted material from theses and dissertations
ACS extends blanket permission to students to include in their theses and dissertations their own articles, or portions thereof, that have been published in ACS journals or submitted to ACS journals for publication, provided that the ACS copyright credit line is noted on the appropriate page(s).

Publishing **implications** of electronic publication of theses and dissertation material
Students and their mentors should be aware that posting of theses and dissertation material on the Web prior to submission of material from that thesis or dissertation to an ACS journal may affect publication in that journal. Whether Web posting is considered prior publication may be evaluated on a case-by-case basis by the journal's editor. If an ACS journal editor considers Web posting to be "prior publication", the paper will not be accepted for publication in that journal. If you intend to submit your unpublished paper to ACS for publication, check with the appropriate editor prior to posting your manuscript electronically.

Reuse/Republication of the Entire Work in Theses or Collections: Authors may reuse all or part of the Submitted, Accepted or Published Work in a thesis or dissertation that the author writes and is required to submit to satisfy the criteria of degree-granting institutions. Such reuse is permitted subject to the ACS' "Ethical Guidelines to Publication of Chemical Research" (http://pubs.acs.org/page/policy/ethics/index.html); the author should secure written confirmation (via letter or email) from the respective ACS journal editor(s) to avoid potential conflicts with journal prior publication*/embargo policies. Appropriate citation of the Published Work must be made. If the thesis or dissertation to be published is in electronic format, a direct link to the Published Work must also be included using the ACS Articles on Request author-directed link - see
http://pubs.acs.org/page/policy/articlesonrequest/index.html

* Prior publication policies of ACS journals are posted on the ACS website at
http://pubs.acs.org/page/policy/prior/index.html

If your paper has not yet been published by ACS, please print the following credit line on the first page of your article: "Reproduced (or 'Reproduced in part') with permission from [JOURNAL NAME], in press (or 'submitted for publication'). Unpublished work copyright [CURRENT YEAR] American Chemical Society." Include appropriate information.

If your paper has already been published by ACS and you want to include the text or portions of the text in your thesis/dissertation in **print or microfilm formats**, please print the ACS copyright credit line on the first page of your article: "Reproduced (or 'Reproduced in part') with permission from [FULL REFERENCE CITATION.] Copyright [YEAR] American Chemical Society." Include appropriate information.

Submission to a Dissertation Distributor: If you plan to submit your thesis to UMI or to another dissertation distributor, you should not include the unpublished ACS paper in your thesis if the thesis will be disseminated electronically, until ACS has published your paper. After publication of the paper by ACS, you may release the entire thesis (**not the individual ACS article by itself**) for electronic dissemination through the distributor; ACS's copyright credit line should be printed on the first page of the ACS paper.

v1.2

Gratis licenses (referencing $0 in the Total field) are free. Please retain this printable license for your reference. No payment is required.

If you would like to pay for this license now, please remit this license along with your payment made payable to "COPYRIGHT CLEARANCE CENTER" otherwise you will be invoiced within 48 hours of the license date. Payment should be in the form of a check or money order referencing your account number and this invoice number RLNK10976288.
Once you receive your invoice for this order, you may pay your invoice by credit card. Please follow instructions provided at that time.

Make Payment To:
Copyright Clearance Center
Dept 001
P.O. Box 843006
Boston, MA 02284-3006

For suggestions or comments regarding this order, contact Rightslink Customer Support: customercare@copyright.com or +1-877-622-5543 (toll free in the US) or +1-978-646-2777.

A3.2 *Ln*(Ag,Al,Si)$_2$ (Ln = Ce and Gd)

3/17/2011

To whom it may concern

I am currently preparing my dissertation tentatively titled *Synthesis and Characterization of Rare Earth – Copper Containing Ternary and Quaternary Aluminides and Alumosilicide* and I would appreciate permission to reproduce all figures in both print and electronic editions of the Journal and in all subsequent future editions of the Journal, any derivative products and in publisher authorized distribution by third party distributors, aggregators and other licensees such as abstracting and indexing services. I should be grateful for nonexclusive perpetual world rights in all languages and media. Unless you indicate otherwise, I will use the complete reference given below as the credit line.

Brenton L Drake *et al* 2010 *J. Phys.: Condens. Matter* **22** 426002; doi: 10.1088/0953-8984/22/42/426002.

In case you do not control these rights, I would appreciate it if you could let me know to whom I should apply for permissions.

1. We are requesting use of all figures associated with the above reference.

Figures 1 – 8, Crystal growth, structure, and physical properties of Ln(Ag, Al, Si)$_2$ (Ln = Ce and Gd), Brenton L Drake, Michael J Kangas, C Capan, N Haldolaarachchige, Y Xiong, P W Adams, D P Young and Julia Y Chan, Journal of Physics: Condensed Matter, 22, 426002, p 1 - 9, 2010.)

For material being published electronically a link to the version of record will be provided back to the original article via DOI.

For your information, Institute of Physics Publishing is a not-for-profit subsidiary of the UK Institute of Physics and is a signatory to the STM guidelines on use and republication of figures/tables in science publishing.

For your convenience a copy of this letter may serve as a release form: the duplicate copy may be retained for your files.

Thank you for your prompt attention to this request. Permission is being requested of the authors and the publisher separately.

Yours sincerely

Brenton L. Drake

PERMISSION TO REPRODUCE AS REQUESTED IS GIVEN PROVIDED THAT:

(a) the consent of the author(s) is obtained
(b) the source of the material including author, title of article, title of journal, volume number, issue number (if relevant), page range (or first page if this is the only information available), date and publisher is acknowledged.
(c) for material being published electronically, a link back to the original article should be provided (via DOI).

IOP Publishing Ltd
Dirac House
Temple Back
BRISTOL
BS1 6BE

23/03/11
Date

T McGlashan
Rights & Permissions

A3.3 *Ln*(Cu,Al)$_{12}$ (Ln = Y, Ce, Pr, Sm, and Yb)

3/17/2011

To whom it may concern

I am currently preparing my dissertation tentatively titled *Synthesis and Characterization of Rare Earth – Copper Containing Ternary and Quaternary Aluminides and Alumosilicide* and I would appreciate permission to reproduce all figures in both print and electronic editions of the Journal and in all subsequent future editions of the Journal, any derivative products and in publisher authorized distribution by third party distributors, aggregators and other licensees such as abstracting and indexing services. I should be grateful for nonexclusive perpetual world rights in all languages and media. Unless you indicate otherwise, I will use the complete reference given below as the credit line.

Brenton L Drake *et al* 2010 *J. Phys.: Condens. Matter* **22** 066001; doi: 10.1088/0953-8984/22/6/066001.

In case you do not control these rights, I would appreciate it if you could let me know to whom I should apply for permissions.

1. We are requesting use of all figures associated with the above reference. Figures 1 – 14, Crystal growth, structure, and physical properties of Ln(Cu,Al)$_{12}$ (Ln = Y, Ce, Pr, Sm, and Yb) and Ln(Cu,Ga)$_{12}$ (Ln = Y, Gd–Er, and Yb), Brenton L Drake, C Capan, Jung Young Cho, Y Nambu, K Kuga, Y M Xiong, A B Karki, S Nakatsuji, P W Adams, D P Young and Julia Y Chan, Journal of Physics: Condensed Matter, 22, 066001, p 1-14, 2010.)

For material being published electronically a link to the version of record will be provided back to the original article via DOI.

For your information, Institute of Physics Publishing is a not-for-profit subsidiary of the UK Institute of Physics and is a signatory to the STM guidelines on use and republication of figures/tables in science publishing.

For your convenience a copy of this letter may serve as a release form: the duplicate copy may be retained for your files.

Thank you for your prompt attention to this request. Permission is being requested of the authors and the publisher separately.

Yours sincerely

Brenton L. Drake

PERMISSION TO REPRODUCE AS REQUESTED IS GIVEN PROVIDED THAT:

(a) the consent of the author(s) is obtained
(b) the source of the material including author, title of article, title of journal, volume number, issue number (if relevant), page range (or first page if this is the only information available), date and publisher is acknowledged.
(c) for material being published electronically, a link back to the original article should be provided (via DOI).

IOP Publishing Ltd
Dirac House
Temple Back
BRISTOL
BS1 6BE

23/03/11
Date

T M C Gushan
Rights & Permissions

VITA

Brenton Leon Drake was born on August 31, 1984, at Memorial Hospital in Gassaway, West Virginia, to his parents, Debra Kay Drake, youngest daughter of Floyd James and Nannie Marie Rose, and Rickey Leon Drake, youngest son of Donald Houston and Helen Marie Drake, of Burnsville, West Virginia. He is the oldest of six siblings, 5 sisters and 1 brother (one biological, two adopted, and 3 stepsibling from his stepmother Christina Workman): Beverly Kay Drake, Brittany Marie Drake, Brandy Nicole Drake, Andrea Shane Hacker (Workman), Melissa Dawn Workman, and Robert Christopher Workman, respectively. He is the nephew of 5 paternal and 8 maternal aunts and uncles and has a total of 18 cousins.

Brenton graduated Spring of 2002 from Braxton County High School in Flatwoods, West Virginia with a full scholarship from the state, the Promise Scholarship for tuition for college. He received additional funding from the Chisler Scholarship for books and fees.

Brenton attended Glenville State College, in Glenville, West Virginia, from the Fall of 2002 through the Spring of 2007. His studies were guided by the hands of Dr. Kevin Evans (Organic Chemistry) and Dr. Joe Evans (Science Education). He graduated *summa cum laude*, with honors from Chi Beta Phi (math and science honorary), and the Toth Math and Science Award. Additionally, he was awarded, at the graduation ceremony, the Student Leadership Award. He received his Bachelor of Arts in Chemistry and a Bachelor of Science in Education with a minor in mathematics. He is certified in both West Virginia and Louisiana to teach chemistry, physics, and general science.

Brenton then focused his attention to his graduate studies at Louisiana State University. Brenton was awarded Economic Development Assistantship from Louisiana State University. He began class work in the Fall of 2007, starting his research under the advisement of Prof. Julia

Chan in the Spring of 2008. Brenton will be the second member of his family to graduate with a Doctor of Philosophy degree and the first to graduate with his Doctor of Philosophy in chemistry in December 2011 with his contemporaries William Adam Phelan and Melissa C. Menard. At the culmination of his graduate career he has published:

1. J. F. DiTusa, Z. Shoubao, K. Yamaura, Y. Xiong, **B. L. Drake**; B. Fulfer, P. W. Adams, D. A. Browne, and Julia Y. Chan. MnGe a cubic noncentrosymmetric ferromagnet, *XXXXXX*, 2011, *Submitted*
2. Phelan, W. A.; Kangas, M. J.; Menard, M. C.; **Drake, B. L**.; Chan, J. Y.; Adventures in Crystal Growth: Synthesis and Characterization of Single Crystals of Complex Intermetallic Compounds, *Chem. Mater*. **2011**, *Submitted.*
3. Menard, M. C.; Drake, B. L.; Thomas, K. R.; Haldolaarachchige, N.; Young, D. P.; DiTusa, J.; Chan, J. Y. A Tale of Two Polymorphs – Growth and Characterization of α-*Ln*$NiGa_4$ (*Ln* = Y, Gd–Yb) and β-*Ln*$Ni_{1-x}Ga_4$ (*Ln* = Tb–Er). *Eur. J. Inorg. Chem.* **2011**, S*ubmitted.*
4. Drake, B. L.; Kangas, M. J.; Haldolaarachchige, N.; Xiong, Y.; Adams, P. W.; Young, D. P.; Chan, J. Y. Crystal growth, structure, and physical properties of *Ln*$(Ag,Al,Si)_2$ (*Ln* = Ce and Gd). *J. Phys: Cond. Mat.* **2010**, *22*, 426002.
5. Menard, M.C.; Xiong, Y.; Karki, A.B.; Drake, B.L.; Adams, P.W.; Fronczek, F.R.; Young, D.P.; Chan, J.Y., Crystal growth and properties of $Ln_2Ag_{1-x}Ga_{10-y}$ (*Ln* = La, Ce), a disordered variant of the Ce_2NiGa_{10} structure type. *J. Solid State Chem.* **2010**, *183*(9), 1935-1942.
6. Drake, B. L.; Capan, C.; Cho, J. Y.; Nambu, Y.; Kuga, K.; Xiong, Y. M.; Karki, A. B.; Nakatsuji, S.; Adams, P. W.; Young, D. P.; Chan, J. Y. Crystal growth, structure, and physical properties of $Ln(Cu,Al)_{12}$ (Ln = Y, Ce, Pr, Sm, and Yb) and $Ln(Cu,Ga)_{12}$ (Ln = Y, Gd–Er, and Yb). *J. Phys. Cond. Mat.* **2010**, *22*(6), 066001.
7. Drake, B. L.; Grandjean, F.; Kangas, M. J.; Okudzeto, E. K.; Karki, A. B.; Sougrati, M. T.; Young, D. P.; Long, G. J.; Chan,J. Y. Crystal Growth, Transport, and the Structural and Magnetic Properties of Ln_4FeGa_{12} with Ln = Y, Tb, Dy, Ho, and Er. *Inorg. Chem.* **2010**, *49*(2), 445.

With the following manuscripts in preparation:

1. Kangas, M. J.; Drake, B. L.; Haldolaarachchige, N.; Xiong, Y.; Young, D. P.; Adams, P. W.; Chan, J. Y. Crystal growth, structure, and physical properties of Ln_2PdGa_{12} (*Ln* = Pr, Nd, and Sm). *J. Alloy. Compd. To be submitted.*
2. Drake, B. L; Phelan, W. A.; Kangas, M. J.; Xiong, Y.; Adams, P. W.; DiTusa, J.; Chan, J. Y. Crystal growth, structure, and physical properties of $LnCu_2(Al,Si)_5$ (Ln = La and Ce). *To be submitted.*
3. Phelan, W. A.; McCandless, G. T.; Kangas, M. J.; Drake, B. D.; Haldolaarachchige, N.; Xiong, Y. Adams, P. W.; Young, D. P.; Chan, J. Y. Crystal growth, neutron structure, and physical properties of $Ln(Cu,Al,Ga)_{13}$ (Ln = La, Ce, Pr, and Eu).